THE TITLE OF THESIS. CAPITALIZED, CENTERED, SINGLE SPACED

by

Full Name of The Scholar
Registration Number

Research Supervisor:
Name of Research Supervisor

2024

Department Name
Polytechnic University of Turin

ABSTRACT

This comprehensive study investigates the mechanical and damping characteristics of various aluminum-based materials, including Aluminum 6016 Plate, Aluminum Foam, Al-Zn Sandwich and Al-2%-Zn Sandwich. The experimental investigation of Aluminum 6016 Plate reveals a correlation between Young's modulus and shear modulus with material density, indicating a notable relationship observed in the study Aluminum Foam displays an upward trend in Young's and shear moduli with increasing density, while internal friction coefficient rises inversely. Al-Zn Sandwich and Al-2%-Zn Sandwich exhibit density-dependent behaviors in Young's and shear moduli, with intriguing shifts in internal friction coefficient.

Tensile tests underscore SD Al6016 Al Zn's superior peak stress resistance, contrasting with Aluminum Foam's lower stress levels. A positive correlation between peak stress and strain is observed across materials, offering insights into strength and ductility. Comparative analysis between theoretical and experimental values unveils notable disparities, particularly in Aluminum Foam, SD Al6016 Al Zn, and SD Al6016 Al 2 Zn, emphasizing the complexity of predicting material behaviors.

Failure analyses elucidate unique failure modes, with Aluminum Foam sandwich demonstrating robust bonding strength, a finding supported by delamination in lower modulus samples. RFDA testing aligns with tensile results, highlighting the versatility of bonding materials in influencing elastic moduli. This study provides critical insights into the mechanical behavior of diverse aluminum sandwich materials, emphasizing the need for nuanced considerations in material selection for specific engineering applications.

ACKNOWLEDGMENTS

I extend my profound gratitude to my family for their unwavering encouragement and steadfast support during the entirety of this research journey. A special acknowledgment is reserved for Professor Graziano Ubertalli whose exceptional guidance and mentorship played a pivotal role in shaping the direction of this study. The invaluable contribution of the laboratory staff is duly recognized, as their expertise and assistance were instrumental in the seamless execution of complex experiments. Additionally, I express my heartfelt thanks to my esteemed colleagues whose collaborative spirit and insightful discussions significantly enriched the depth and breadth of this research.

TABLE OF CONTENTS

Page

ABSTRACT vi

ACKNOWLEDGMENTS vii

TABLE OF CONTENTS viii

LIST OF FIGURES xii

LIST OF TABLES xviii

NOMENCLATURE xx

1. CHAPTER 1 - ALUMINUM FOAM SANDWICHES STRATEGIES FOR THEIR PREPARATION AND MAIN APPLICATIONS 21

1.1. ALUMINUM FOAM SANDWICH 21

1.2. CHARACTERISTICS OF ALUMINUM FOAM SANDWICH 22

1.3. STRUCTURE OF ALUMINUM FOAM SANDWICH 22

1.4. EXISTING TECHNIQUES FOR PRODUCTION OF AFS 23

1.4.1. PREPARATION TECHNIQUES OF ALUMINUM FOAM 24

1.4.2. Alporas Type Technique 25

1.4.3. EX-SITU BONDING TECHNIQUE 25

1.4.4. IN-SITU BONDING TECHNIQUE 27

1.5. APPLICATIONS OF ALUMINUM FOAM SANDWICH 29

1.5.1. TECHNOLOGICAL APPLICATIONS 30

1.5.2. ELECTROMAGNETIC SHIELDING 30

1.5.3. SOLAR THERMAL APPLICATIONS 31

1.5.4. CUTLERY ITEMS 31

1.5.5. ARCHITECTURAL APPLICATIONS 32

1.6. ECONOMICS OF ALUMINUM FOAM SANDWICH 33

1.7. CONCLUSION 33

2. CHAPTER 2 - MECHANICAL PROPERTIES OF ALUMINUM FOAM SANDWICHES: EXPERIMENTAL CHARACTERIZATIONS AND MODELLING 35

2.1. EXPERIMENTAL ANALYSIS 36

2.2. NUMERICAL ANALYSIS 41

2.3. CONCLUSION 44

3. CHAPTER 3 – MATERIALS AND METHODS 47

3.1. SAMPLE PREPARATION OF ASF BY JOINING MATERIALS 47

3.1.1. MATERIALS USED 48

3.2. EXPERIMENTAL SAMPLE 48

3.3. RESONANT FREQUENCY AND DAMPING ANALYZER (RFDA) 55

3.3.1. RESONANT FREQUENCY ANALYSIS 55

3.3.2. DAMPING ANALYSIS 55

3.3.3. RFDA INSTRUMENT OPERATION 55

3.3.4. APPLICATIONS 56

3.4. EXPERIMENT 1 – RFDA EXPERIMENTAL SETUP 57

3.5. EXPERIMENT 2 – TENSILE TESTING EXPERIMENTAL SETUP 59

3.6. ELECTRON MICROSCOPY 65

4. CHAPTER 4 – RESULTS 67

4.1. SAMPLE DATA COLLECTION 67

4.2. RESULTS FOR ALUMINUM 6016 PLATE 70

4.2.1. RESULTS FOR AL 6016 S1 70

4.2.2. RESULTS FOR AL 6016 S2 73

4.2.3. RESULTS FOR AL 6016 S3 75

4.2.4. RESULTS FOR AL 6016 COMBINED 77

4.3. RESULTS FOR ALUMINUM FOAM 78

4.3.1. RESULTS FOR AL FOAM S1 78

4.3.2. RESULTS FOR AL FOAM S2 80

4.3.3. RESULTS FOR AL FOAM S3 82

4.3.4. RESULTS FOR AL FOAM COMBINED 84

4.4. RESULTS FOR AL-ZN SANDWICH (SD AL6016 AL ZN) 85

4.4.1. RESULTS FOR SD AL6016 ZN S1 85

4.4.2. RESULTS FOR SD AL6016 ZN S2 87

4.4.3. RESULTS FOR SD AL6016 ZN S3 90

4.4.4. RESULTS FOR SD AL6016 ZN COMBINED 92

4.5. RESULTS FOR AL-2%-ZN SANDWICH (SD AL6016 AL 2 ZN) 93

4.5.1. RESULTS FOR SD AL6016 ZN2AL S1 93

4.5.2. RESULTS FOR SD AL6016 ZN2AL S2 95

4.5.3. RESULTS FOR SD AL6016 ZN2AL S3 97

4.5.4. RESULTS FOR SD AL6016 ZN2AL COMBINED 99

4.6. COMPARISON PLOTS 100

4.7. RESULTS FOR TENSILE TEST EXPERIMENT 102

4.8. RESULTS FOR ELECTRON MICROSCOPY 111
5. CHAPTER 5 – DISCUSSION 120
5.1. ANALYSIS OF RESULTS 120
5.1.1. ALUMINUM 6016 PLATE 120
5.1.2. ALUMINUM FOAM 120
5.1.3. Al-Zn Sandwich (SD Al6016 Al Zn) 121
5.1.4. Al-2%-Zn Sandwich (SD Al6016 Al 2 Zn) 122
5.1.5. COMPARATIVE ANALYSIS BETWEEN THEORETICAL AND EXPERIEMNTAL VALUES 122
5.2. BEHAVIORAL & STRUCTURAL RESPONSE OF SAMPLES 125
5.3. ANALYSIS OF TENSILE TEST RESULTS 128
5.4. ANALYSIS OF FAILURE MODE IN TENSILE TEST 129
6. CONCLUSION 134
BIBLIOGRAPHY 136
APPENDICES 138

LIST OF FIGURES

Figure Page

Figure 1.1: The summary of manufacturing methods of aluminum sandwich foam[8] ... 29

Figure 2.1: Force-displacement curves of specimens with various face sheet thickness under the impact energies: (a) 1150 J, (b) 2300 J, and (c) 4600 J..... 37

Figure 2.2: Comparison of energy absorption indicators of sandwich structures with various face sheet thickness under the impact energies: (a) 1150 J, (b) 2300 J, and (c) 4600 J. 42

Figure 2.3: Force-displacement curves of specimens with various core heights under the impact energies: (a) 1150 J, (b) 2300 J, and (c) 4600 J. 44

Figure 3.1: Aluminum Plate sample 50

Figure 3.2: Aluminum Foam sample 51

Figure 3.3: Al-Zn Sandwich (SD Al6016 Al Zn) sample..... 52

Figure 3.4: Al-2%-Zn Sandwich (SD Al6016 Al 2 Zn) sample 53

Figure 3.5: IMCE RFDA-HT1600 model..... 56

Figure 3.6: Mounted sample on RFDA with sensor in position 58

Figure 3.7: MTS Tensile Tester, model LPS.504 with a capacity of 50 kN..... 60

Figure 3.8: QATM auto cut off machine for sizing and cutting metal samples 61

Figure 3.9: Cut off sample of aluminum foam sandwich from QATM auto cutoff machine 61

Figure 3.10: MTS tensile tester with Aluminum foam sample mounted in the holder with adhesive bonding..... 63

Figure 3.11: MTS tensile tester with Aluminum sandwich foam sample mounted in the holder with adhesive bonding 63

Figure 3.12: Ruptured sample of aluminum sandwich foam SD Al6016 Al Zn 64

Figure 3.13: JEOL JCM-6000Plus electron microscope 65

Figure 4.1: Resonant frequency, loss rate & damping in Torsional & Flexural measurement mode for Al6016 S1 sample. 70

Figure 4.2: Youngs Modulus for Al6016 S1 Plate 71

Figure 4.3: Internal Friction Coefficient in flexion for Al6016 S1 Plate..... 71

Figure 4.4: Shear Modulus for Al6016 S1 Plate..... 72

Figure 4.5: Internal Friction Coefficient in torsion for Al6016 S1 Plate..... 72

Figure 4.6: Youngs Modulus for Al6016 S2 Plate 73

Figure 4.7: Internal Friction Coefficient in flexion for Al6016 S2 Plate..... 73

Figure 4.8: Shear Modulus for Al6016 S2 Plate..... 74

Figure 4.9: Internal Friction Coefficient in torsion for Al6016 S2 Plate..... 74

Figure 4.10: Youngs Modulus for Al6016 S3 Plate 75

Figure 4.11: Internal Friction Coefficient in flexion for Al6016 S3 Plate..... 75

Figure 4.12: Shear Modulus for Al6016 S3 Plate..... 76

Figure 4.13: Internal Friction Coefficient in torsion for Al6016 S2 Plate..... 76

Figure 4.14: Mean Young and Shear Moduli for Al6016 Plate - Combined..... 77

Figure 4.15: Mean Internal Friction Coefficient in flexion and torsion for Al6016 Plate - Combined 77

Figure 4.16: Youngs Modulus for Al Foam S1 78

Figure 4.17: Internal Friction Coefficient in flexion for Al Foam S1 79

Figure 4.18: Shear Modulus for Al Foam S1 79

Figure 4.19: Internal Friction Coefficient in torsion for Al Foam S1 80

Figure 4.20: Youngs Modulus for Al Foam S2 80

Figure 4.21: Internal Friction Coefficient in flexion for Al Foam S2 81

Figure 4.22: Shear Modulus for Al Foam S2 81

Figure 4.23: Internal Friction Coefficient in torsion for Al Foam S2 82

Figure 4.24: Youngs Modulus for Al Foam S3 83

Figure 4.25: Internal Friction Coefficient in flexion for Al Foam S3 83

Figure 4.26: Shear Modulus for Al Foam S3 83

Figure 4.27: Internal Friction Coefficient in torsion for Al Foam S3 84

Figure 4.28: Mean Young and Shear Moduli for Al Foam - Combined 84

Figure 4.29: Mean Internal Friction Coefficient in flexion and torsion for Al Foam - Combined 85

Figure 4.30: Youngs Modulus for SD Al6016 Zn S1 86

Figure 4.31: Internal Friction Coefficient in flexion for SD Al6016 Zn S1 86

Figure 4.32: Shear Modulus for SD Al6016 Zn S1 87

Figure 4.33: Internal Friction Coefficient in torsion for SD Al6016 Zn S1 87

Figure 4.34: Youngs Modulus for SD Al6016 Zn S2 88

Figure 4.35: Internal Friction Coefficient in flexion for SD Al6016 Zn S2 88

Figure 4.36: Shear Modulus for SD Al6016 Zn S2 89

Figure 4.37: Internal Friction Coefficient in torsion for SD Al6016 Zn S2 89

Figure 4.38: Youngs Modulus for SD Al6016 Zn S3 90

Figure 4.39: Internal Friction Coefficient in flexion for SD Al6016 Zn S3 90

Figure 4.40: Shear Modulus for SD Al6016 Zn S3 91

Figure 4.41: Internal Friction Coefficient in torsion for SD Al6016 Zn S3 91

Figure 4.42: Mean Young and Shear Moduli for SD Al6016 Zn - Combined 92

Figure 4.43: Mean Internal Friction Coefficient in flexion and torsion for SD Al6016 Zn - Combined 92

Figure 4.44: Youngs Modulus for SD Al6016 Zn2Al S1 93

Figure 4.45: Internal Friction Coefficient in flexion for SD Al6016 Zn2Al S1 94

Figure 4.46: Shear Modulus for SD Al6016 Zn2Al S1 94

Figure 4.47: Internal Friction Coefficient in torsion for SD Al6016 Zn2Al S1 95

Figure 4.48: Youngs Modulus for SD Al6016 Zn2Al S2 95

Figure 4.49: Internal Friction Coefficient in flexion for SD Al6016 Zn2Al S2 96

Figure 4.50: Shear Modulus for SD Al6016 Zn2Al S2 96

Figure 4.51: Internal Friction Coefficient in torsion for SD Al6016 Zn2Al S2 97

Figure 4.52: Youngs Modulus for SD Al6016 Zn2Al S3 97

Figure 4.53: Internal Friction Coefficient in flexion for SD Al6016 Zn2Al S3 98

Figure 4.54: Shear Modulus for SD Al6016 Zn2Al S3 98

Figure 4.55: Internal Friction Coefficient in torsion for SD Al6016 Zn2Al S3 99

Figure 4.56: Mean Young and Shear Moduli for SD Al6016 Zn2Al - Combined 99

Figure 4.57: Mean Internal Friction Coefficient in flexion and torsion for SD Al6016 Zn2Al - Combined 100

Figure 4.58: Comparison plot for Youngs Modulus of Al 60616 plate, Al foam, SD Al6016 Zn and SD Al6016 Zn2Al 101

Figure 4.59: Comparison plot for Internal Friction coefficient in Flexion Al 60616 plate, Al foam, SD Al6016 Zn and SD Al6016 Zn2Al 101

Figure 4.60: Comparison plot for Shear Modulus of Al 60616 plate, Al foam, SD Al6016 Zn and SD Al6016 Zn2Al 102

Figure 4.61: Comparison plot for Internal Friction coefficient in Torsion Al 60616 plate, Al foam, SD Al6016 Zn and SD Al6016 Zn2Al 102

Figure 4.62: Load vs extension plot for test 1 – AlZn S1 104

Figure 4.63: Load vs extension plot for test 2 – AlZn S2 104

Figure 4.64: Load vs extension plot for test 3 – AlZn S3 105

Figure 4.65: Load vs extension plot for test 4 – Al2Zn S1 105

Figure 4.66: Load vs extension plot for test 5 – Al2Zn S3 106

Figure 4.67: Load vs extension plot for test 6 – Al Foam S1 106

Figure 4.68: Load vs extension plot for test 7 – Al Foam S2 107

Figure 4.69: Load vs extension plot for test 8 – Al Foam S3 107

Figure 4.70: Load vs displacement plot for tensile test experiment 108

Figure 4.71: Comparison of mean and standard deviation of elastic modulus between tested materials 109

Figure 4.72: Comparison of mean and standard deviation of strain % between tested materials 110

Figure 4.73: Comparison of percentage strain observed by each sample of material at peak stress 110

Figure 4.74: Comparison of peak load observed by each sample of various material ... 111

Figure 4.75: Comparison of elastic modulus depicted by each sample of various material 111

Figure 4.76: Varying magnification images of Aluminum foam 112

Figure 4.77: Varying magnification images of AFS component brazed with pure Zn foil as soldering material (SD Al6016 Zn) 116

Figure 4.78: Varying magnification images of AFS component brazed with pure Zn2Al foil as soldering material (SD Al6016 Zn2Al)..... 117

Figure 4.79: EDS Spectra results of SD Al6016 foam sandwich 118

Figure 5.1: Aluminum foam core failure mode 130

Figure 5.2: Failure mode showing failure of adhesive bond between Al foam and holder 131

Figure 5.3: Failure of adhesive bond between aluminum face plate and foam core of the sandwich panel SD Al6016 Al 2 Zn 132

Figure 5.4: Failure of adhesive bond between aluminum face plate and foam core of the sandwich panel SD Al6016 Al Zn 133

Figure 5.5: Failure of foam core of the sandwich panel SD Al6016 Al Zn..... 133

LIST OF TABLES

Table Page

Table 3.1: Theoretical values for Aluminum 6016 49

Table 3.2: Theoretical values for Aluminum Foam 50

Table 3.3: Theoretical values ranges for Alporas Aluminum Sandwich Foam 51

Table 3.4: Sample sizes and dimensions of first material Al 6016 Plate 53

Table 3.5: Sample sizes and dimensions of second material Aluminum Foam 53

Table 3.6: Sample sizes and dimensions of third material sandwich Al6016 Al Zn 54

Table 3.7: Sample sizes and dimensions of third material sandwich Al6016 Al 2 Zn 54

Table 4.1: Flexural resonant frequency data for Al6016 S1 sample 68

Table 4.2: Torsional resonant frequency data for Al6016 S1 sample 69

Table 4.3: Details of Test 1 to 8 103

Table 4.4: Tensile test results for Al foam and AFS 109

Table 4.5: EDS results with composition (wt%) 118

Table 5.1: Experimental results of Youngs and Shear Moduli & internal friction coefficient for varying densities of Al 6016 Plate 120

Table 5.2: Experimental results of Youngs and Shear Moduli & internal friction coefficient for varying densities of Al Foam 121

Table 5.3: Experimental results of Youngs and Shear Moduli & internal friction coefficient for varying densities of SD Al6016 Al Zn 121

Table 5.4: Experimental results of Youngs and Shear Moduli & internal friction coefficient for varying densities of SD Al6016 Al 2 Zn 122

Table 5.5: Disparity between theoretical and experimental values of Youngs Modulus 123

Table 5.6: Disparity between theoretical and experimental values of Shear Modulus... 124

NOMENCLATURE

Symbol	Description
ASF	Aluminum Sandwich Foam

1. CHAPTER 1 - ALUMINUM FOAM SANDWICHES STRATEGIES FOR THEIR PREPARATION AND MAIN APPLICATIONS

In this chapter, aluminum foam sandwich composite is defined and its components are studied in detail. The Aluminum foam sandwiches are a novel material that is prepared from multiple techniques on a commercial scale, an account of which is given in detail. The applications of Aluminum foam sandwiches in the modern age have also been discussed.

1.1. ALUMINUM FOAM SANDWICH

An Aluminum Foam Sandwich (AFS) is a composite structure that consists of an aluminum foam core sandwiched between two dense metallic face sheets. It is a unique and innovative structure that offers several advantages in various industries. AFS provides increased mechanical stability and effective sealing compared to metal foam parts with thin outer skins. The dense face sheets protect the porous foam and enhance compression strength. This design allows to produce complex shapes while maintaining structural integrity. The use of AFS offers numerous benefits in different industries. One significant advantage is its lightweight construction. Metal foams have higher stiffness-to-mass ratios compared to dense materials, making them ideal for applications that require weight reduction without compromising strength. Although optimized structures like honeycomb or stringer-stiffened plates exhibit greater stiffness than AFS, metal foam cores still provide enough stiffness across various load situations. The statistical distribution of "dead material" in foams may not contribute to mechanical performance in a targeted manner, but overall, they perform well in average circumstances. The benefits

of AFS go beyond stiffness, encompassing factors like cost, damage tolerance, joining technologies, and other properties relevant to specific applications.

1.2. CHARACTERISTICS OF ALUMINUM FOAM SANDWICH

AFS is a versatile material that possesses several desirable properties and characteristics. Its lightweight construction and high stiffness-to-mass ratio make it ideal for applications where weight reduction is crucial without compromising structural strength. AFS exhibits favorable mechanical properties, including compression, tensional, and flexural strength, allowing it to withstand heavy loads and resist deformation. It also demonstrates good thermal insulation capabilities due to the presence of air-filled voids within its foam structure, providing thermal stability. AFS's excellent damping behavior enables it to absorb vibrations and impact energy, making it suitable for applications requiring vibration control and impact resistance. Furthermore, AFS can be engineered to be non-inflammable, offering fire resistance and ensuring safety in fire-prone environments.

1.3. STRUCTURE OF ALUMINUM FOAM SANDWICH

The structure of a typical AFS involves creating a three-layer composite consisting of a foamable layer and face sheets. The three-layer composite for AFS production is created using metallic precursors that can be filled into complex molds or used to foam plates if suitable molds are available. The composite comprises a foamable layer in the center and two face sheets. The composite is heated to a temperature where the lower-melting foamable layer expands, while the higher-melting face sheets remain

solid. This expansion results in the formation of an AFS panel with metallic bonding between the core and face sheets. To ensure flatness, a hot calibration step is often performed after foaming.

1.4. EXISTING TECHNIQUES FOR PRODUCTION OF AFS

In the past, the alloy combination AlSi6Cu4 or AlSi6Cu6 was commonly used for the foamable core in AFS production. However, the presence of copper in these alloys made them heavy, expensive, and prone to corrosion. A replacement alloy was sought, and the Al-Mg-Si system was found to be suitable. Among various alloys in this system, the alloy AlSi8Mg4 emerged as a favorable choice due to its good foaming behavior, including expansion and the formation of small and regular pores. AlSi8Mg4 is now widely used in AFS production. The precise conditioning of all metal powders used is crucial for improving foam quality. Contaminations, such as atmospheric moisture or dust, can adversely affect the uniformity of pore size distributions in the foam. To avoid weak points in the foam structure, which can lead to larger pores and compromised mechanical properties, careful attention is given to preventing contamination on the metal powders used. Additionally, the replacement of copper with magnesium in the alloy composition improves the corrosion resistance of the foam.

Aluminum Foam Sandwich (AFS) is a remarkable material known for its lightweight properties, impressive strength, and exceptional abilities in energy absorption and thermal insulation. This composite structure comprises a core composed of aluminum foam, enclosed between two outer face sheets typically constructed from aluminum or alternative metals.

Several distinct manufacturing techniques are employed in the production of AFS. Among the most prevalent methods used previously are:

1.4.1. PREPARATION TECHNIQUES OF ALUMINUM FOAM

The closed-cell metal foams, having better mechanical properties, are manufactured primarily by two techniques named powder metallurgy technology [1] and melting metallurgy technology [2]. However, it has been reported that aluminum foam developed through powder metallurgy yields superior mechanical properties in terms of compressive strength [3].

The powder metallurgy technique has been recommended for the preparation of aluminum foam. In this approach, a foaming agent is introduced in aluminum powder which is subjected to compaction, forming a coherent mass. Subsequently, the compacted aluminum powder is subjected to sintering at elevated temperatures. This process results in the creation of a robust porous material with an intricate internal structure. Another technique utilized in production of aluminum foams is foaming. This technique commences with the melting of aluminum, followed by the addition of a foaming agent to generate a liquid infused with gas bubbles. This aluminum foam-imbued liquid is subsequently poured into a mold and allowed to cool and solidify. As a result, the outcome is a core material characterized by a porous structure, denoting foamed aluminum. The powder metallurgy technique utilizes aluminum powder mixed with a foaming agent or a blowing agent. The commonly used foaming agent is Titanium hydride TiH2. The powder is thoroughly mixed, compressed, and then heated to above the melting point of aluminum. This allows the bonded hydrogen in the foaming agent to escape leaving behind a pore-like structure, resulting in the formation of aluminum foam.

The aluminum foam is then subjected further to either of the techniques of ex-situ binding or in-situ bonding. The in-situ bonding can be further classified into AFS technology [4] and AAS technology [5] which differs among themselves in joining methods.

1.4.2. ALPORAS TYPE TECHNIQUE

The production method employed for our foam involves the Alporas type, utilizing an in-situ gas generation process within the molten metal. This technique entails the introduction of gas-forming agents or compounds into the molten metal, triggering a reaction that generates gas bubbles throughout the material. As the molten metal solidifies, these gas bubbles become trapped, resulting in a foam-like structure with a cellular morphology.

The in-situ gas generation process begins by incorporating specific gas-forming agents or compounds into the molten metal. These agents undergo a chemical reaction within the molten metal, releasing gas that forms bubbles dispersed throughout the material. The choice of gas-forming agents and their proportions is critical, as it influences the size, distribution, and stability of the resulting foam structure.

During the production process, precise control over temperature, composition, and mixing is essential to ensure uniform gas bubble formation and distribution. Once the desired foam structure is achieved, the molten metal can solidify, preserving the foam's cellular morphology.

1.4.3. EX-SITU BONDING TECHNIQUE

Ex-situ bonding techniques involve bonding the face sheets and foam core using external means. This includes methods such as adhesive bonding, brazing, and diffusion bonding. Adhesive bonding involves the application of an adhesive material to join the face sheets and the foam core. This adhesive acts as a bonding agent, creating a robust connection. Adhesive bonding is chosen for its ability to distribute stresses evenly, resulting in a strong bond. Zinc-based brazing material are notable examples of adhesive materials used in AFS fabrication [6]. These adhesives have proven effective in securing face sheets to the foam core, providing both structural integrity and vibration damping.

Brazing is a technique that employs a filler material with a lower melting point than the face sheets. The process involves heating the assembly to a temperature where the filler material liquefies and wets the contact surfaces of the face sheets and the foam core. Upon cooling, the filler solidifies, creating a robust bond. Brazing is favored for its ability to produce high-strength joints without compromising the structural integrity of the face sheets or the foam core. This method ensures a hermetic seal and is particularly valuable when airtight or pressure-resistant AFS structures are required. Diffusion bonding relies on applying pressure and heat to allow atomic diffusion between the face sheets and foam core, resulting in a solid bond. Diffusion bonding relies on the principles of atomic diffusion to create a solid bond between the face sheets and the foam core. The process involves applying pressure and heat to the assembly, facilitating the movement of atoms at the interface. As atoms migrate and intermingle across the boundary, a metallurgical bond forms, resulting in a cohesive structure. Diffusion bonding is esteemed for its ability to generate joints with exceptional strength and integrity. It is

often employed when the AFS requires a bond that is as robust as the constituent materials themselves.

Ex-situ bonding techniques, such as adhesive bonding, brazing, and diffusion bonding, offer distinct advantages and considerations in AFS fabrication. Adhesive bonding stands out for its ease of application, stress distribution capabilities, and vibration damping properties. However, it may exhibit temperature sensitivity, environmental susceptibility, and prolonged curing times. Brazing excels in delivering high-strength joints and hermetic seals, accommodating a wide range of materials. Nevertheless, it demands high temperatures, skilled personnel, and potentially higher costs. Diffusion bonding boasts exceptional joint strength, hermetic sealing capabilities, and fewer material compatibility concerns. Yet, it necessitates elevated temperatures and pressures, extended processing times, and skilled oversight.

The selection of the appropriate ex-situ bonding method hinges on project-specific criteria, including strength requirements, material compatibility, temperature constraints, and cost considerations. Engineers must carefully weigh these pros and cons to determine the most suitable bonding technique for their AFS application, ensuring the optimal balance between structural integrity and manufacturing feasibility.

1.4.4. IN-SITU BONDING TECHNIQUE

In-situ bonding techniques combine the foaming process with the bonding of the face sheets and foam core. The in-situ production process is mold-free and does not require a separate bonding step unlike ex-situ bonding. A three-layer composite is used, consisting of a central foam layer and two face sheets. The central core layer if rolled in the mentioned configuration and then heated results in AFS technology while if the

central foam layer is first extruded and then cut into smaller pieces and then joined with face sheets results in AAS technology. By heating the composite to a temperature that allows the foam core layer to expand without melting the higher-melting face sheets, the composite expands and forms an AFS panel. The bonding between the core and face sheets remains metallic before and after foaming. A hot calibration step after foaming is recommended to ensure the flatness of the resulting AFS.

The rolling technique has been preferred for larger batches of ASF panels as the rolling requires an excess amount of effort however, the aluminum foam core is heated more quickly. The extruded technique not only carries the advantage of less energy utilization as compared to rolling but is also favored due to easiness of aluminum foam core extrusion [7]. However, the extruded process only allows for a shorter period of time for face sheet to form bond with the foam core [5]. The Figure 1.1 below shows the summary of manufacturing methods of metal foams and ultimately formation of Aluminum Sandwich Foam.

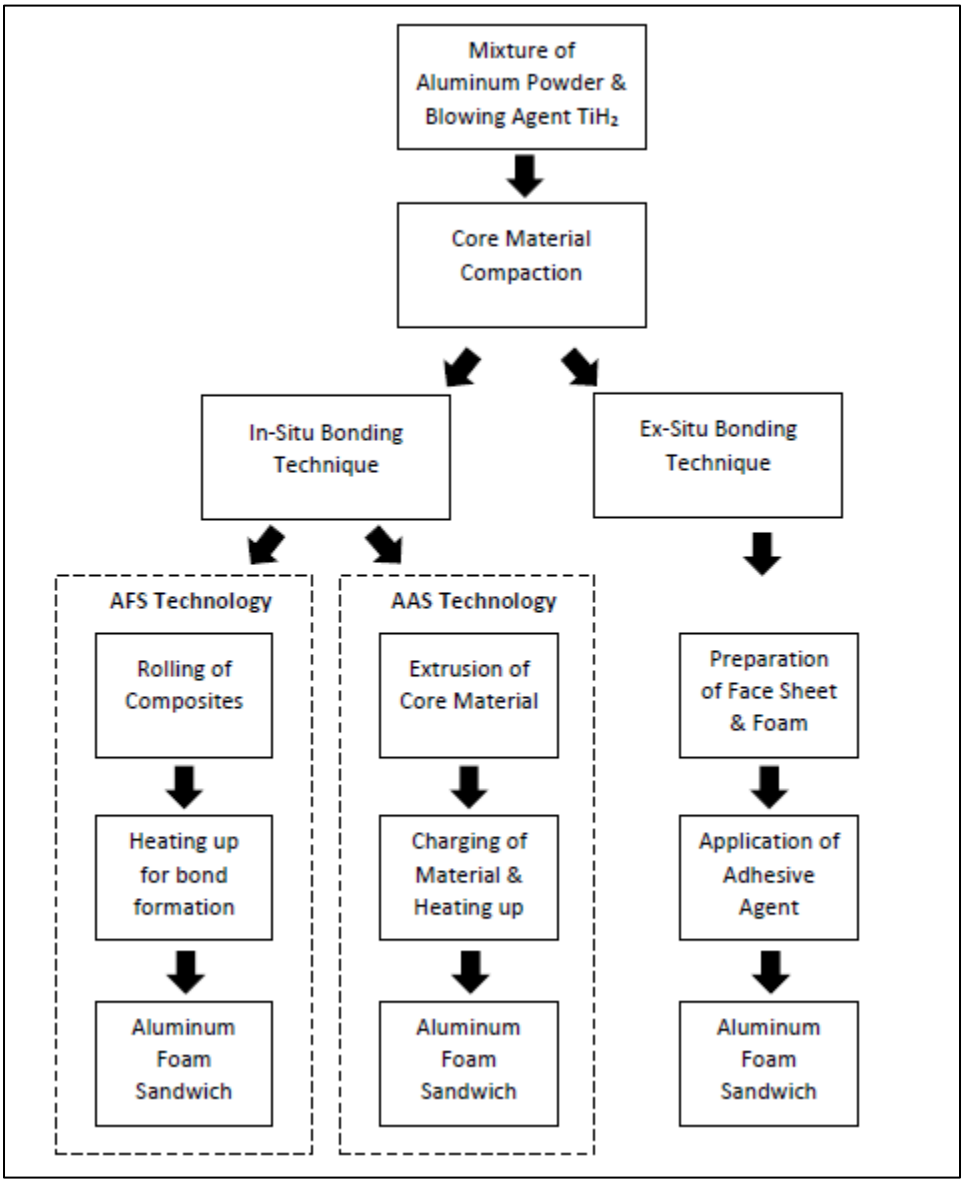

Figure 1.1: The summary of manufacturing methods of aluminum sandwich foam[8]

1.5. APPLICATIONS OF ALUMINUM FOAM SANDWICH

The use of AFS panels has been successfully applied in various industries, highlighting its versatility and advantages.

1.5.1. TECHNOLOGICAL APPLICATIONS

In the telescope lifting system developed by Teupen GmBH, AFS panels were incorporated into the support structure, allowing for increased working height and outreach while keeping the vehicle weight low [9]. The structure exhibited excellent performance under multi-axial cyclic loads, surpassing the required number of cycles without failure and weighing significantly less than the conventional steel counterpart. Alimex, another German company, introduced AFS sandwich panels to their product line of high-precision aluminum plates [10]. These AFS plates demonstrated a weight reduction of over 50% compared to solid counterparts while maintaining 92% of their stiffness. The plates are suitable for applications in metrology and machine engineering. Additionally, AFS technology has been utilized in the production of an Ariane 5 rocket adaptor prototype, a bicycle crank arm, and even cookware [11]. The AFS-based rocket adaptor prototype exhibited enough strength, while efforts are underway to enhance its stiffness further. AFS forging was applied in the production of a lightweight crank arm for racing bicycles, resulting in a 30% weight reduction compared to conventional parts. In the cookware industry, AFS base plates were found to distribute heat more evenly, leading to improved cooking performance. These examples highlight the wide-ranging potential and benefits of AFS in various fields, including increased strength-to-weight ratio, cost reduction, and enhanced thermal properties.

1.5.2. ELECTROMAGNETIC SHIELDING

In recent years, AFS panels have been applied in various new and diverse applications. One notable application is in the field of electromagnetic shielding, where AFS panels have proven to be effective in shielding electromagnetic waves while

offering mechanical rigidity and electrical conductivity. Prototype boxes made of AFS exhibited superior electromagnetic damping compared to aluminum sheet counterparts. It has been reported that Aluminum sandwich foams possess good EMI shielding effectiveness of 25–75 dB when subjected to the plane electromagnetic wave within the frequency of 130–1800 MHz [12] as compared to the 60 dB value of aluminum sheet for moderate thicknesses of sheet. It has also been reported that EMI shielding effectiveness of ASF generally increases with increasing porosity and decreases with increasing frequency.

1.5.3. SOLAR THERMAL APPLICATIONS

AFS has also shown potential in solar thermal energy generation, particularly in the design of parabolic trough mirrors. These mirrors can be constructed using AFS panels, which provide the necessary bending capabilities and thermal stability for concentrating sunlight onto a fluid collector. This design offers advantages in terms of lifetime durability and resistance to thermal warping. The thermal conductivity of aluminum foam can range from 5 to 40 W/mK, depending on the porosity of the foam. This is significantly higher than the thermal conductivity of air, which is 0.024 W/mK [13].

1.5.4. CUTLERY ITEMS

Cooking equipment has also benefited from the use of AFS due to its excellent heat diffusion and conduction properties. AFS plates have been used in barbecue plates, baking ovens, and cooking utensils such as frying pans and saucepans. These applications demonstrate energy efficiency, reduced heating times, and improved heat distribution

compared to traditional materials. Aluminum foam sandwiches can conduct heat well, which could cause food to cook unevenly. This could be mitigated by using a thicker foam core or by adding a protective coating to the crockery.

1.5.5. ARCHITECTURAL APPLICATIONS

Architectural panels have found use in AFS as well, leveraging its flexibility, ease of processing, non-inflammability, and corrosion resistance. AFS panels can be visually appealing and functional, offering sound absorption properties and enabling various surface modifications. They have been employed in staircase railings, where the open-pore structure of AFS panels is visible and contributes to the aesthetic appeal.

AFS panels, in combination with stone plates, have been utilized for protection against bullets and explosions. This configuration has shown effectiveness in stopping bullets and dissipating energy. The combination of AFS and stone provides a lightweight and visually appealing solution for architectural purposes, particularly in high-security buildings or public structures.

Additionally, AFS has been employed in the construction of protective housings for high-speed turning machines, offering reliable protection against potential hazards. These AFS casings have been successfully implemented in industrial settings to safeguard against flying debris. Aluminum foam can also be used as insulation to prevent heat loss. The foam's closed-cell structure traps air, which is a poor conductor of heat. This makes aluminum foam a good choice for applications such as building insulation and pipe insulation [14].

1.6. ECONOMICS OF ALUMINUM FOAM SANDWICH

The widespread adoption of AFS panels faces several obstacles. Firstly, the cost of AFS panels is higher compared to traditional materials, limiting their affordability and feasibility. AFS panels exhibit material anisotropy and variations in mechanical properties, making it challenging to predict and control their performance. Thirdly, the lack of comprehensive technical parameters and reference applications hinders their adoption, as designers and engineers require standardized guidelines and reference cases. Lastly, the limited availability of AFS panels creates supply chain challenges and longer lead times. Overcoming these obstacles requires addressing technical parameters, establishing reference applications, reducing costs through improved manufacturing processes, and increasing material availability. Research and development efforts, industry collaborations, and investment in production capabilities are crucial to promote wider acceptance and adoption of AFS panels.

1.7. CONCLUSION

Aluminum foam technology and here mainly AFS technology has led to several promising small-scale applications. What is important for the development of the market is the availability of materials in quantities of tens of thousands of square meters annually. Experience in the past has shown that without a source of material, the search for applications in companies is slow which, in turn, slows down the development of manufacturing technologies. This is the well-known ‘‘chicken and egg problem’’ of new materials. The past years have seen an improvement in foam quality. Pore size distributions are now more uniform and large pores that have a negative effect on the

entire AFS can be avoided. What has remained very much the same is the cost of the product. Strategies to reduce costs include combining various process steps into fewer integrated steps, for example, combining powder pressing and rolling as suggested. Such integrated technologies have been found to be difficult to control and sometimes to have a negative impact on foam quality but still, they are the right way to go. Finally, the search for applications must focus more on finding the unique selling points of AFS, that is, as many as possible of the properties mentioned above should be combined in a given application, thus representing multi-functionality.

2. CHAPTER 2 - MECHANICAL PROPERTIES OF ALUMINUM FOAM SANDWICHES: EXPERIMENTAL CHARACTERIZATIONS AND MODELLING

This chapter focuses on understanding how strong and lightweight Aluminum Foam Sandwiches (AFS) behave when subjected to different types of forces. We'll explore their mechanical properties through experiments and computer models. AFS materials are known for their strength and ability to absorb energy, making them useful in industries like aerospace and automotive. By studying how AFS responds to pressure, bending, and other forces, we can better design structures and improve materials in engineering.

Theoretical analysis, experimental testing, and numerical simulation have been used to investigate the dynamic response of sandwich structures to low-velocity impact. Experimental methods have provided valuable insights into the energy absorption and damage patterns of sandwich structures. However, experiments can be costly and time-consuming. Numerical simulations offer a cost-effective alternative and have been employed to study the mechanical response of sandwich structures under low-velocity impact. Crashworthiness and optimization design of sandwich structures under impact loading have also been explored. The research focuses on the dynamic characteristics and energy absorption capability of aluminum foam sandwich structures through both experiments and numerical simulations. It evaluates the influence of various parameters on the energy absorption effect and deformation and damage modes of sandwich

structures, providing valuable data for the optimum design of sandwich structures against low-velocity impact loads.

2.1. EXPERIMENTAL ANALYSIS

The experiment focused on aluminum foam sandwich structures comprising of two mild steel face sheets and a closed-cell aluminum foam core, bonded together using silicone structural adhesive. Four types of sandwich panels were tested, varying in face sheet thickness (1 mm, 2 mm, and 3 mm) and foam core height (30 mm and 50 mm). A total of 36 specimens were prepared, with three specimens for each configuration to minimize experimental error. The low-velocity impact tests were conducted using a drop hammer tester. The tester consisted of a free-falling carriage system with a crosshead, impactor, and force transducer. The sandwich specimen was placed between the impactor and a rigid support platen. The impactor, shaped like a hemisphere with a diameter of 50 mm and a total counterweight of 230 kg, was used to deliver the impact. The rigid support platen had inner and outer diameters of 100 mm and 240 mm, respectively. The initial impact energy was controlled by adjusting the height of the impactor using computer automation. The impactor was raised to predetermined heights (0.5 m, 1.0 m, and 2 m) to achieve initial impact energies of 1150 J, 2300 J, and 4600 J, respectively.

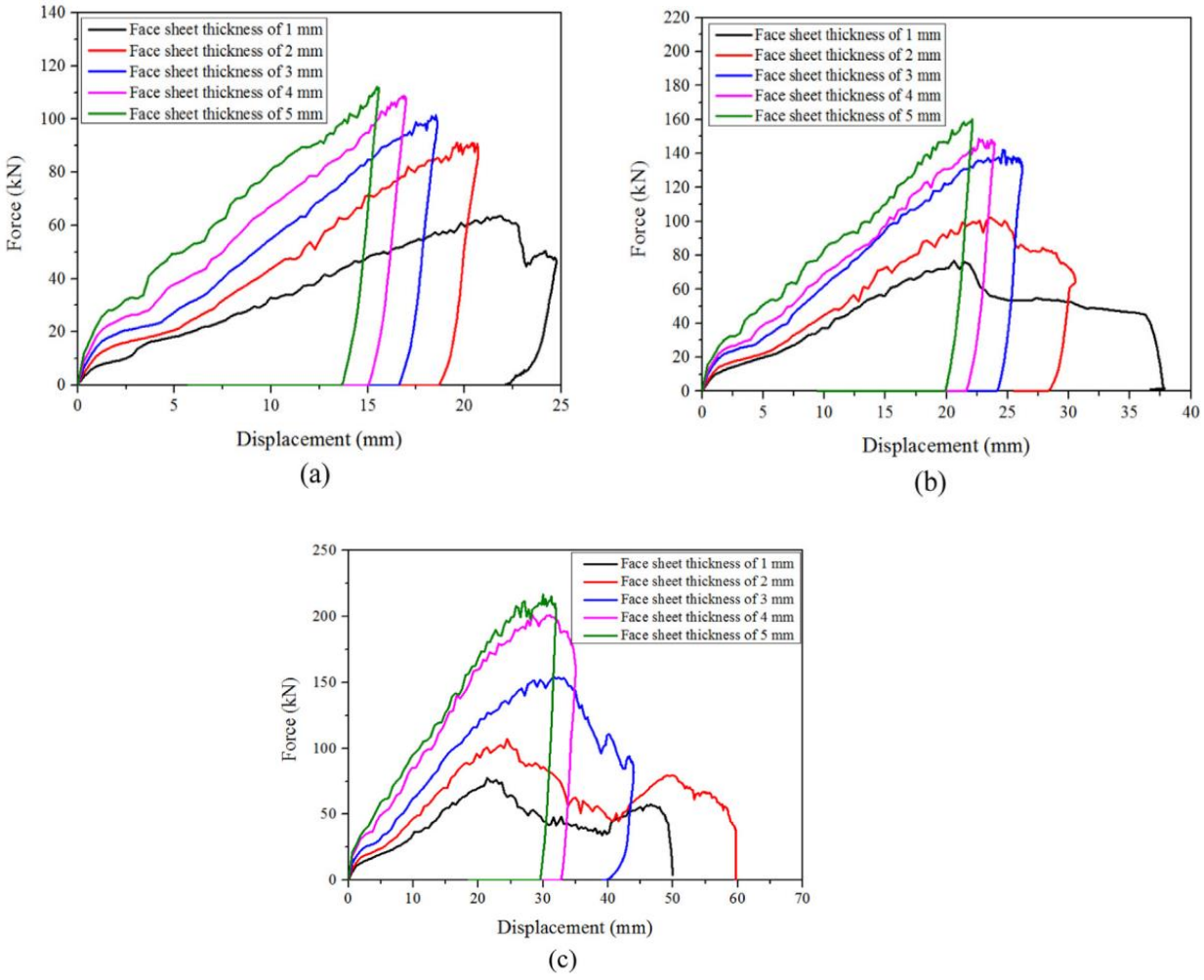

Figure 2.1: Force-displacement curves of specimens with various face sheet thickness under the impact energies: (a) 1150 J, (b) 2300 J, and (c) 4600 J

The corresponding initial impact velocities were calculated based on the law of energy conservation (3.16 m/s, 4.47 m/s, and 6.32 m/s, respectively). During the test, the force transducer measured the impact force-time history curve to analyze the low-velocity impact process. The impactor was released, free-falling along guide columns to impact the central position of the specimen. Fig. 1 compares the curves of force–displacement for specimens with various face sheet thickness suffering from different impact energies

by numerical calculation. The results show that face sheet thickness exhibits a dramatic effect on the force–displacement curves for sandwich structures.

The experimental setup allowed for controlled and repeatable impact tests at different energy levels. The sandwich structure consists of a closed-cell aluminum foam core and two mild steel face sheets. The material properties of the aluminum foam were determined through quasi-static uniaxial compressive tests, while the mild steel material properties were obtained through quasi-static uniaxial tensile tests. The aluminum foam specimens were cut into cylinders, and three specimens were tested for each density. The stress-strain curves for aluminum foam and mild steel were obtained and used in the numerical simulations. The crushable foam model with isotropic hardening was employed to represent the plastic behavior of the aluminum foam in the numerical analysis. The material properties and densities of the aluminum foam were provided in the respective tables. For the mild steel face sheets, the bilinear isotropic hardening model was utilized, and its material properties were summarized in a table.

Shear failure criteria were used to describe the deformation and damage of the mild steel face sheets and aluminum foam core. The fracture strain values for mild steel and aluminum foam with different densities were determined, and the shear failure model was based on the equivalent plastic strain. Damage was assumed to occur when the failure parameter reached a value of 1, triggering the removal of elements in the numerical simulation. Overall, the material properties and failure criteria were established for the aluminum foam and mild steel components, forming the basis for the subsequent numerical simulations of the sandwich structures' low-velocity impact response.

The determination of material properties, particularly the elastic and damping characteristics, is of paramount importance in various engineering applications. In the context of metallic foams, such as ductile aluminum foam, the evaluation of these properties is essential for designing lightweight structures that can effectively mitigate noise and vibration issues. Since, this study focuses on the experimental investigation of these properties, employing standardized procedures outlined in ASTM E 1876, which provides guidelines for the characterization of mechanical properties of materials[15].

1. Young's Modulus (E) Calculation:

Young's Modulus (E) is calculated using the following formula:

$$E = \frac{4L^3}{3bd^3} \times \left(\frac{f_{flexural}}{f_{torsion}}\right)^2$$

Where,

E is Youngs Modulus

L is the length of the rectangular bar sample

b is the width of the rectangular bar sample

d is the thickness of the rectangular bar sample

$f_{flexural}$ is the fundamental flexural resonant frequency

$f_{torsion}$ is the torsional resonant frequency

2. Shear Modulus (G) Calculation:

Shear Modulus (G) can be calculated using the following formula:

$$G = \frac{\pi^2 pd(f_{torsion})^2}{16L^2}$$

Where,

G is the Shear Modulus

L is the length of the rectangular bar sample

ρ is the density of the rectangular bar sample in kg/m^2

d is the thickness of the rectangular bar sample

$f_{torsion}$ is the torsional resonant frequency

3. Internal Friction Coefficient Q^{-1} Calculation

The Internal Friction Coefficient Q^{-1} can be determined using the following formula:

$$Q^{-1} = \frac{k}{\pi . f_r}$$

Where,

Q^{-1} is the Internal friction coefficient

k is the exponential decay parameter of the vibration component of frequency f_r

f_r is the resonant frequency in Hertz (Hz)

4. Young's Modulus (E) Calculation Using Resonant Frequency:

In addition to traditional stress-strain analysis, this study employs the resonant frequency method for calculating Young's Modulus (E). This method, rooted in the resonant frequency and damping analyzer (RFDA), offers an alternative approach to assessing the stiffness of materials based on their vibration response. Young's Modulus (E) can also be calculated using the fundamental flexural resonant frequency $f_{flexural}$ with the following formula:

$$E = \frac{\rho \times \left(f_{flexural}\right)^2 \times L^4}{3bd^3}$$

Where,

E is Youngs Modulus

L is the length of the rectangular bar sample

ρ is the density of the rectangular bar sample in kg/m^2

b is the width of the rectangular bar sample

d is the thickness of the rectangular bar sample

$f_{flexural}$ is the fundamental flexural resonant frequency

2.2. NUMERICAL ANALYSIS

A numerical model of the same aluminum foam sandwich structure undergoing drop-hammer impact was created using ABAQUS/Explicit software. The model consisted of the face sheet, foam core, impactor, and support platen, all meshed using 8-node hexahedral elements. The impactor and support platen were treated as rigid constraints. Surface-surface contact elements were utilized to simulate the interaction between the impactor and front face sheet, with a coefficient of friction of 0.3. The support platen was fixed at the bottom, while the impactor and sandwich structure were free. Impact energies of 1150 J, 2300 J, and 4600 J were applied, corresponding to initial velocities of 3.16 m/s, 4.47 m/s, and 6.32 m/s, respectively.

Five various thicknesses of face sheet were considered for sandwich structures with the same core height (30 mm) and core density (0.48 g/cm^3) in the impact simulation of low-velocity to evaluate effects of face sheet thickness.

For more direct and quantitative comparison, Fig. 2 shows the energy absorbing indicators for sandwich structures which have decreased when its thickness increased to a certain value, which prevented momentum transfer to the aluminum foam core.

The sandwich structure of three various core heights (30 mm, 40 mm, and 50 mm) with the same density of 0.48 g/cm^3 were considered to discuss the influences of the aluminum foam core height on impact performance. All the specimens were fabricated with mild steel face sheets of 2 mm thickness.

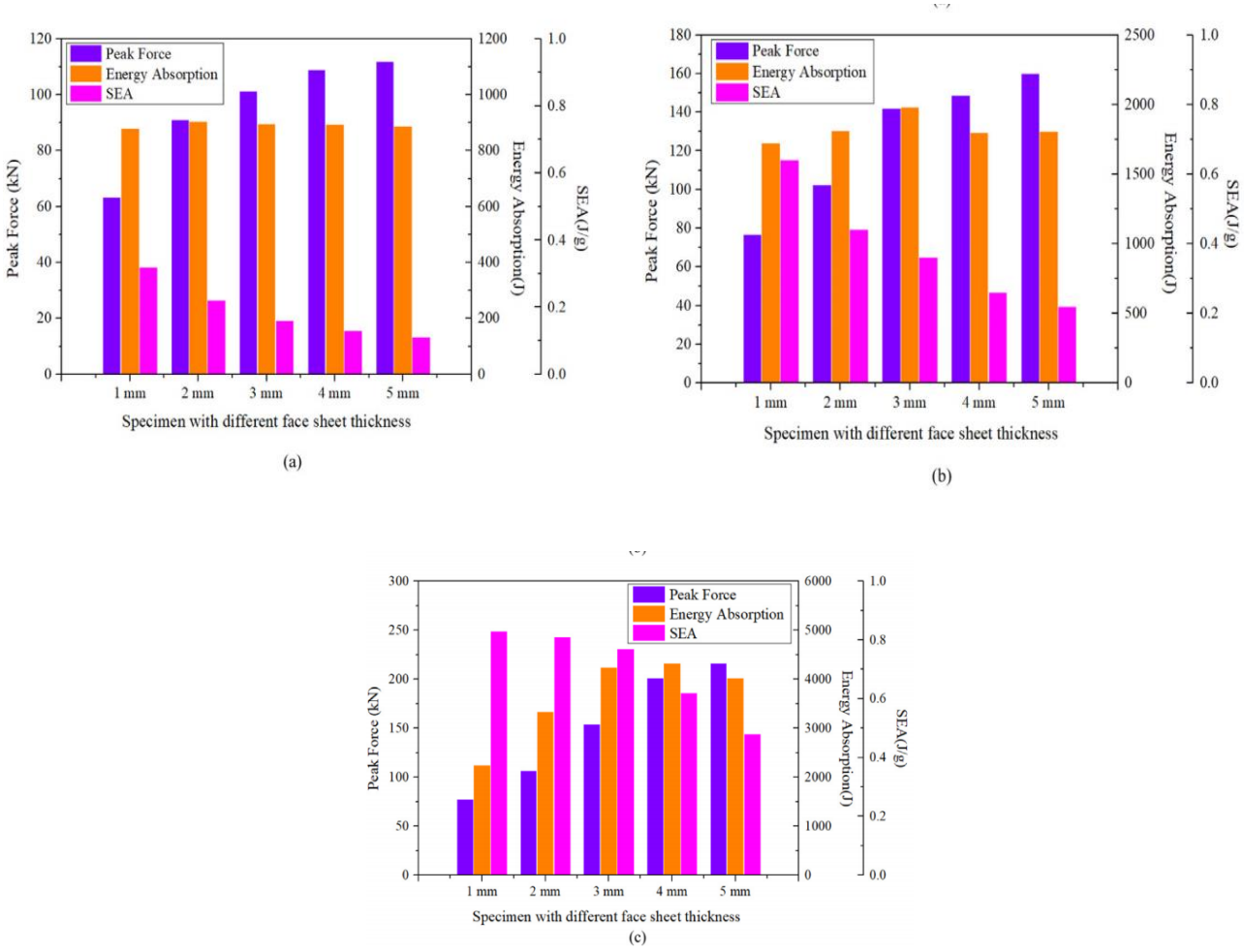

Figure 2.2: Comparison of energy absorption indicators of sandwich structures with various face sheet thickness under the impact energies: (a) 1150 J, (b) 2300 J, and (c) 4600 J.

Fig. 3 exhibits the force–displacement curves of specimens with various core heights subjecting to various impact energies by numerical calculation. It was discovered that

various core heights have little effect on the force–displacement curves suffering from lower impact energy (1150 J). When subjected to higher impact energy, such as 2300 J and 4600 J, the core height can influence the force–displacement distance, but did not change configuration of the impact force curves suffering from the same impact energy. Fig. 3 exhibits the force–displacement curves of specimens with various core heights subjecting to various impact energies by numerical calculation. It was discovered that various core heights have little effect on the force–displacement curves suffering from lower impact energy (1150 J). When subjected to higher impact energy, such as 2300 J and 4600 J, the core height can influence the force–displacement distance, but did not change configuration of the impact force curves suffering from the same impact energy.

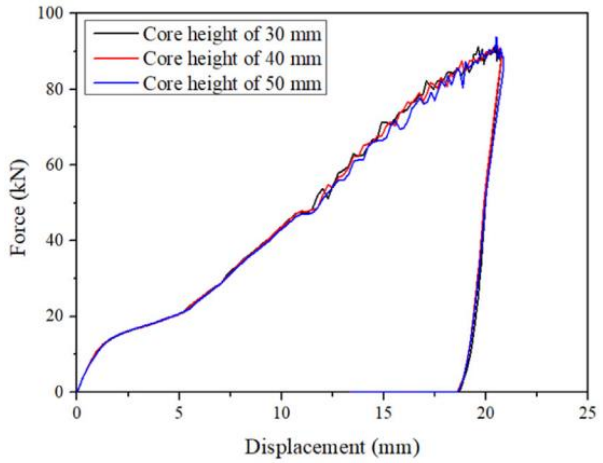

(a)

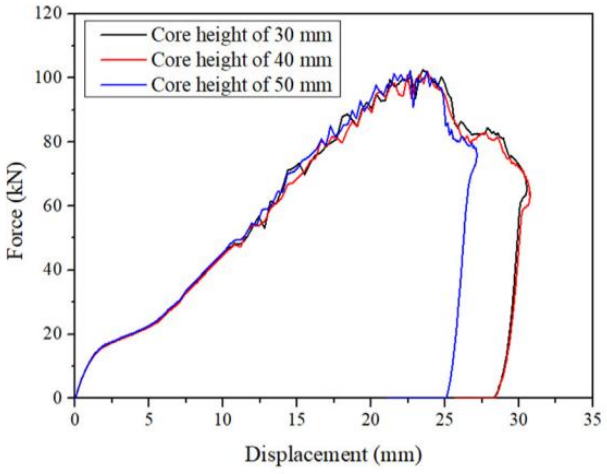

(b)

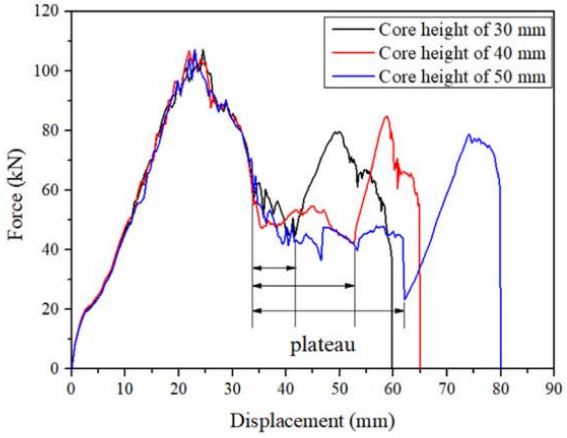

(c)

Figure 2.3: Force-displacement curves of specimens with various core heights under the impact energies: (a) 1150 J, (b) 2300 J, and (c) 4600 J.

2.3. CONCLUSION

During the experimental investigation, a comprehensive analysis was being performed to study the mechanical response of Aluminum Foam Sandwich (AFS) structures subjected to low-velocity impacts. These AFS configurations consisted of two mild steel face sheets bonded to a closed-cell aluminum foam core using silicone structural adhesive. Through a meticulous approach encompassing varying face sheet

thicknesses (1 mm, 2 mm, and 3 mm) and foam core heights (30 mm and 50 mm), we explored the influence of these parameters on the impact behavior of the structures. The experimental tests, executed with precision and rigor, provided crucial insights into the performance of AFS under controlled impact conditions. Force-displacement curves, as depicted in Figure 1, elucidated the substantial impact of face sheet thickness on the force-displacement response of the sandwich structures. These findings underscore the importance of tailoring AFS designs to meet specific load and deformation requirements. Furthermore, material properties for both the aluminum foam core and mild steel face sheets were meticulously characterized, enabling the development of numerical models that faithfully captured the observed behavior. Utilizing the crushable foam model with isotropic hardening for aluminum foam and the bilinear isotropic hardening model for mild steel, we conducted simulations that revealed the complex interplay of material properties and geometrical parameters in AFS structures.

Incorporating shear failure criteria and fracture strain values, our analysis comprehensively addressed deformation and damage mechanisms in the mild steel face sheets and aluminum foam core. The numerical simulations, informed by experimental data, provided invaluable insights into the low-velocity impact response of AFS structures, enabling a deeper understanding of their behavior under varying loading conditions.

This study, therefore, not only contributes to the fundamental knowledge of AFS behavior but also paves the way for informed design choices in diverse engineering applications. The findings presented herein offer a foundation for optimizing AFS designs, enhancing their structural performance, and guiding future research endeavors.

As AFS materials continue to garner attention for their unique properties, this investigation stands as a testament to the potential of these versatile composite structures in a range of engineering and industrial contexts.

3. CHAPTER 3 – MATERIALS AND METHODS

In this chapter, the foundation is being laid for the research work by detailing the materials being used and the methods being employed. The aim of this chapter is to provide a clear and concise roadmap of how the experiments and investigations were conducted. The chapter also discusses in detail the manufacturing methods being utilized for preparation of aluminum sandwich foam which were tested in the forthcoming chapters. The literature comprises of prevalent manufacturing methods of ASF and the methodology being utilized for the preparation of samples, by using zinc based joining materials, for the study under discussion. This chapter serves as a guide, offering transparency into the tools and techniques that underpin the scientific journey.

3.1. SAMPLE PREPARATION OF ASF BY JOINING MATERIALS

In this preparation technique, the objective was to establish a robust bond between AL-6016, a prevalent aluminum alloy in the automobile industry, and lightweight aluminum foam, using Zn-based brazing alloy. The process began with thorough surface preparation, encompassing cleaning, abrading, and activation to ensure effective bonding. Selections were made for joining materials, comprising pure Zn foil and Zn with 2% Al strip. The application of Al-6 flux facilitated chemical bonding and averted oxidation.

The assembly was subjected to controlled heating within a tubular furnace, maintaining an argon atmosphere to prevent oxidation. Optimization efforts yielded specific time/temperature combinations, resulting in the ideal bonding conditions. The subsequent cooling phase was executed slowly to eliminate residual stresses. The joining process was performed in a previous work according to Ubertalli et. al.[6]

This procedure, designed with scalability in mind, provided the framework for generating robust joints between dissimilar materials. Following this, mechanical testing, was carried out to assess the quality and strength of the joints that had been established. The detailed account is given below.

3.1.1. MATERIALS USED

- Skin Material: Aluminum Alloy (AA)-6016 (Al 98.75% + Mg 0.25% + Si 1%), 1.2 mm thick, which is commonly being used in the automobile industry.
- Core Material: Ultralight aluminum foam plate (9 mm thick, average density 0.28 g/cm3) with closed cells, which is being supplied by Foamtech, South Korea.
- Soldering Materials: Pure Zn foil (250 μm thick) and Zn with 2% Al strip (350 μm thick) provided by Lucas Milhaupt, USA.
- Flux: Al-6 flux (working temperature 420–470 °C), supplied by Stella srl-Italy, applied to facilitate chemical bonding and prevent oxidation.

3.2. EXPERIMENTAL SAMPLE

In this experiment, we conducted a comprehensive study on four distinct materials, each with different compositions. The aim was to understand and compare their mechanical properties and behaviors. The materials chosen for investigation were:

- Aluminum 6016 Plate
- Aluminum Foam
- Al-Zn Sandwich (SD Al6016 Al Zn)
- Al-2%-Zn Sandwich (SD Al6016 Al 2 Zn)

Aluminum 6016 Plate: This material is a commonly used aluminum alloy known for its excellent combination of strength and corrosion resistance. It is widely employed in various engineering applications, particularly in the automotive and aerospace industries. The theoretical mechanical properties of Aluminum 6016 are as follows [16]:

Table 3.1: Theoretical values for Aluminum 6016

Mechanical Properties	**Theoretical Values**
Tensile strength	310 MPa
Yield strength	276 MPa
Shear strength	207 MPa
Fatigue strength	96.5 MPa
Elastic modulus	68.9 GPa
Shear modulus	26 GPa
Poisson's ratio	0.33
Elongation	12-17%
Hardness, Brinell	95

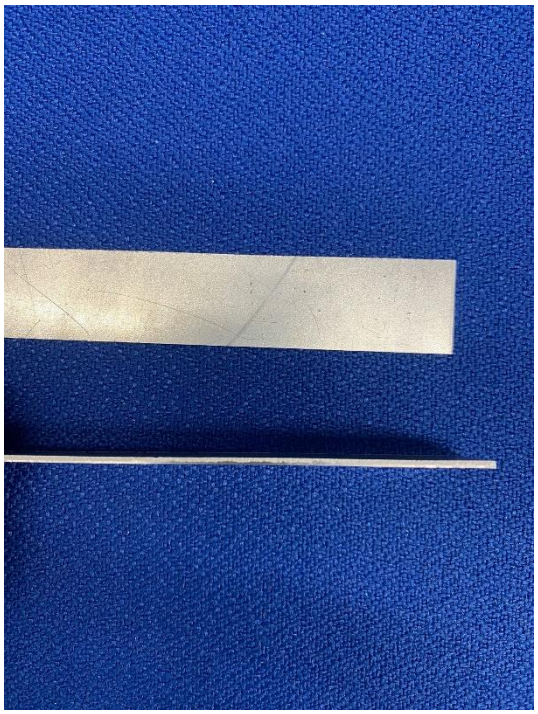

Figure 3.1: Aluminum Plate sample

Aluminum Foam: Aluminum foam is a lightweight, porous material that exhibits remarkable energy-absorbing properties. Its unique structure makes it suitable for applications involving impact resistance, sound absorption, and lightweight structural components. The theoretical mechanical & thermal properties of Aluminum foam are as follows represented in table 3.2 [17]:

Table 3.2: Theoretical values for Aluminum Foam

Properties	**Stochastic or reticulated foam**
Material	Aluminum 98.5% (Aluminum 6101 alloy)
Standard cell size	2 to 16 pores/cm
Foam topology	Open, interconnected
Relative density	4 to 10%
Nominal Density (unclad foam)	0.11 to 0.27 g/cm^3
Maximum service temperature	450°C
Melting point	660°C
Compression Strength	2.53 MPa
Tensile Strength	1.24 MPa
Shear Strength	1.31 MPa
Modulus of Elasticity (Comp.)	103.08 MPa
Modulus of Elasticity (Tension)	101.84 MPa
Shear Modulus	199.95 MPa
Specific Heat	0.895 J/g-C
Bulk Thermal Conductivity	5.8 W/m-C
Coefficient of Thermal Expansion (0-100°C)	23.58 x 10-6 m/m—C
Bulk Resistivity	7.2 x 10-5 ohm - cm

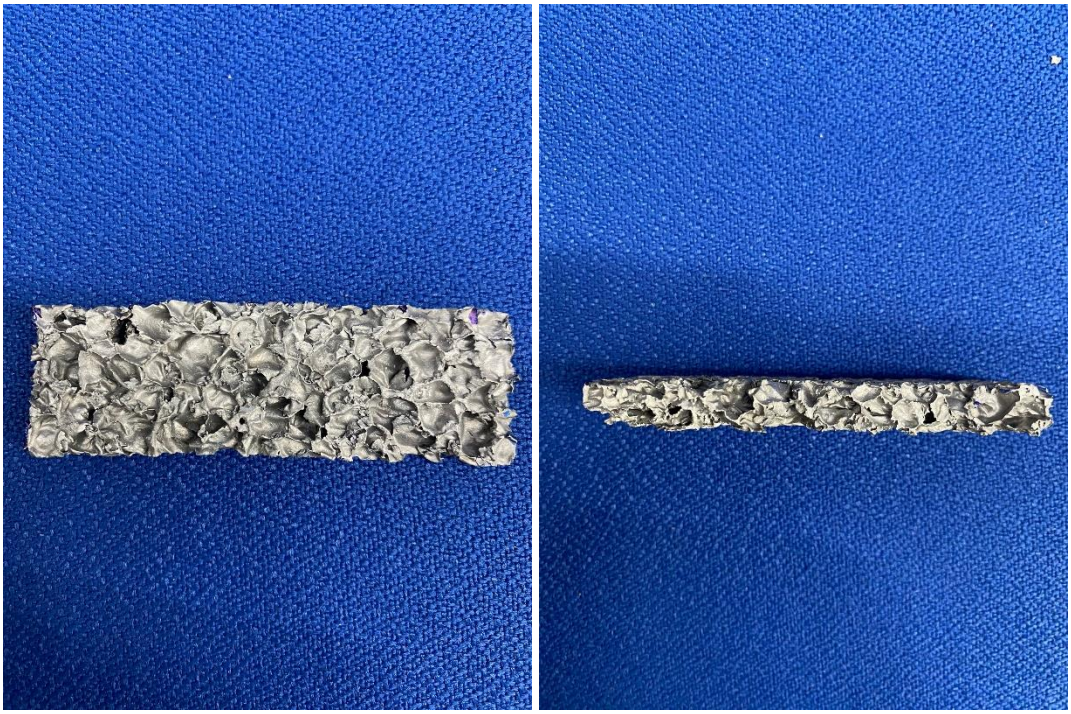

Figure 3.2: Aluminum Foam sample

Al-Zn Sandwich (SD Al6016 Al Zn): The sandwich is made with two Al6016 layers and an aluminum foam core which are joined by zinc brazing alloy. Such sandwich structures are known for their potential in achieving a balance between strength and weight reduction, making them valuable in structural applications. The theoretical mechanical & thermal properties of Alporas Aluminum foam are as follows represented in table 3.3 [18]:

Table 3.3: Theoretical values ranges for Alporas Aluminum Sandwich Foam

Properties	**Theoretical Values**
Material	Alporas
Relative Density	0.08 – 0.1
Structure	Closed cell
Density (mg/m3)	0.2 – 0.25
Young's Modulus (GPa), E	0.4 – 1.0
Shear Modulus (GPa), G	0.3 – 0.35

Bulk Modulus (GPa), K	0.9 – 1.2
Flexural Modulus (GPa), Ef	0.9 – 1.2
Poisson's Ratio	0.31 – 0.34
Comp. Strength (MPa)	1.3 – 1.7
Tensile Strength (MPa)	1.6 – 1.9
Hardness	2.0 – 2.2

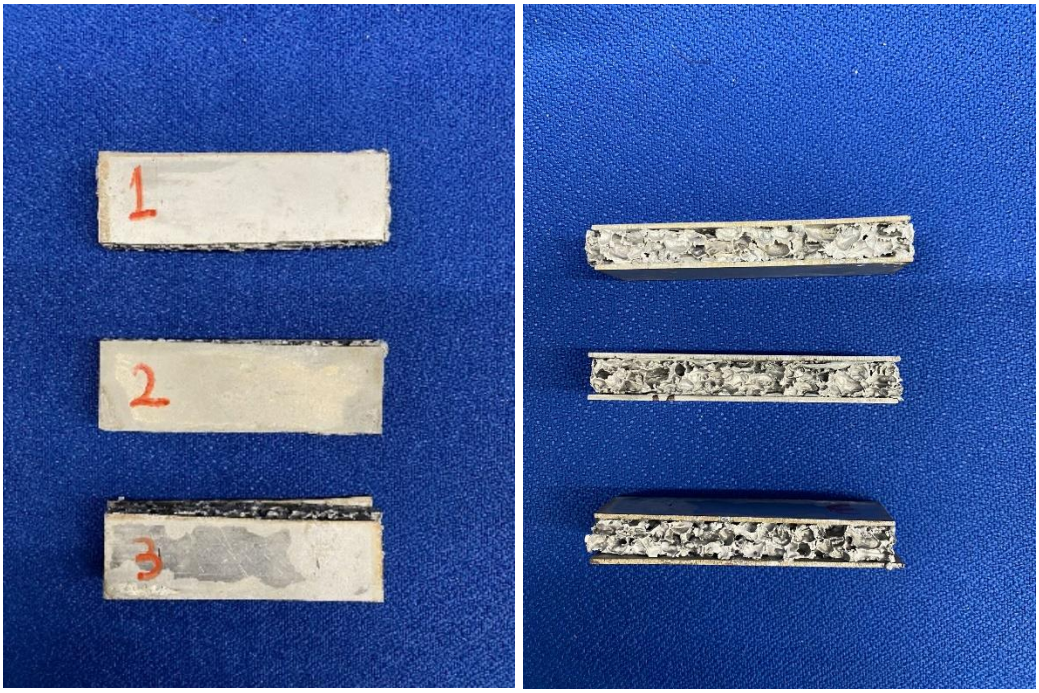

Figure 3.3: Al-Zn Sandwich (SD Al6016 Al Zn) sample

Al-2%-Zn Sandwich (SD Al6016 Al 2 Zn): The sandwich is made with two Al6016 layers and an aluminum foam core which are joined by zinc2Al alloy as brazing alloy. This variation was chosen to investigate how altering the alloy composition affects the material's mechanical properties.

Figure 3.4: Al-2%-Zn Sandwich (SD Al6016 Al 2 Zn) sample

The sample materials and their dimensions are given in the tables as follows:

Table 3.4: Sample sizes and dimensions of first material Al 6016 Plate

Sample No.	Material Composition	Shape	Dimension (L×W×T)	Mass (kg)
			mm	*kg*
1	Aluminum 6016 S1	Rectangular Bar	100.2 × 16.96 × 1.28	5.451
2	Aluminum 6016 S2	Rectangular Bar	100.34 × 19.38 × 1.25	6.132
3	Aluminum 6016 S3	Rectangular Bar	100.28 × 19.2 × 1.26	6.121

Table 3.5: Sample sizes and dimensions of second material Aluminum Foam

Sample No.	Material Composition	Shape	Dimension (L×W×T)	Mass (kg)
			mm	*kg*

1	Aluminum Foam S1	Rectangular Bar	75.4 × 25.28 × 8.8	4.834
2	Aluminum Foam S2	Rectangular Bar	80.64 × 25.66 × 8.72	5.174
3	Aluminum Foam S3	Rectangular Bar	75.44 × 24.44 × 8.86	3.323

Table 3.6: Sample sizes and dimensions of third material sandwich Al6016 Al Zn

Sample No.	Material Composition	Shape	Dimension (L×W×T)	Mass (kg)
			mm	*kg*
1	SD Al6016 Al Zn S1	Rectangular Bar	70.04 × 25.45 × 10.88	22.116
2	SD Al6016 Al Zn S2	Rectangular Bar	76.32 × 25.22 × 11.178	20.816
3	SD Al6016 Al Zn S3	Rectangular Bar	77.38 × 24.52 × 11.22	21.296

Table 3.7: Sample sizes and dimensions of third material sandwich Al6016 Al 2 Zn

Sample No.	Material Composition	Shape	Dimension (L×W×T)	Mass (kg)
			mm	*kg*
1	SD Al6016 Al 2 Zn S1	Rectangular Bar	79.2 × 24.82 × 11.14	21.805
2	SD Al6016 Al 2 Zn S2	Rectangular Bar	79.92 × 24.38 × 11.24	21.893
3	SD Al6016 Al 2 Zn S3	Rectangular Bar	79.2 × 24.78 × 11.48	20.506

3.3. RESONANT FREQUENCY AND DAMPING ANALYZER (RFDA)

The Resonant Frequency and Damping Analyzer (RFDA) is an advanced and specialized instrument used in materials science and engineering to conduct in-depth studies of materials' mechanical properties. It employs an Impulse Excitation Technique, which is a non-destructive method for characterizing the dynamic response of materials to vibrations, providing valuable insights into their structural and mechanical behavior.

3.3.1. RESONANT FREQUENCY ANALYSIS

RFDA is primarily utilized to determine the resonant frequencies of materials. Resonant frequency is a fundamental property that defines how materials respond to mechanical vibrations. It is akin to the natural frequency at which a material oscillates most efficiently when subjected to external forces. In practical terms, it's the frequency at which materials "sing" or vibrate most vigorously. By accurately identifying these resonant frequencies, RFDA reveals essential information about a material's structural integrity and its potential applications.

3.3.2. DAMPING ANALYSIS

In addition to resonant frequency analysis, RFDA is instrumental in assessing a material's damping characteristics. Damping measures the ability of a material to absorb and dissipate vibrational energy. It is a crucial parameter because it impacts the material's performance under dynamic loading conditions. Materials with low damping might be more brittle and susceptible to fractures, while those with high damping tend to be more robust and energy-absorbing. The RFDA precisely quantifies the damping ratio, helping researchers evaluate the long-term durability and fatigue resistance of materials.

3.3.3. RFDA INSTRUMENT OPERATION

The RFDA operates by applying a controlled mechanical impulse to the material under investigation. The impulse can be in flexural mode and torsional mode. The RFDA is also capable of applying both modes simultaneously to study the reaction of material under combined modes of impulse. This impulse initiates vibrations in the material, and the RFDA sensors capture the resulting response. This response is then analyzed to determine the material's natural frequencies and damping characteristics. The sensors are highly sensitive, enabling precise measurements even for subtle vibrations. The figure below shows the IMCE RFDA-HT1600 model (in J-TECH @POLITO interdepartmental laboratory) being utilized for experimentation purpose.

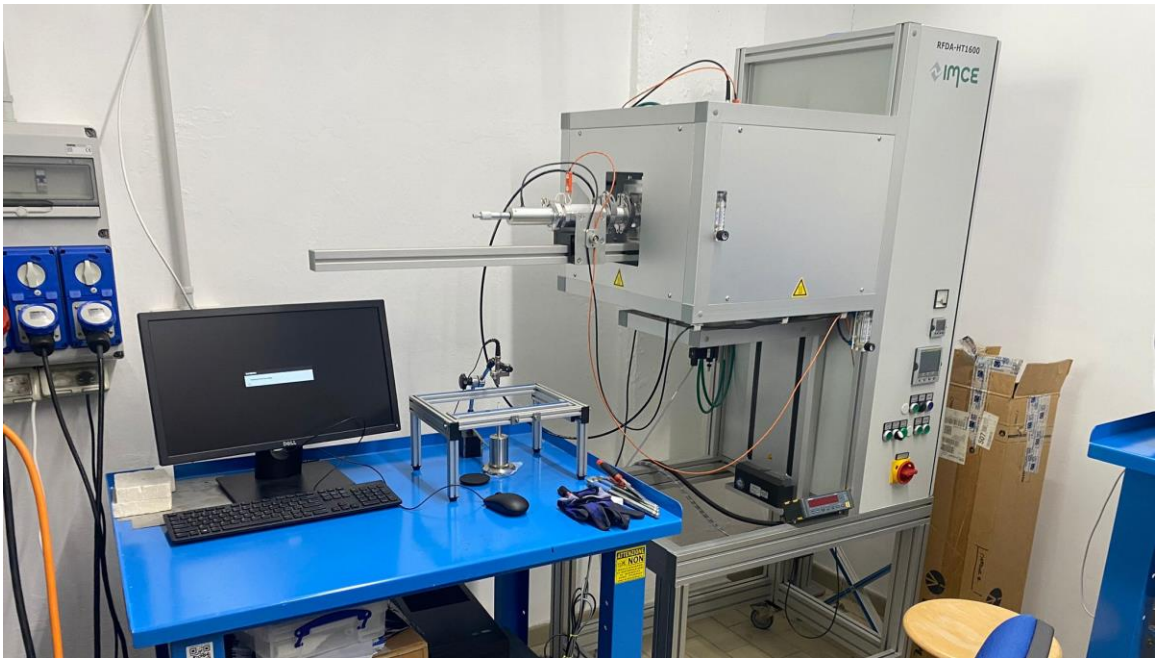

Figure 3.5: IMCE RFDA-HT1600 model

3.3.4. APPLICATIONS

Researchers and engineers use RFDA in various fields, such as aerospace, civil engineering, automotive manufacturing, and materials development. It aids in quality control, structural health monitoring, and design optimization. For instance, in aircraft

design, RFDA assists in selecting materials with specific resonant properties to ensure structural stability and passenger safety.

3.4. EXPERIMENT 1 – RFDA EXPERIMENTAL SETUP

The experiment was performed on Resonant Frequency and Damping Analyzer (RFDA). The experiment started by preparing test samples of each of the four materials mentioned in the previous section: Aluminum 6016 Plate, Aluminum Foam, Al-Zn Sandwich (SD Al6016 Al Zn), and Al-2%-Zn Sandwich (SD Al6016 Al 2 Zn). It was ensured that these samples are of appropriate size and shape for testing. Pretest measurements were performed to feed sample date in the data logger. This included measurements of the sample's dimensions and weight, the dimension was measured using the digital Vernier calipers and the mass of each test sample was measured on a digital scale by Sartorius.

Once baseline measurements were obtained and recorded, the test samples were securely mounted to the RFDA equipment. The samples were left free on the test bench to vibrate. Sensors were affixed to the test samples. The type of sensor used varied depending on the material and the specific information we wanted to collect. Common sensors included accelerometers and strain gauges. It was ensured that the sensors are properly calibrated. The figure below shows the mounting of a sample of RFDA platform.

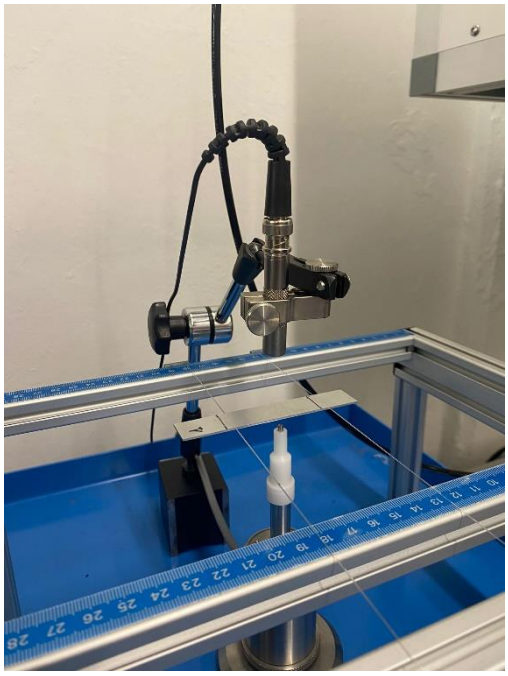

Figure 3.6: Mounted sample on RFDA with sensor in position

The shaker system was calibrated to ensure it generated controlled and repeatable mechanical vibrations. Calibration involved checking the shaker's amplitude, frequency range, and ensuring that it operated within specified tolerance. A controlled testing environment was maintained, including temperature and humidity, to minimize external factors that could affect the results.

The RFDA equipment was set up for the specific test configuration. This included selecting the vibration parameters such as frequency range, amplitude, and waveform. The RFDA MF v10.0.0 software version was utilized to perform the experiment. The sample frequency was set at 200000 Hz with a time interval set for 10 minutes. The respective material file was selected to set the default parameters available in the software. There are two modes in which the sample was tested, flexural and torsional. When the sample is subjected to flexion (out of plane flexure), it measured the Young’s Modulus of the sample, based on the response of the sample, material and

geometrical properties. The flexural resonant frequency obtained can then be used to calculate the elastic modulus. Similarly, when the sample is subjected to torsion, it measured the Shear Modulus of the sample, based on the response of the sample, material and geometrical properties. It is worth mentioning, that the noticeable property of the material that determines the result is the density which was calculated by measuring all dimensions and determining volume and the mass of the sample. The torsional resonant frequency obtained can then be used to calculate the damping modulus.

To perform the experiment and obtain the flexural resonant frequency in flexion and torsional resonant frequency in torsional mode, the RFDA was started to test the sample by gradually increasing the vibration frequency within the predetermined range. The experimental tests were started at a low frequency and swept through a range of frequencies to identify resonant frequencies. The data was collected from the sensors during the vibration tests and was stored in rdf file format. The experiments were repeated for each sample in flexural and torsional mode to perform the analysis and compare experimental and theoretical values.

3.5. EXPERIMENT 2 – TENSILE TESTING EXPERIMENTAL SETUP

The procedure for tensile testing experiment is conducted in the following steps:

1. Tensile Testing Preparation: Before proceeding with the tensile tests, each specimen was rigorously inspected for any visible defects or irregularities. The test setup was carefully calibrated. The testing apparatus used for these experiments was the MTS Tensile Tester LPS.504 with a capacity of 50 kN, a reliable and widely accepted

device for conducting tensile tests. The machine was adjusted to ensure that the tensile force would be applied accurately to the samples. The figure below shows the MTS tensile tester:

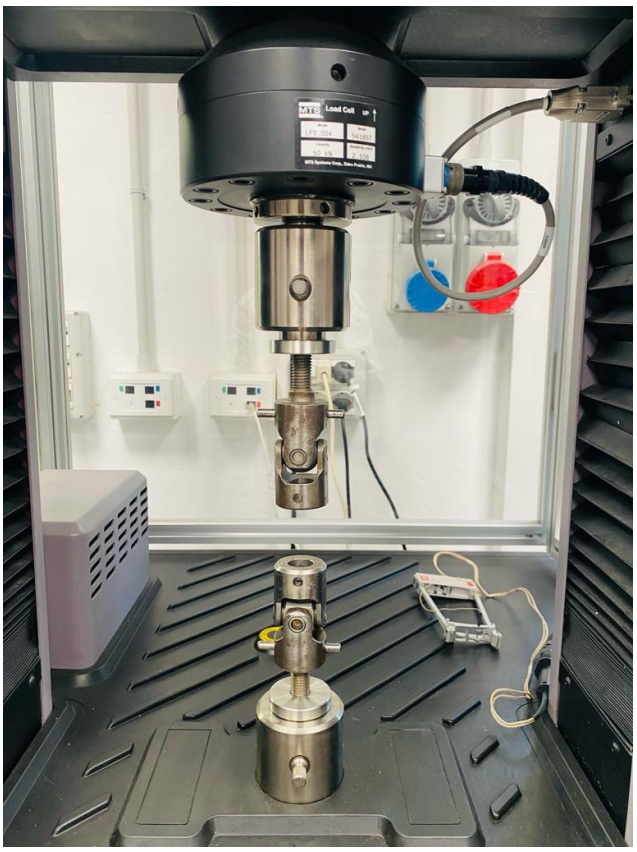

Figure 3.7: MTS Tensile Tester, model LPS.504 with a capacity of 50 kN

2. Sample Preparation and Cutting: The samples of aluminum foam, aluminum foam sandwich SD Al6016 Al Zn and aluminum foam sandwich SD Al6016 Al 2 Zn were prepared and cut to size using QATM auto cut off machine which utilized black alumina blade to cut the metal samples. The QATM auto cut off machine is shown in figure below:

Figure 3.8: QATM auto cut off machine for sizing and cutting metal samples

The samples were placed on the holder of the machine and the blade was tightened. It was made sure that sample was safely secured. Cooling oil was sprinkled during the process of cutting to avoid overheating of the alumina blade and damaging during operation. The figure below shows the cut off samples of aluminum foam sandwich.

Figure 3.9: Cut off sample of aluminum foam sandwich from QATM auto cutoff machine

3. Mounting the Specimen: The adhesive used for attaching the testing piece to the holder was 3M™ Scotch-Weld™ DP-490 Black Structural Adhesive Kit. This adhesive is known for its high strength and durability, ensuring that the samples were securely fastened to the testing apparatus. The testing piece was aligned within the machine's grips, ensuring that the load would be evenly distributed.
4. Sample Alignment and Heat Treatment: To ensure precise alignment and consistency in the direction of the tensile force, a custom-designed fixture was used. This fixture featured holes that allowed for accurate positioning of the samples. Prior to testing, a heat treatment process was conducted to cure the adhesives. The samples were placed in a controlled environment within a furnace, held at a temperature of 80 degrees Celsius for a duration of one hour.
5. Strain Measurement: Strain gauges or extensometers were carefully attached to the specimens to measure strain during the test. These devices provided real-time data on how the specimen deformed under the applied load.
6. Test Execution: The tensile test was carried out by applying a controlled axial load to the specimen at a constant rate. The MTS Tensile Tester gradually increased the force applied to the sample until it reached the point of failure or rupture. During this process, various parameters, such as the load, deformation, and time, were continuously recorded by the testing machine. This allowed for the generation of stress-strain curves that depicted the material's behavior under load.

Figure 3.10: MTS tensile tester with Aluminum foam sample mounted in the holder with adhesive bonding

Figure 3.11: MTS tensile tester with Aluminum sandwich foam sample mounted in the holder with adhesive bonding

7. Data Collection: As the test progressed, the MTS Tensile Tester continuously collected data, including the load in newtons (N), the stress in megapascals (MPa),

and the deformation in percentage. These measurements provided valuable insights into the material's mechanical properties and its response to applied stress.

8. Test Termination: Each test was terminated on the rupture of the specimen. Another reason that resulted in termination of load was due to error occurred in MTS tensile tester due to removal of sample from the machine. The figure below shows the ruptured sample of the aluminum sandwich foam.

Figure 3.12: Ruptured sample of aluminum sandwich foam SD Al6016 Al Zn

9. Post-Test Analysis: Once the specimen failed, the test was concluded. The recorded data were analyzed to determine critical mechanical properties, such as ultimate tensile strength (UTS), yield strength, modulus of elasticity, and elongation at rupture. This analysis was crucial for understanding the material's performance under tensile stress.
10. Adhesive Residue Removal: After the tensile tests were completed, the specimens were subjected to a post-test process for the removal of adhesive residue. To

accomplish this, the samples were exposed to a higher temperature, specifically 400 degrees Celsius, which effectively eliminated any remaining adhesive remnants. The holders were washed in ethanol in an ultrasonic bath after glue removal by the thermal treatment.

3.6. ELECTRON MICROSCOPY

The electron microscopy images permit for a detailed observation of the microtopography of the materials tested. SEM observations were conducted to investigate the fractured surfaces of the samples and study the type. The imaging was performed on a JEOL JCM-6000Plus electron microscope as shown in figure 3.13.

Figure 3.13: JEOL JCM-6000Plus electron microscope

The electron microscope employed for the analysis featured versatile magnification capabilities, ranging from ×10 to ×60,000 for secondary electron images and ×10 to ×30,000 for backscattered electron images, particularly when the image size

was set at 128 mm × 96 mm. The specimen stage allowed manual control for X and Y movements with dimensions of X: 35 mm and Y: 35 mm, accommodating a maximum sample size of 70 mm in diameter and 50 mm in height. Specimen exchange was facilitated through a draw-out mechanism. The microscope was equipped with an image memory capable of storing images at a resolution of 1,280 × 960 × 16 bits, and it supported various image processing functions, including pixel accumulation and recursible image accumulation. The system featured automated functions for full-auto operation, filament adjustment, alignment, focus, stigmator, and exposure. Metrology capabilities included measuring the distance between two points and angles. File formats for image storage included BMP, TIFF, and JPEG.

4. CHAPTER 4 – RESULTS

In this section, the outcomes of the experimentation are presented using the Resonant Frequency and Damping Analyzer (RFDA) on four distinct materials as mentioned in the previous section: Aluminum 6016 Plate, Aluminum Foam, Al-Zn Sandwich (SD Al6016 Al Zn), and Al-2%-Zn Sandwich (SD Al6016 Al 2 Zn). The objective is to provide a detailed account of the findings obtained from the analysis of these materials.

The section commences with a thorough examination of the resonant frequencies exhibited by each material. Resonant frequencies are indicative of the natural vibrational tendencies of materials and can reveal vital insights into their structural properties and potential applications. Following the resonant frequency analysis, we delve into the damping characteristics of the materials. Damping is a crucial parameter that determines a material's ability to dissipate vibrational energy. Understanding the damping properties is essential for assessing the materials' fatigue resistance and structural integrity.

As the results section progresses, it will provide a detailed breakdown of the findings from each material, offering a comprehensive understanding of their resonant properties and damping dynamics. These results serve as a valuable resource for professionals and researchers in the realm of materials science and engineering.

4.1. SAMPLE DATA COLLECTION

The data is being collected in the form of rdf file. The data obtained is being shown in following tables 4.1 & 4.2. The data for flexural and torsional mode is being separated.

Table 4.1: Flexural resonant frequency data for Al6016 S1 sample

Measure no.	Shape	E-modulus	Error E-mod	G-modulus	Error G-mod	Poisson	f flexural	loss rate flex	damp flex
2	Rectangular Bar	55.73	1.46	0	0	0.33	617.624	1.4	0.000744
3	Rectangular Bar	55.73	1.46	0	0	0.33	617.637	1.5	0.000758
4	Rectangular Bar	55.74	1.46	0	0	0.33	617.649	1.5	0.000759
5	Rectangular Bar	55.74	1.46	0	0	0.33	617.682	1.5	0.000759
6	Rectangular Bar	55.74	1.46	0	0	0.33	617.686	1.4	0.00075
7	Rectangular Bar	55.75	1.46	0	0	0.33	617.708	1.4	0.000737
8	Rectangular Bar	55.75	1.46	0	0	0.33	617.715	1.5	0.000758
9	Rectangular Bar	55.75	1.46	0	0	0.33	617.714	1.6	0.000799
10	Rectangular Bar	55.75	1.46	0	0	0.33	617.722	1.5	0.000752
11	Rectangular Bar	55.75	1.46	0	0	0.33	617.745	1.4	0.000728
13	Rectangular Bar	55.75	1.46	0	0	0.33	617.753	1.5	0.000785
14	Rectangular Bar	55.76	1.46	0	0	0.33	617.781	1.4	0.000711
15	Rectangular Bar	55.76	1.46	0	0	0.33	617.775	1.4	0.000742
16	Rectangular Bar	55.76	1.46	0	0	0.33	617.783	1.5	0.000754
17	Rectangular Bar	55.76	1.46	0	0	0.33	617.779	1.4	0.000729
18	Rectangular Bar	55.76	1.46	0	0	0.33	617.788	1.5	0.000763
20	Rectangular Bar	55.76	1.46	0	0	0.33	617.807	1.4	0.000748
42	Rectangular Bar	55.7	1.46	0	0	0.275	617.427	1.6	0.00085

The data shown in table 4.1 is obtained for flexural resonant frequency for Al6016 S1 sample. The data is being cleaned and the NaN applicable values are being omitted for accuracy of results. It can be observed that data set is calculating the Young's Modulus based on the geometrical and material information provided at the time of conducting experiments. Alternatively, flexural loss can be utilized to calculated the flexural resonant frequency and ultimately leading to Young's Modulus. Similarly, the table 4.2 shows the sample data collected for the torsional resonant frequency for Al6016 S1 sample.

Table 4.2: Torsional resonant frequency data for Al6016 S1 sample

Measure no.	Shape	G-Modulus	Error G - Mod	Poisson	f torsion	loss rate tors	damp tors	order tors
41	Rectangular Bar	51.94	0.54	0.275	3359.59	5.8	0.000554	2
43	Rectangular Bar	1.75	0.02	0.275	617.434	1.6	0.000845	3
44	Rectangular Bar	1.75	0.02	0.275	617.438	1.7	0.000872	3
45	Rectangular Bar	1.75	0.02	0.275	617.445	1.7	0.000888	3
46	Rectangular Bar	1.75	0.02	0.275	617.431	1.6	0.000824	2
47	Rectangular Bar	1.75	0.02	0.275	617.435	1.6	0.000834	2
48	Rectangular Bar	1.75	0.02	0.275	617.431	1.6	0.000808	2
49	Rectangular Bar	1.75	0.02	0.275	617.43	1.7	0.000859	3
50	Rectangular Bar	1.75	0.02	0.275	617.423	1.6	0.000817	2
51	Rectangular Bar	1.75	0.02	0.275	617.427	1.7	0.000857	2
52	Rectangular Bar	1.75	0.02	0.275	617.434	1.4	0.000743	2
53	Rectangular Bar	1.75	0.02	0.275	617.428	1.6	0.00081	2
54	Rectangular Bar	1.75	0.02	0.275	617.43	1.7	0.000886	2
55	Rectangular Bar	1.75	0.02	0.275	617.416	1.6	0.000813	2
56	Rectangular Bar	1.75	0.02	0.275	617.409	1.7	0.00086	2
57	Rectangular Bar	1.75	0.02	0.275	617.41	1.6	0.000827	2
58	Rectangular Bar	1.75	0.02	0.275	617.409	1.6	0.000833	2
59	Rectangular Bar	1.75	0.02	0.275	617.419	1.6	0.000815	2

The remaining data for the samples has been compiled in Annexure A. In addition, the figure represents the frequency, loss rate and damping of the Al6016 S1 sample is flexural and torsional measurement modes. It can be observed form the amplitude-time and amplitude-frequency spectrum that impulse excitation technique is clearly indicative, with no signal filters, showing damping in amplitude with the passage of time interval. It can also be observed that Youngs Modulus is reported as 55.75 GPa while the shear modulus is calculated as 1.75 GPa.

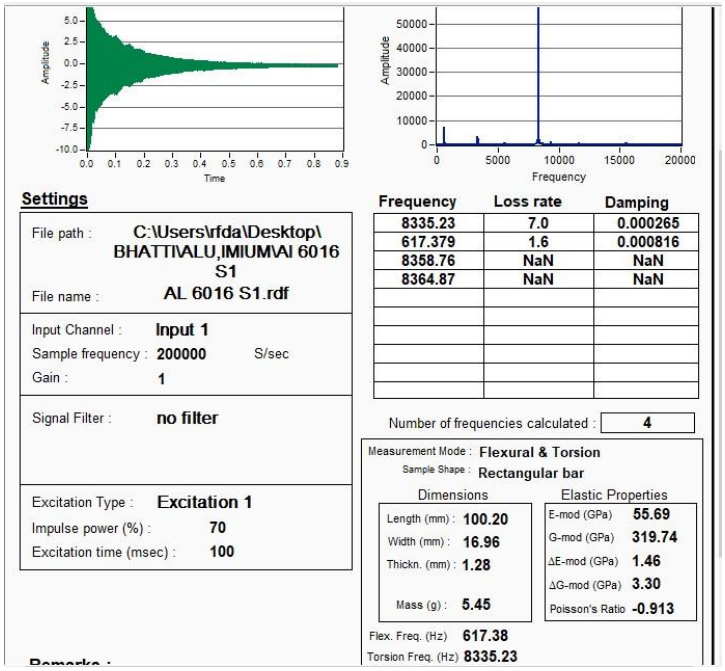

Figure 4.1: Resonant frequency, loss rate & damping in Torsional & Flexural measurement mode for Al6016 S1 sample.

4.2. RESULTS FOR ALUMINUM 6016 PLATE

The results for Aluminum 6016 plate are being obtained for Youngs Modulus, internal friction coefficient in flexion, shear modulus and internal friction coefficient in torsion. These plots are segregated for each of the three samples S1, S2 and S3. The combined plots are then prepared for elastic and shear moduli of the Aluminum 6016 plate and internal friction coefficient in flexion and torsion by averaging the values obtained for each run of the data.

4.2.1. RESULTS FOR AL 6016 S1

The figures below represent the elastic and shear modulus and internal coefficient of friction in flexion and torsion for Al 6016 S1.

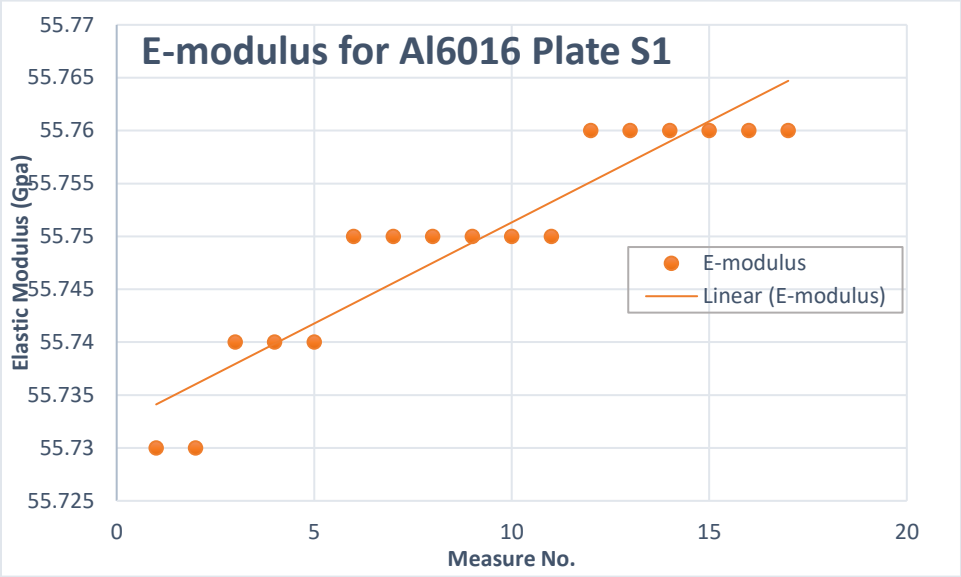

Figure 4.2: Youngs Modulus for Al6016 S1 Plate

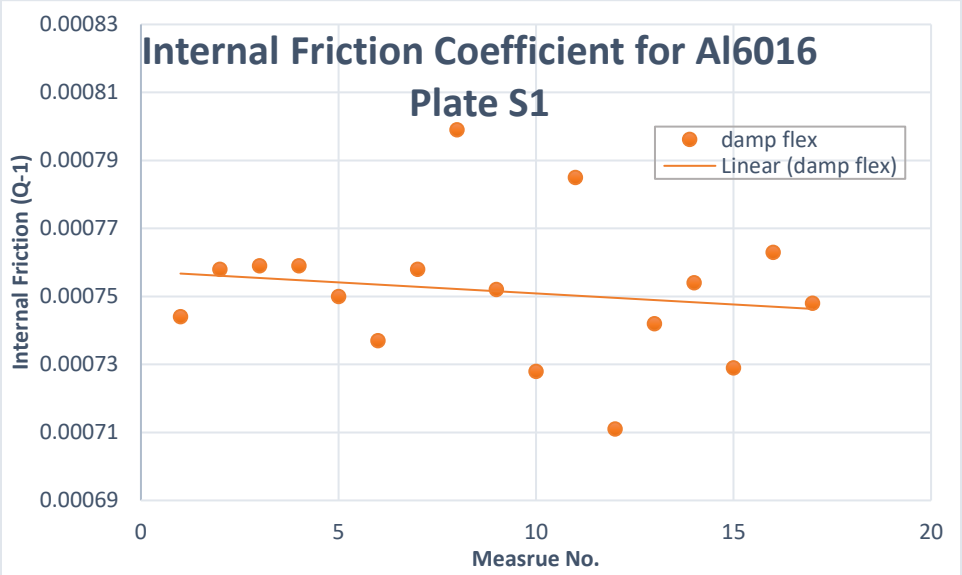

Figure 4.3: Internal Friction Coefficient in flexion for Al6016 S1 Plate

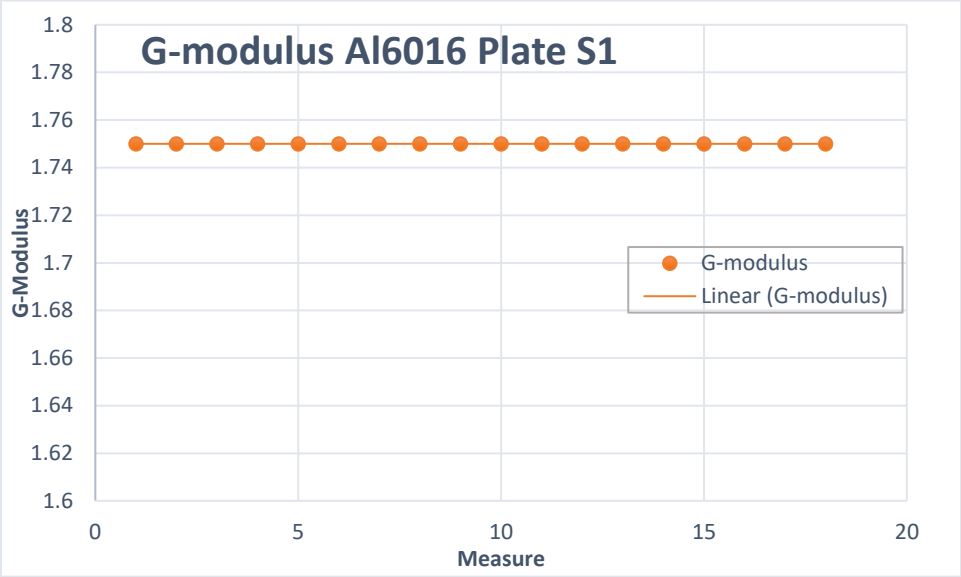

Figure 4.4: Shear Modulus for Al6016 S1 Plate

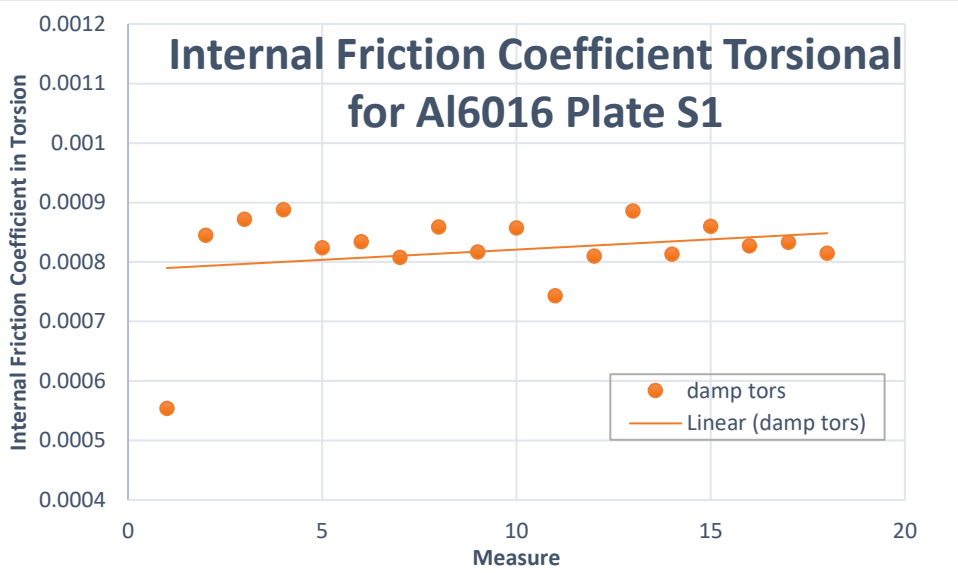

Figure 4.5: Internal Friction Coefficient in torsion for Al6016 S1 Plate

4.2.2. RESULTS FOR AL 6016 S2

The figures below represent the elastic and shear modulus and internal coefficient of friction in flexion and torsion for Al 6016 S2.

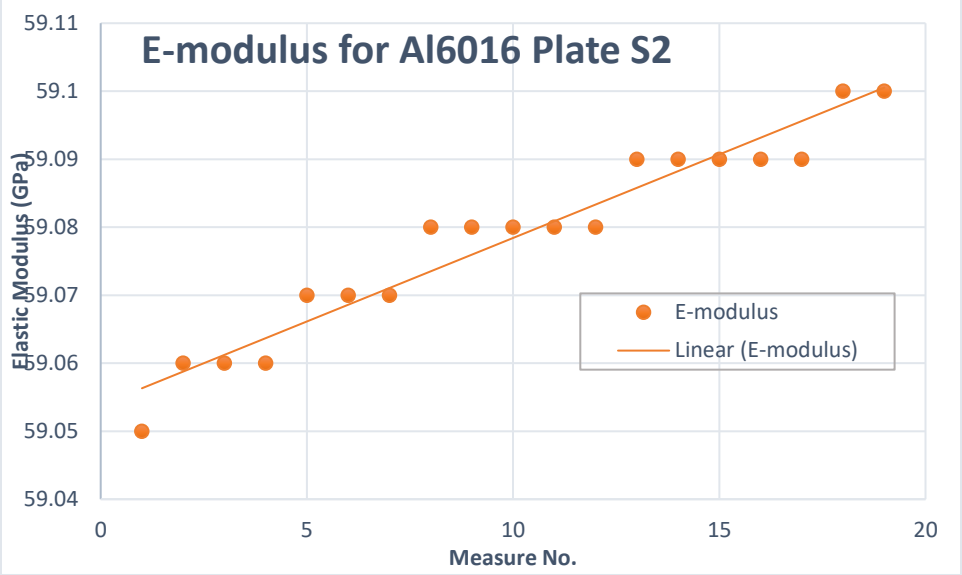

Figure 4.6: Youngs Modulus for Al6016 S2 Plate

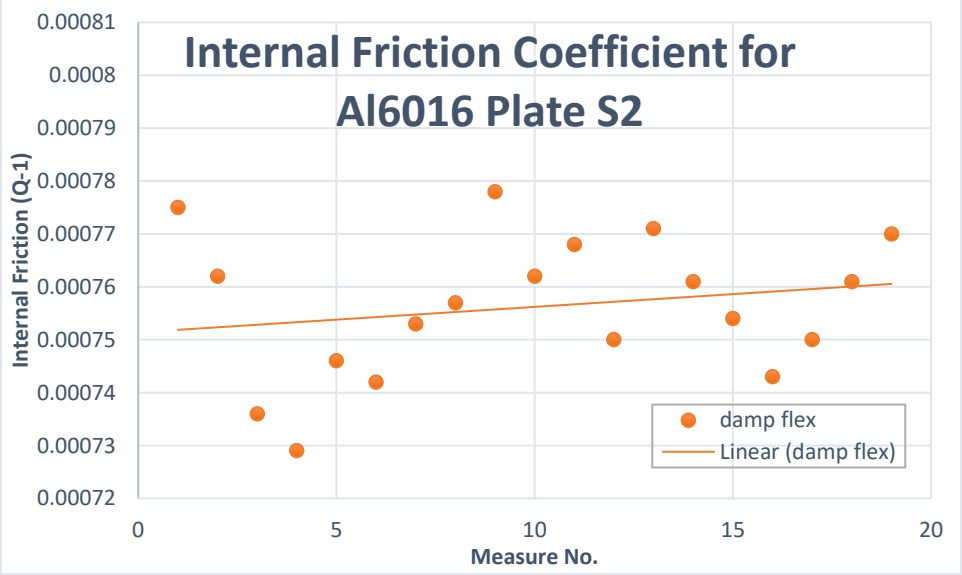

Figure 4.7: Internal Friction Coefficient in flexion for Al6016 S2 Plate

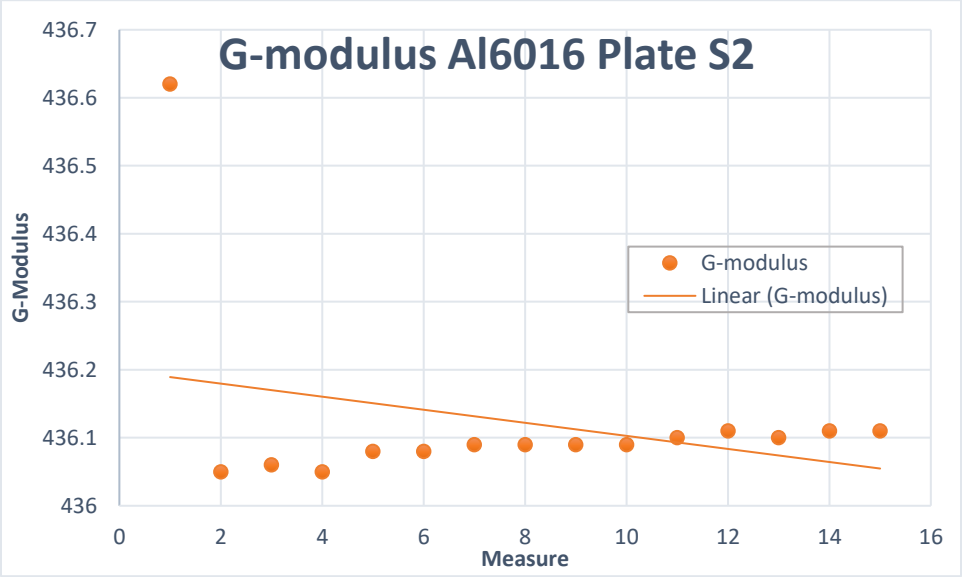

Figure 4.8: Shear Modulus for Al6016 S2 Plate

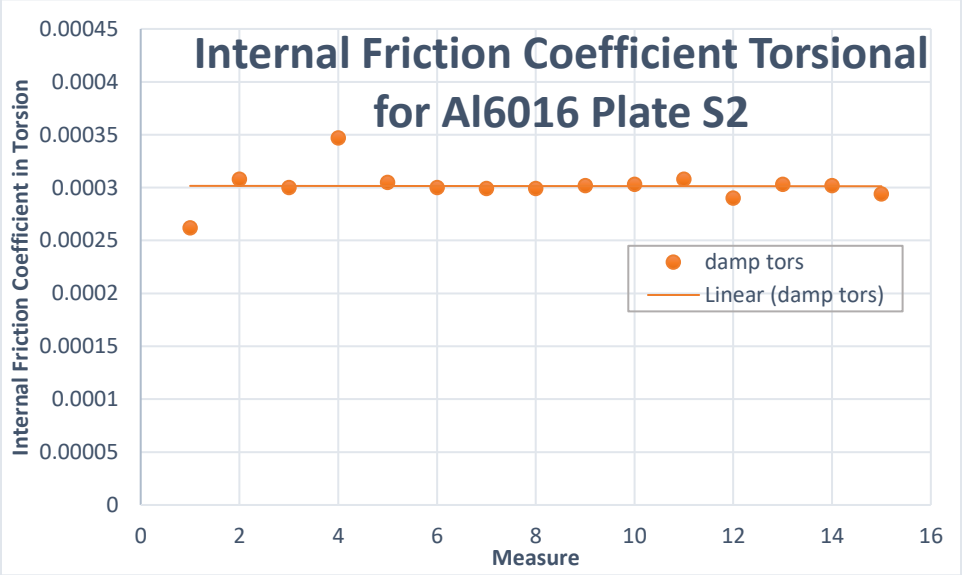

Figure 4.9: Internal Friction Coefficient in torsion for Al6016 S2 Plate

4.2.3. RESULTS FOR AL 6016 S3

The figures below represent the elastic and shear modulus and internal coefficient of friction in flexion and torsion for Al 6016 S3.

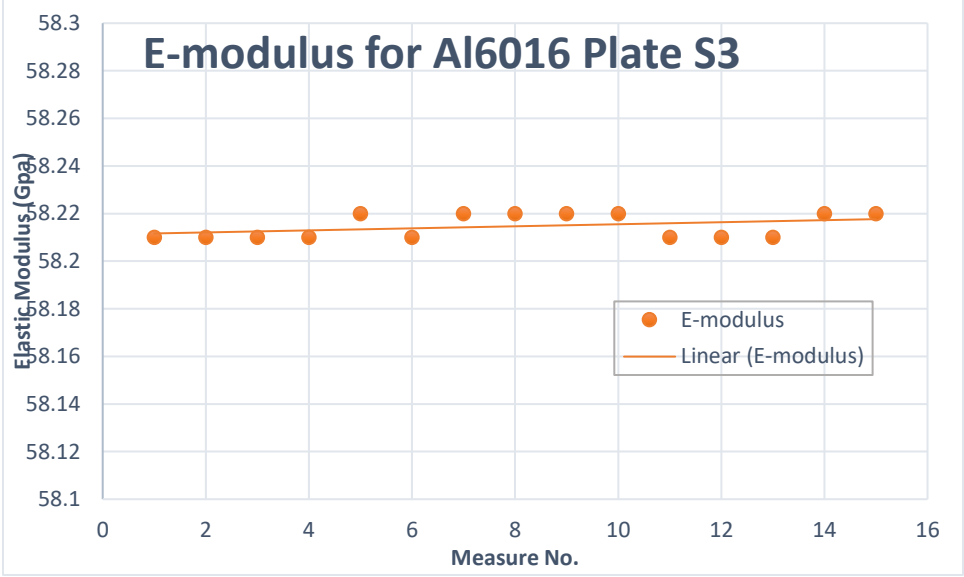

Figure 4.10: Youngs Modulus for Al6016 S3 Plate

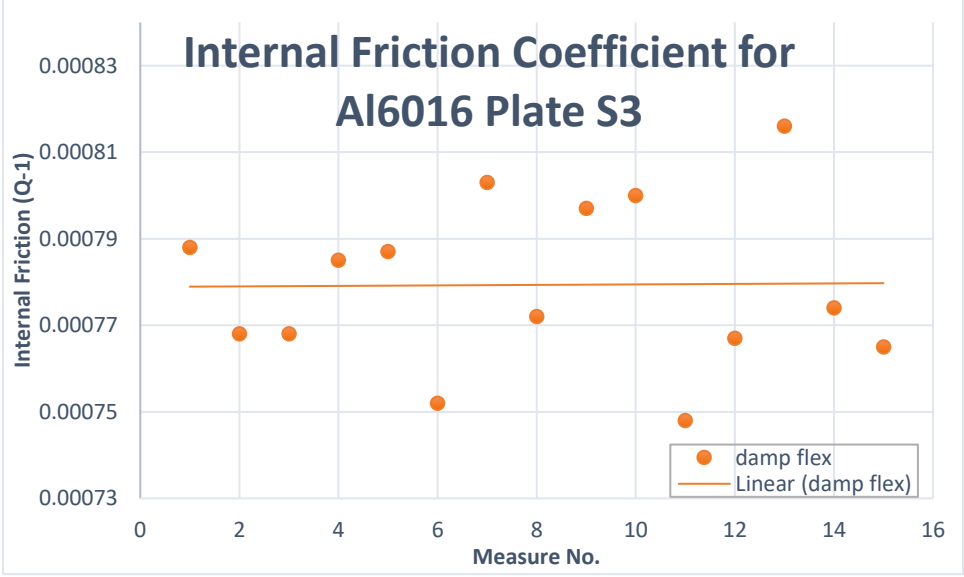

Figure 4.11: Internal Friction Coefficient in flexion for Al6016 S3 Plate

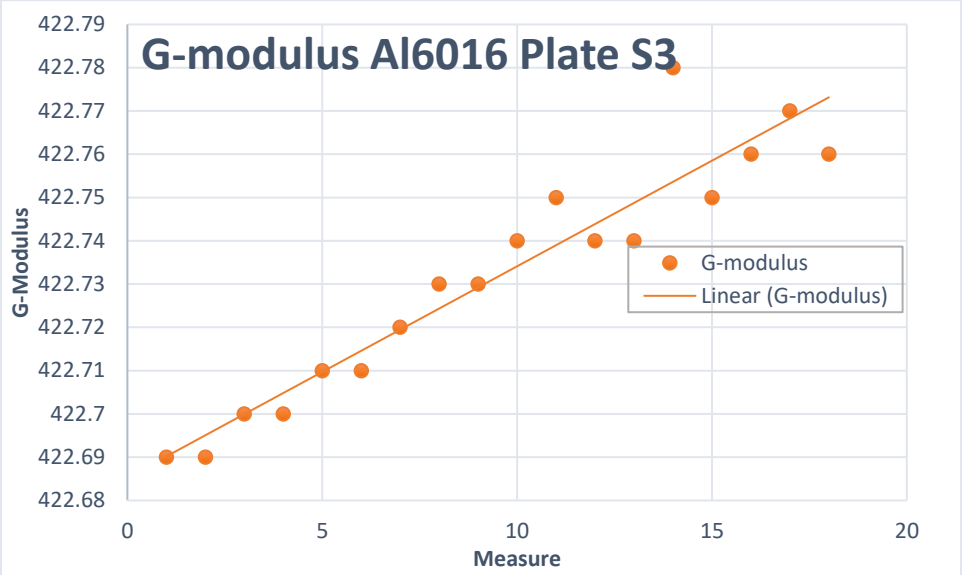

Figure 4.12: Shear Modulus for Al6016 S3 Plate

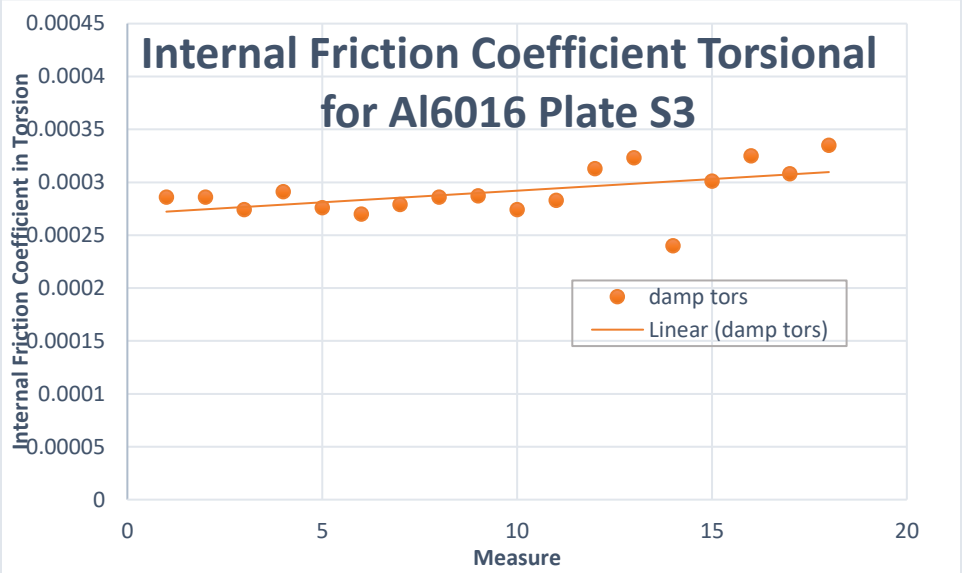

Figure 4.13: Internal Friction Coefficient in torsion for Al6016 S2 Plate

4.2.4. RESULTS FOR AL 6016 COMBINED

The figures below represent the mean elastic and shear moduli and internal friction coefficient in flexion and torsion combined for Al6016 plate.

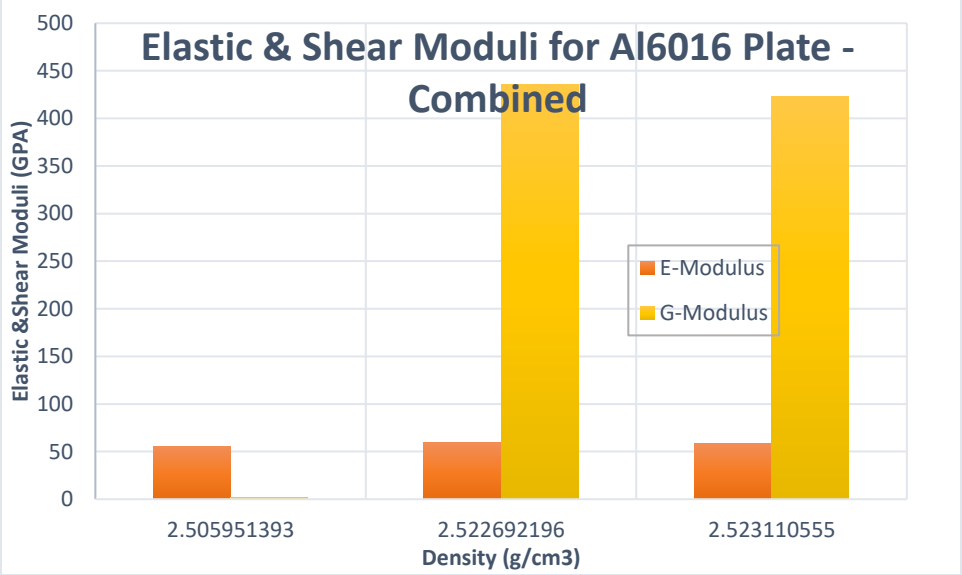

Figure 4.14: Mean Young and Shear Moduli for Al6016 Plate - Combined

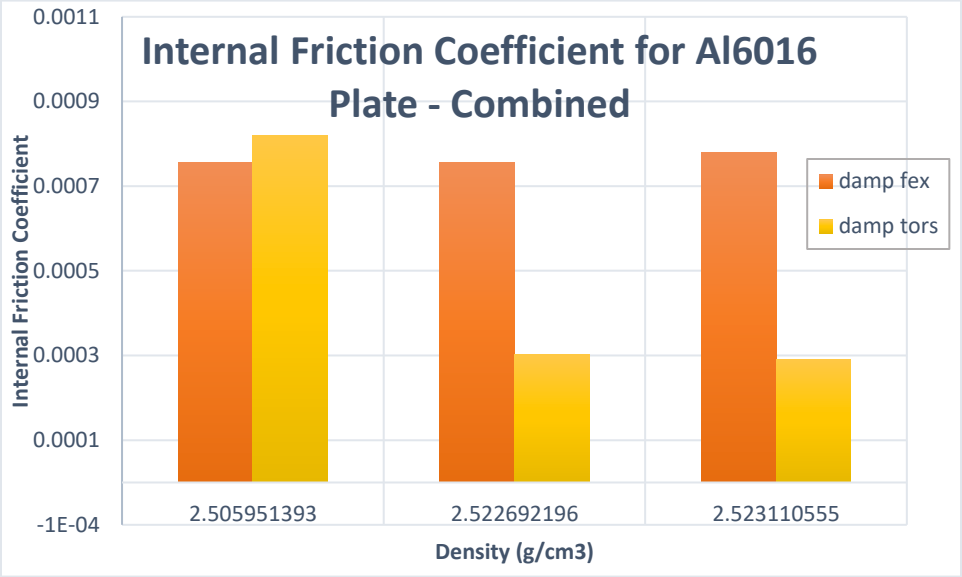

Figure 4.15: Mean Internal Friction Coefficient in flexion and torsion for Al6016 Plate - Combined

4.3. RESULTS FOR ALUMINUM FOAM

The results for Aluminum foam are being obtained for Youngs Modulus, internal friction coefficient in flexion, shear modulus and internal friction coefficient in torsion. These plots are segregated for each of the three samples S1, S2 and S3. The combined plots are then prepared for elastic and shear moduli of the Aluminum 6016 plate and internal friction coefficient in flexion and torsion by averaging the values obtained for each run of the data.

4.3.1. RESULTS FOR AL FOAM S1

The figures below represent the elastic and shear modulus and internal coefficient of friction in flexion and torsion for Al foam S1.

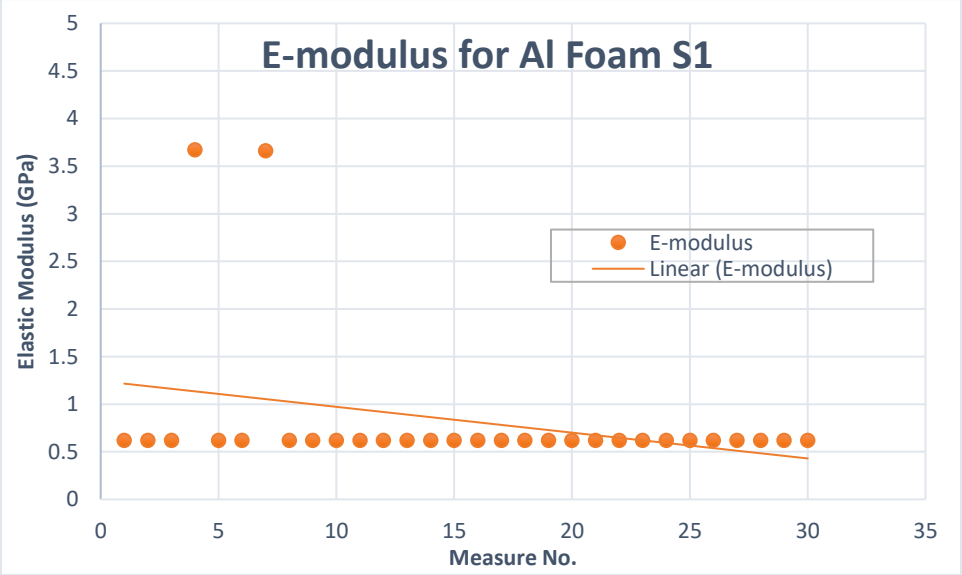

Figure 4.16: Youngs Modulus for Al Foam S1

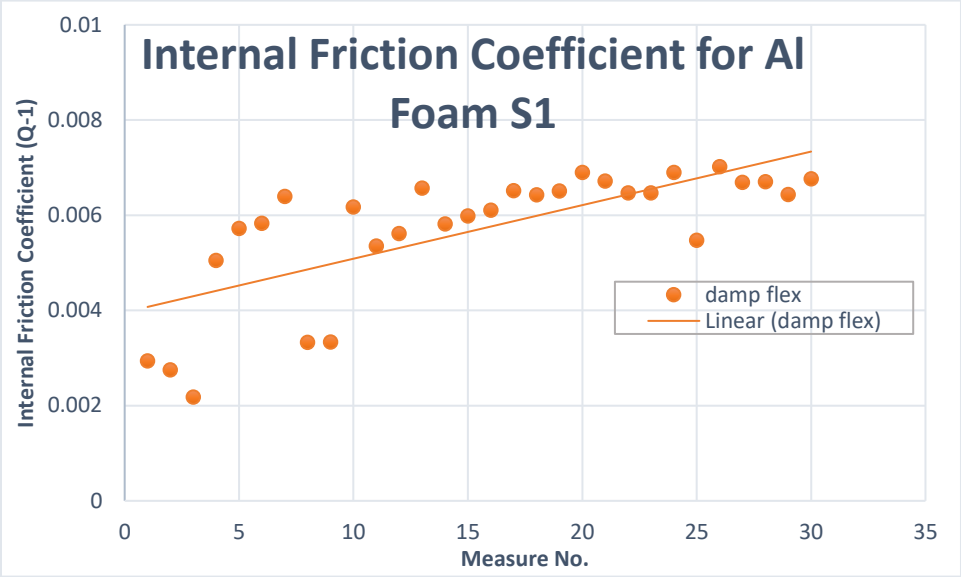

Figure 4.17: Internal Friction Coefficient in flexion for Al Foam S1

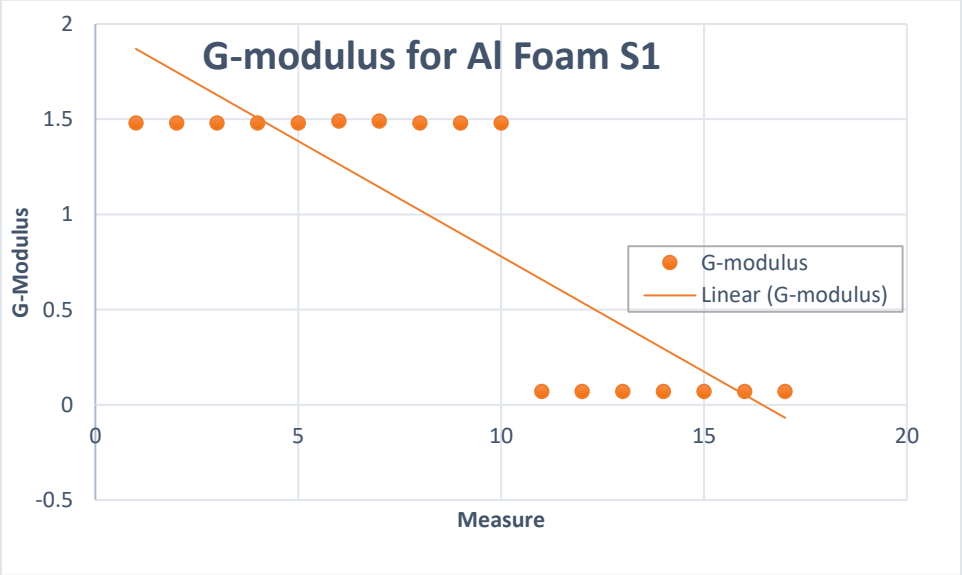

Figure 4.18: Shear Modulus for Al Foam S1

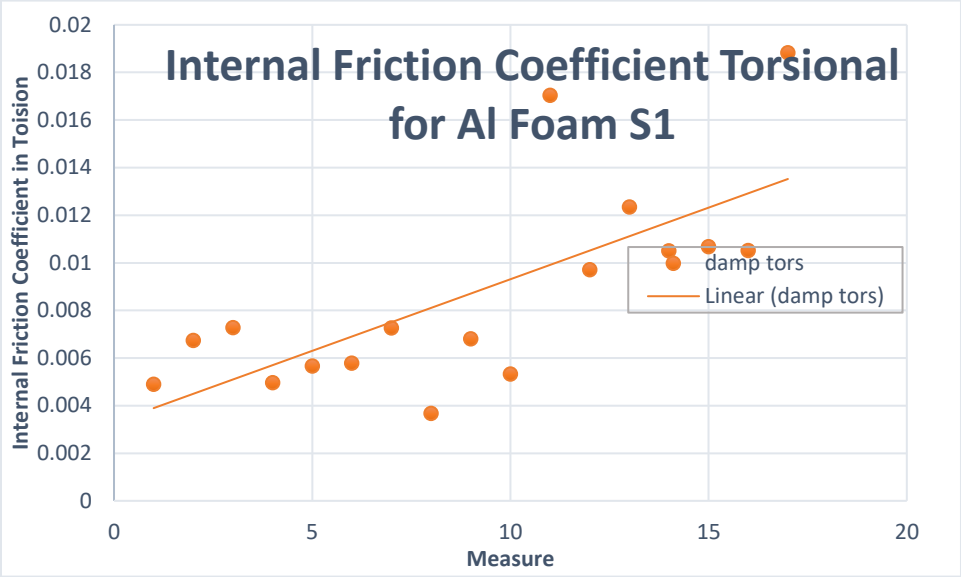

Figure 4.19: Internal Friction Coefficient in torsion for Al Foam S1

4.3.2. RESULTS FOR AL FOAM S2

The figures below represent the elastic and shear modulus and internal coefficient of friction in flexion and torsion for Al foam S2.

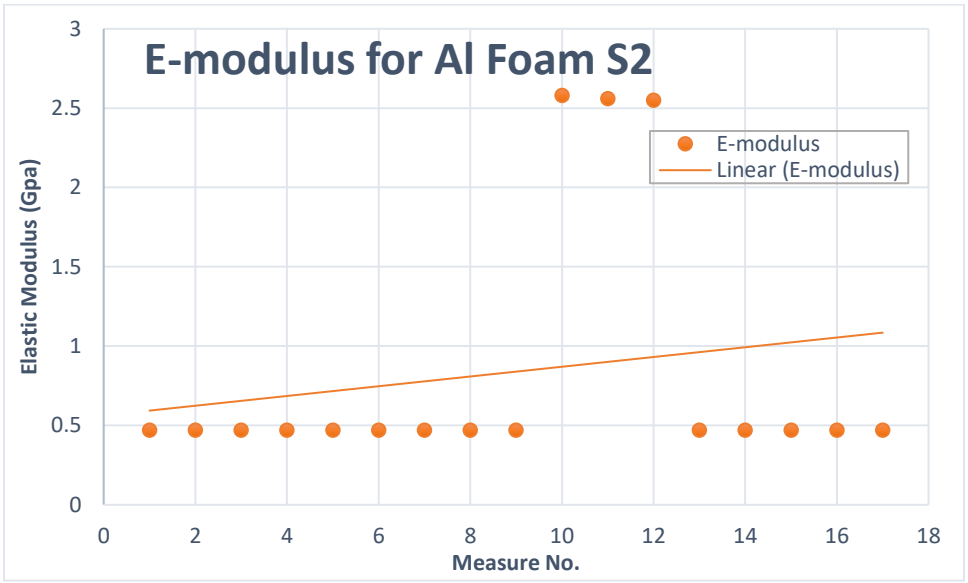

Figure 4.20: Youngs Modulus for Al Foam S2

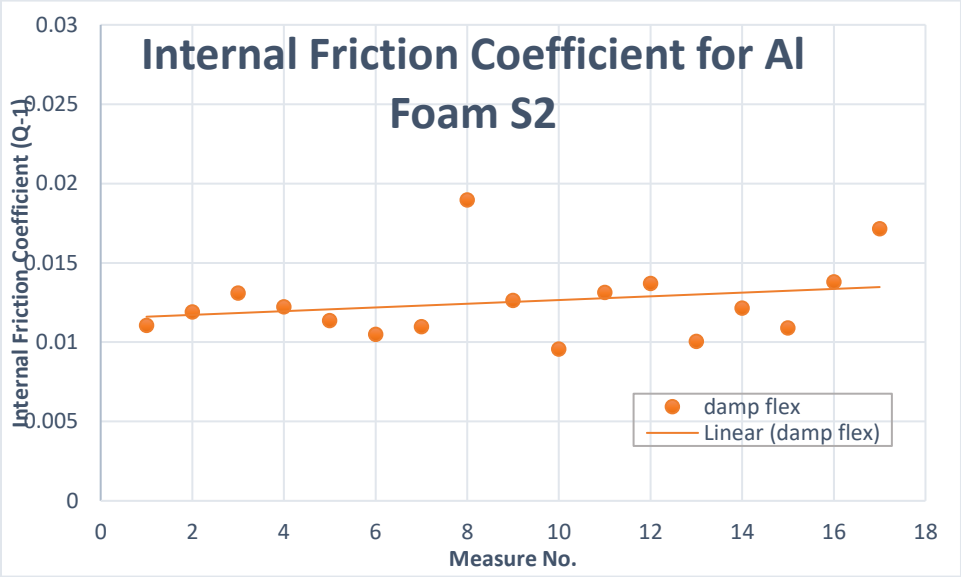

Figure 4.21: Internal Friction Coefficient in flexion for Al Foam S2

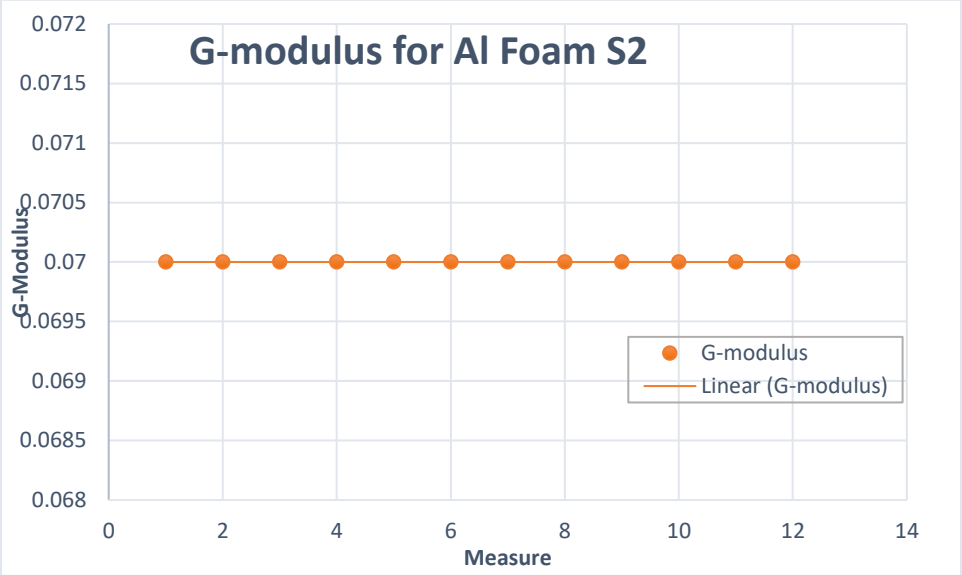

Figure 4.22: Shear Modulus for Al Foam S2

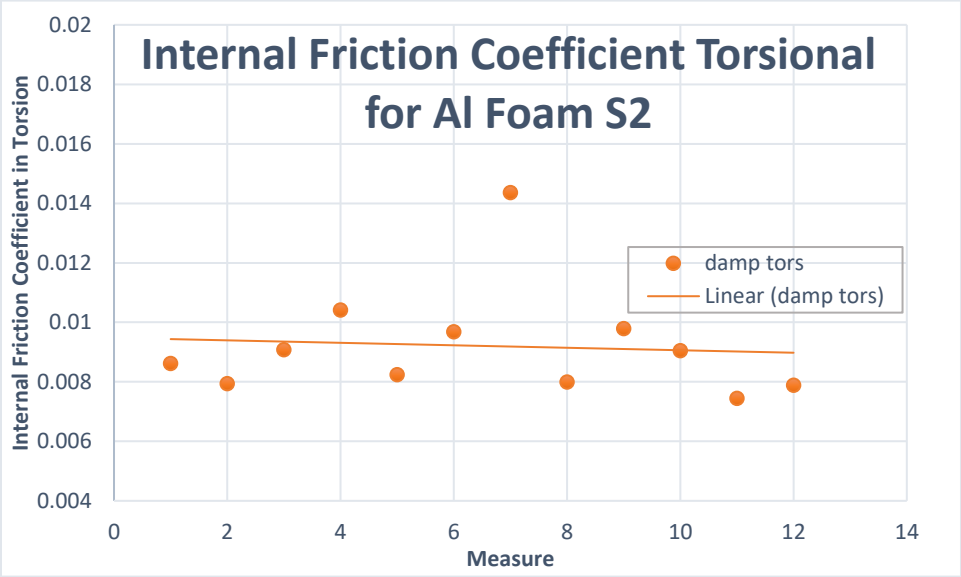

Figure 4.23: Internal Friction Coefficient in torsion for Al Foam S2

4.3.3. RESULTS FOR AL FOAM S3

The figures below represent the elastic and shear modulus and internal coefficient of friction in flexion and torsion for Al foam S3.

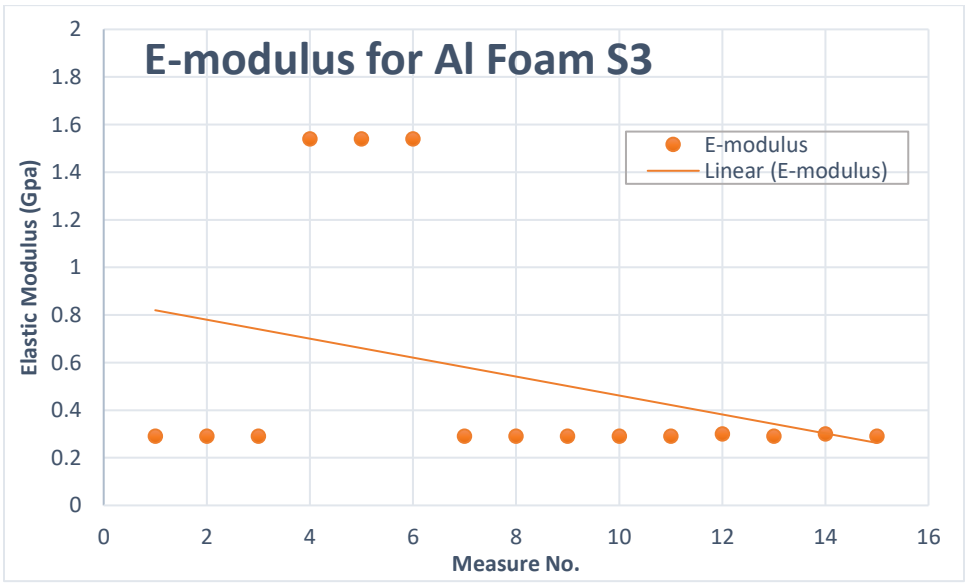

Figure 4.24: Youngs Modulus for Al Foam S3

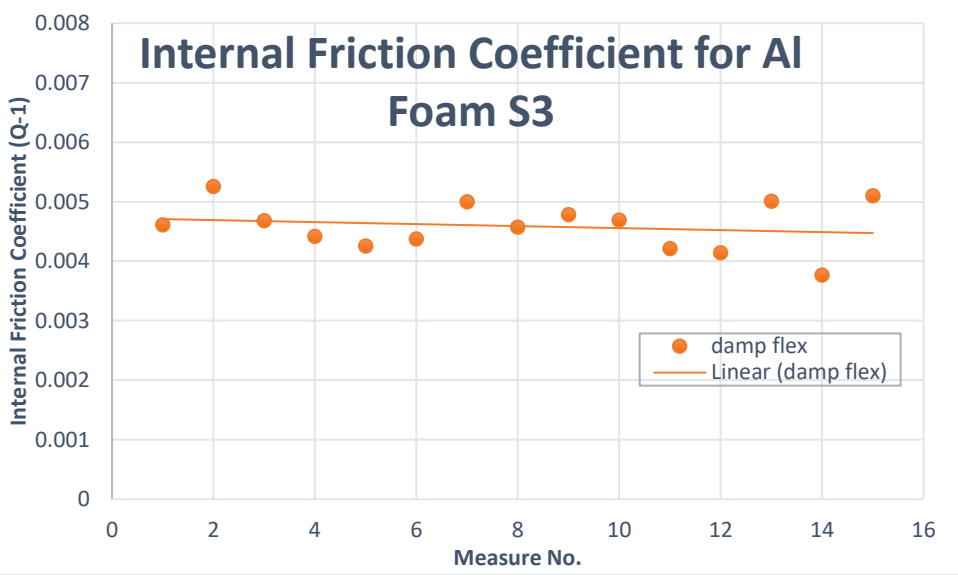

Figure 4.25: Internal Friction Coefficient in flexion for Al Foam S3

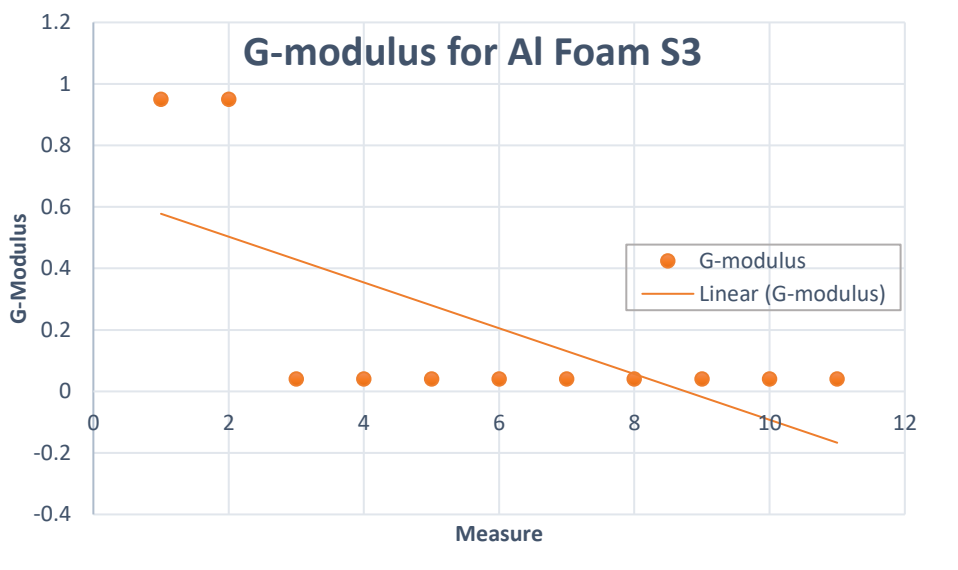

Figure 4.26: Shear Modulus for Al Foam S3

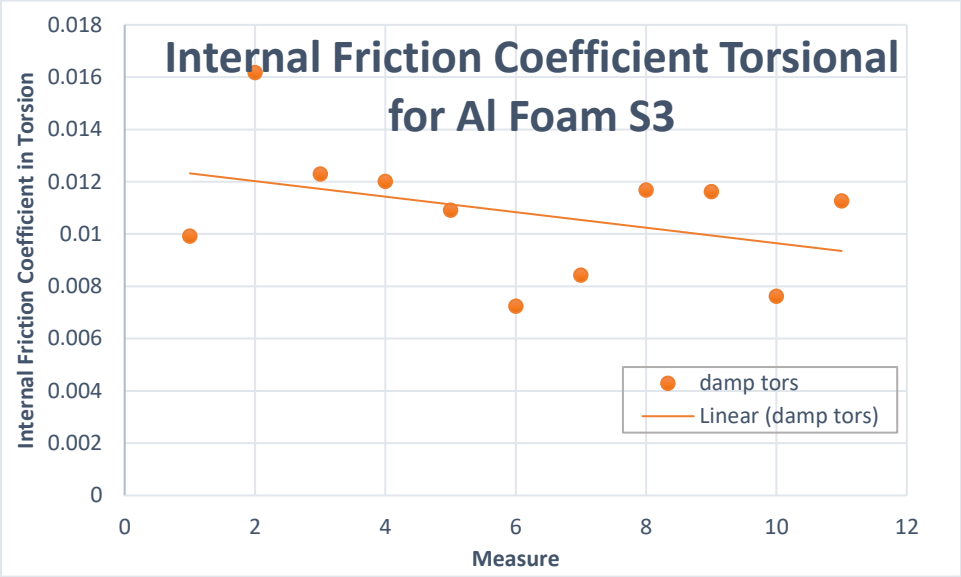

Figure 4.27: Internal Friction Coefficient in torsion for Al Foam S3

4.3.4. RESULTS FOR AL FOAM COMBINED

The figures below represent the mean elastic and shear moduli and internal friction coefficient in flexion and torsion combined for Al foam.

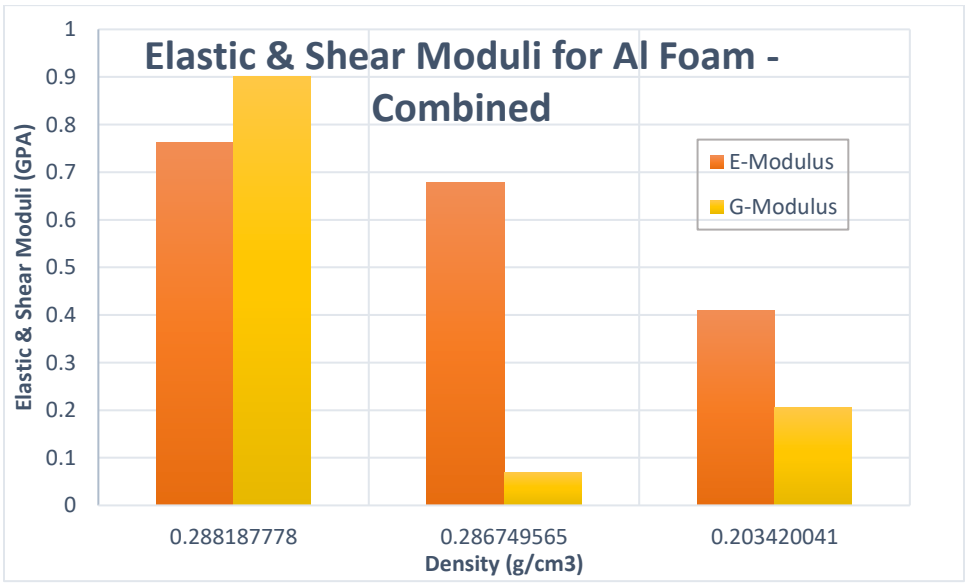

Figure 4.28: Mean Young and Shear Moduli for Al Foam - Combined

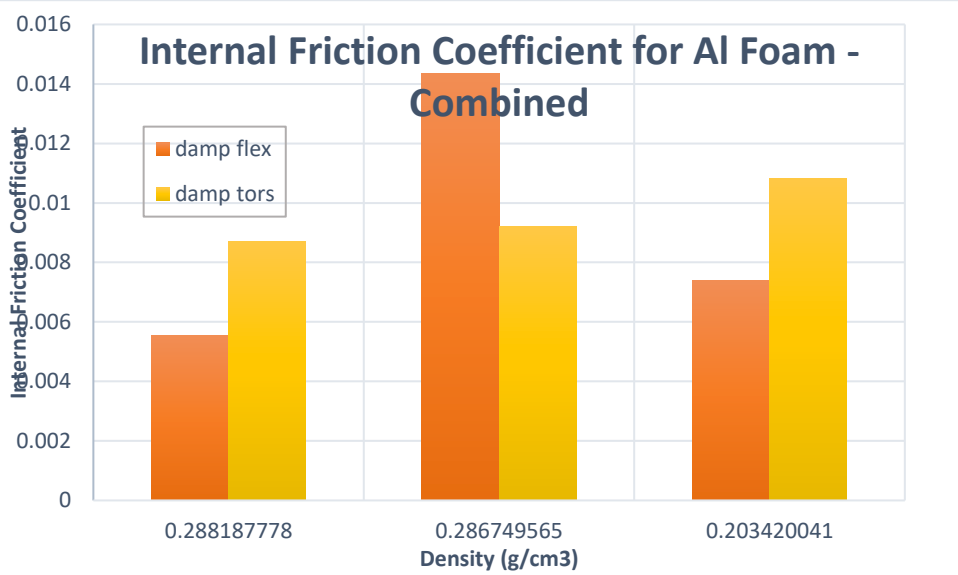

Figure 4.29: Mean Internal Friction Coefficient in flexion and torsion for Al Foam - Combined

4.4. RESULTS FOR AL-ZN SANDWICH (SD AL6016 AL ZN)

The results for Al-Zn Sandwich (SD Al6016 Al Zn) are being obtained for Youngs Modulus, internal friction coefficient in flexion, shear modulus and internal friction coefficient in torsion. These plots are segregated for each of the three samples S1, S2 and S3. The combined plots are then prepared for elastic and shear moduli of the Aluminum 6016 plate and internal friction coefficient in flexion and torsion by averaging the values obtained for each run of the data.

4.4.1. RESULTS FOR SD AL6016 ZN S1

. The figures below represent the elastic and shear modulus and internal coefficient of friction in flexion and torsion for SD Al6016 Zn S1.

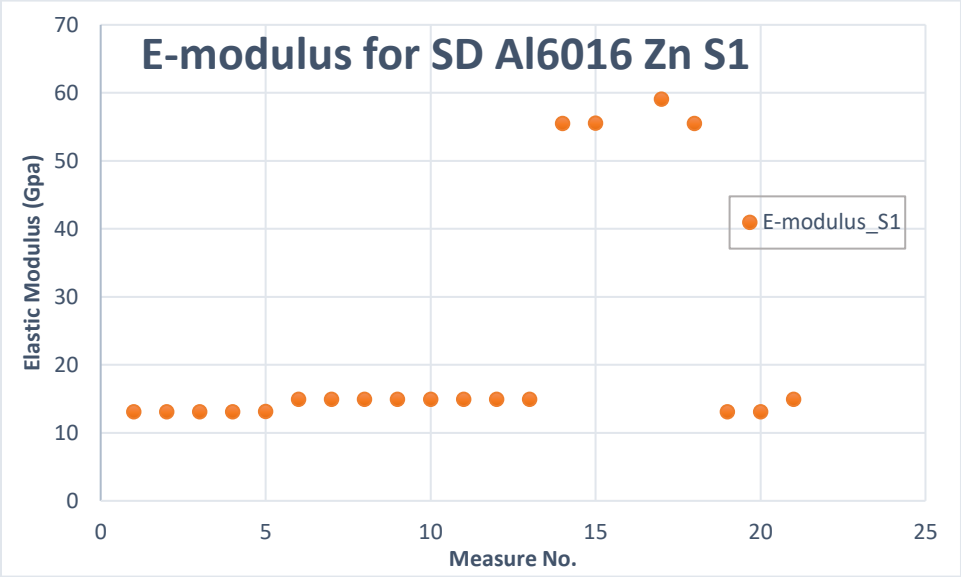

Figure 4.30: Youngs Modulus for SD Al6016 Zn S1

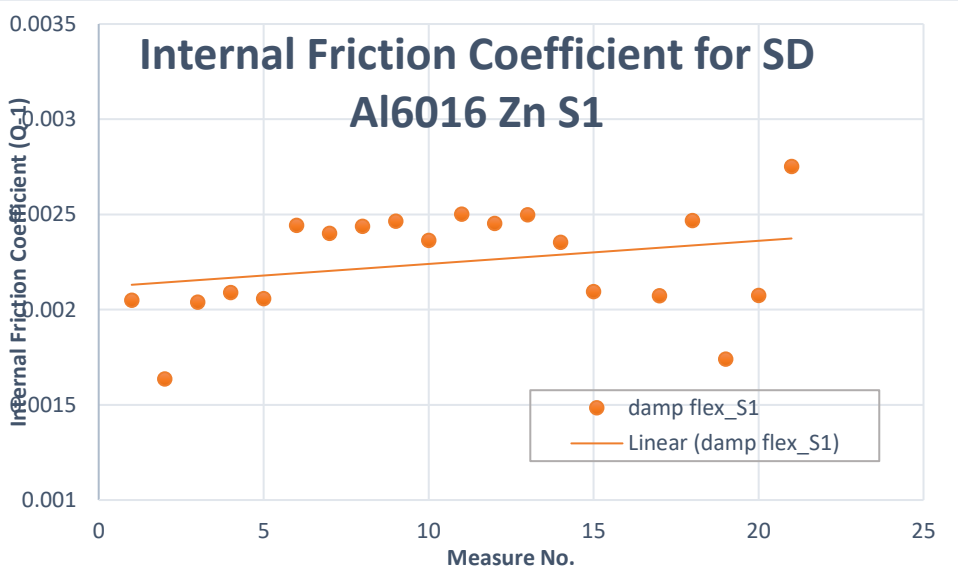

Figure 4.31: Internal Friction Coefficient in flexion for SD Al6016 Zn S1

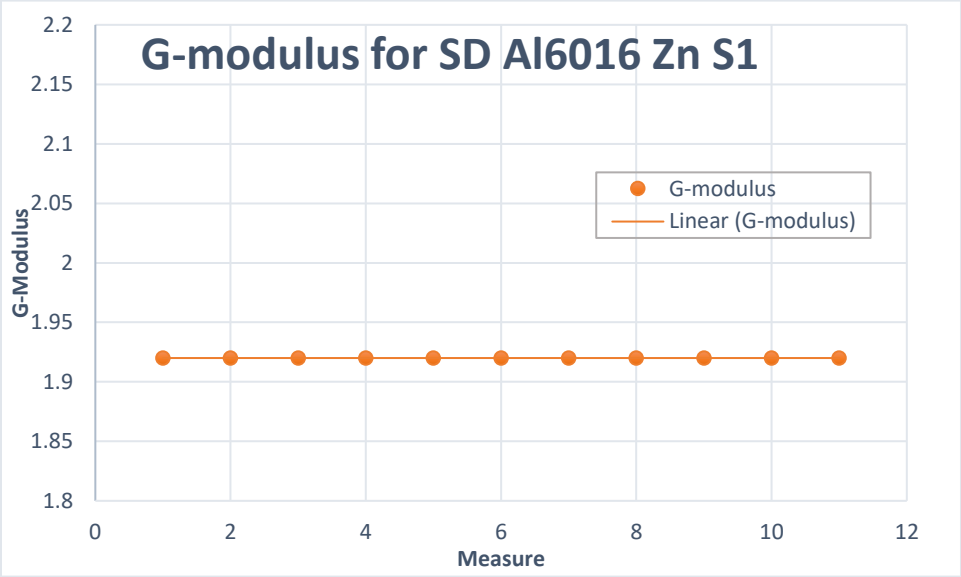

Figure 4.32: Shear Modulus for SD Al6016 Zn S1

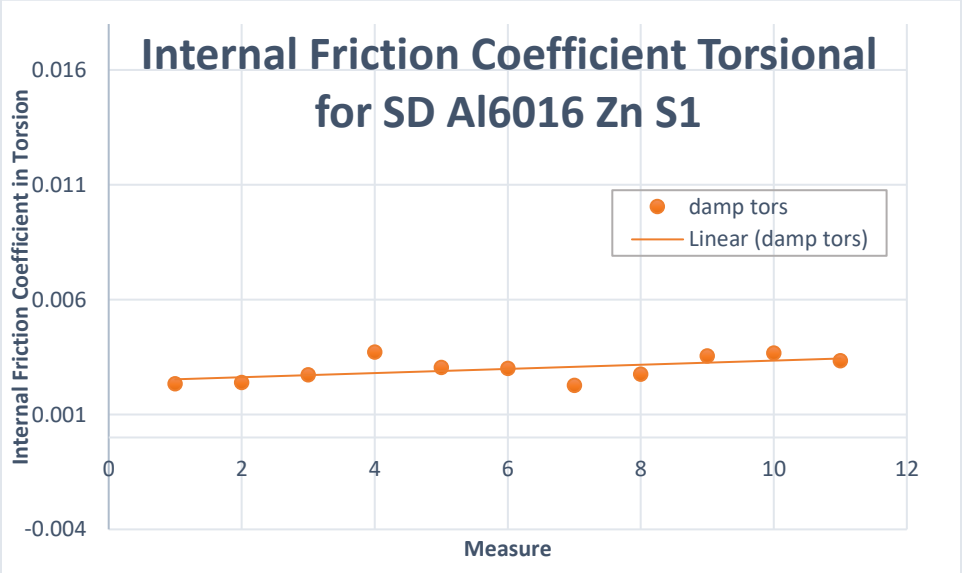

Figure 4.33: Internal Friction Coefficient in torsion for SD Al6016 Zn S1

4.4.2. RESULTS FOR SD AL6016 ZN S2

The figures below represent the elastic and shear modulus and internal coefficient of friction in flexion and torsion for SD Al6016 Zn S2.

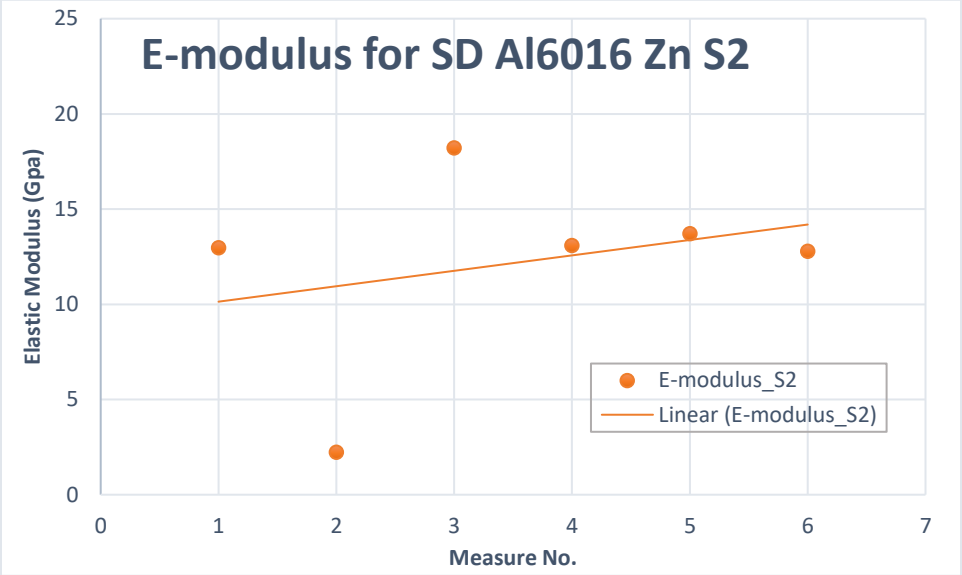

Figure 4.34: Youngs Modulus for SD Al6016 Zn S2

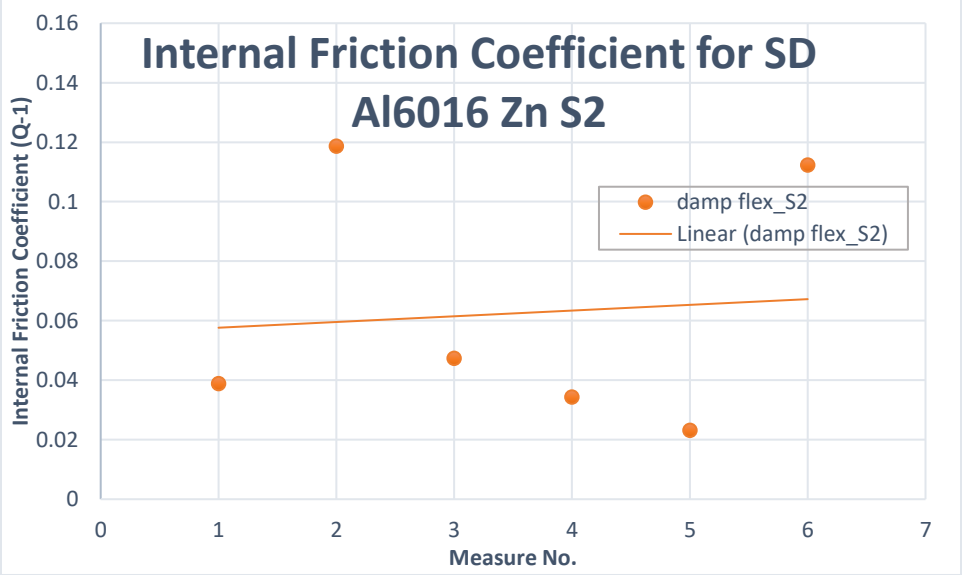

Figure 4.35: Internal Friction Coefficient in flexion for SD Al6016 Zn S2

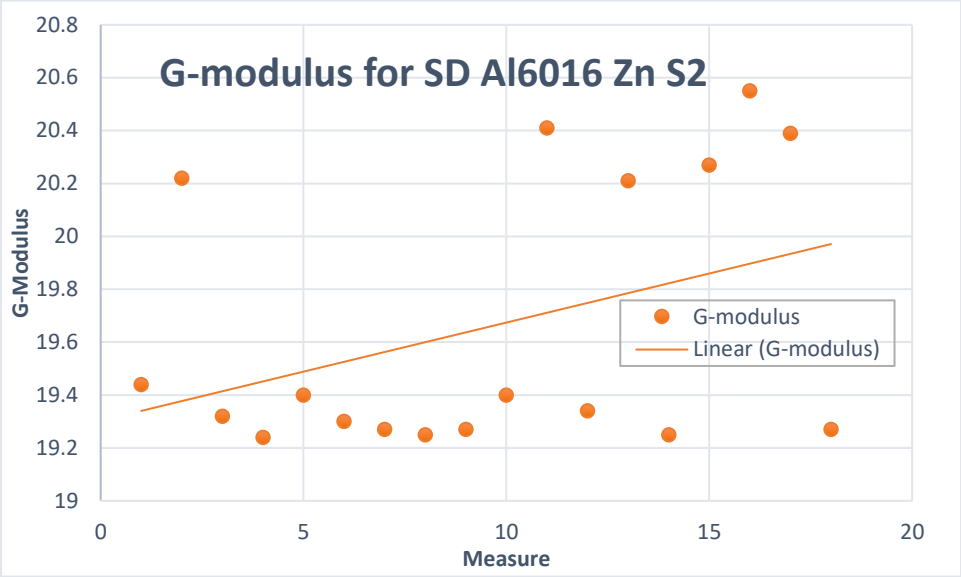

Figure 4.36: Shear Modulus for SD Al6016 Zn S2

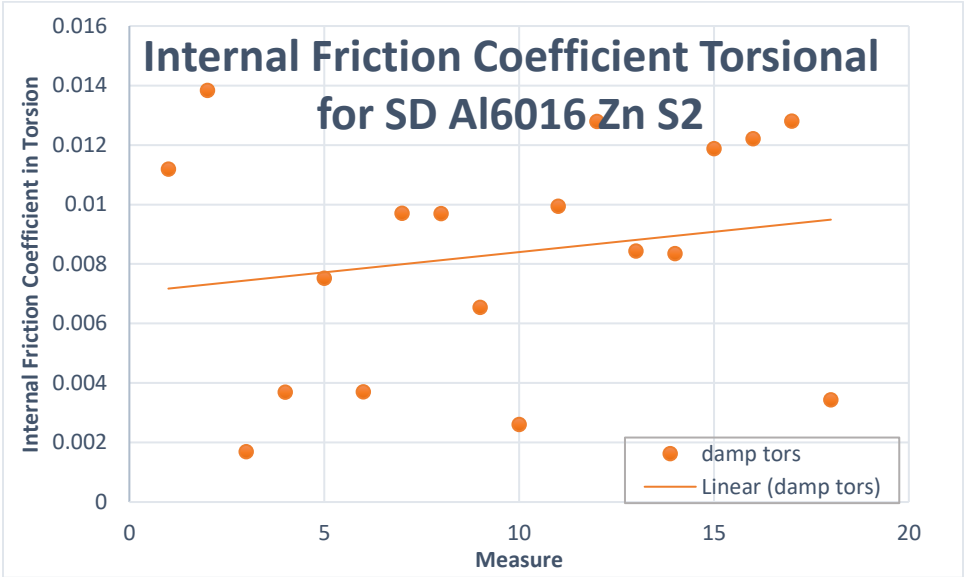

Figure 4.37: Internal Friction Coefficient in torsion for SD Al6016 Zn S2

4.4.3. RESULTS FOR SD AL6016 ZN S3

The figures below represent the elastic and shear modulus and internal coefficient of friction in flexion and torsion for SD Al6016 Zn S3.

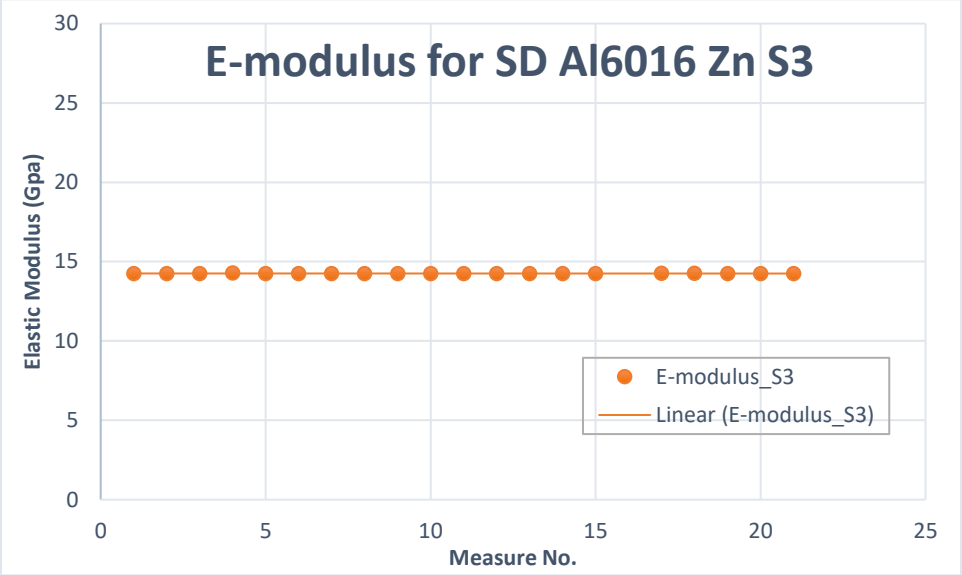

Figure 4.38: Youngs Modulus for SD Al6016 Zn S3

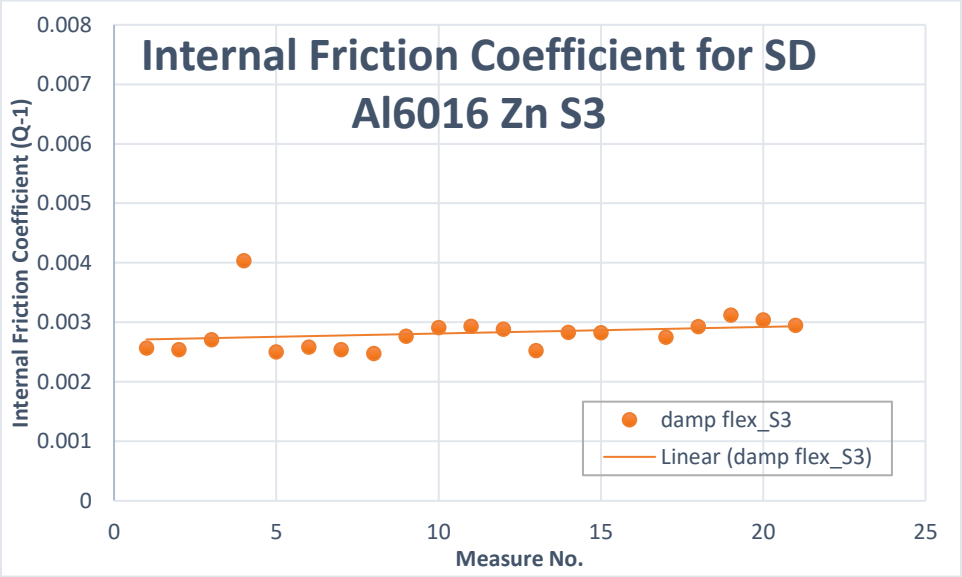

Figure 4.39: Internal Friction Coefficient in flexion for SD Al6016 Zn S3

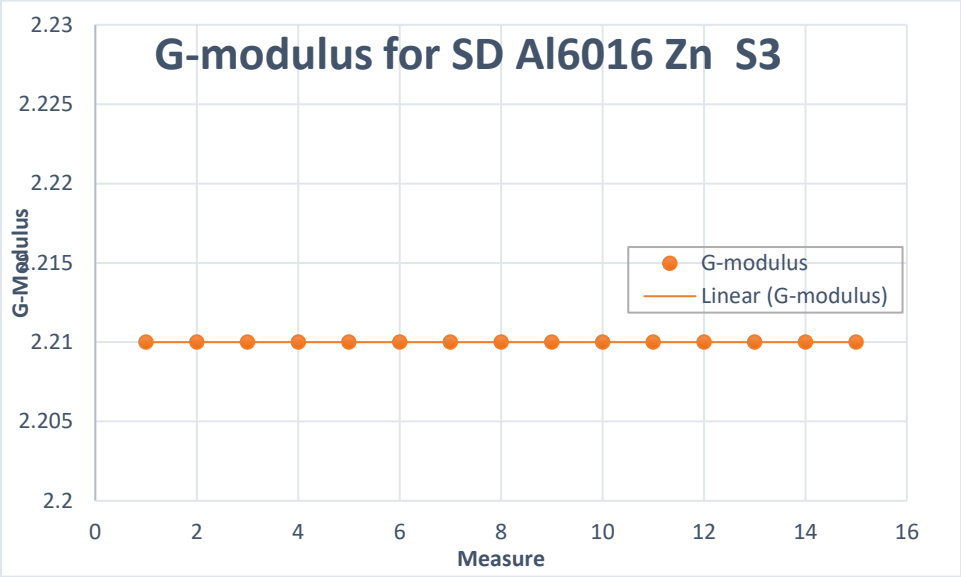

Figure 4.40: Shear Modulus for SD Al6016 Zn S3

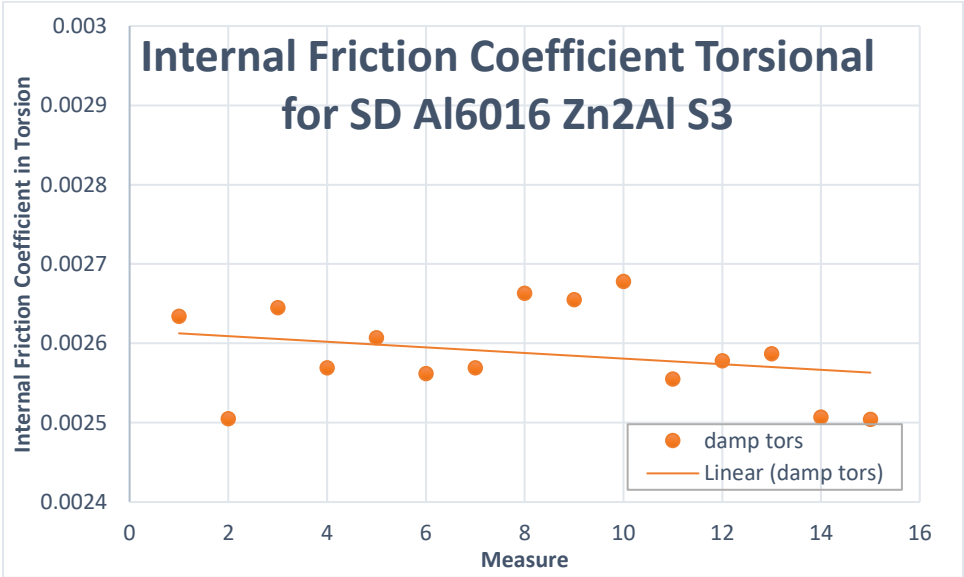

Figure 4.41: Internal Friction Coefficient in torsion for SD Al6016 Zn S3

4.4.4. RESULTS FOR SD AL6016 ZN COMBINED

The figures below represent the mean elastic and shear moduli and internal friction coefficient in flexion and torsion combined for SD Al6016 Zn.

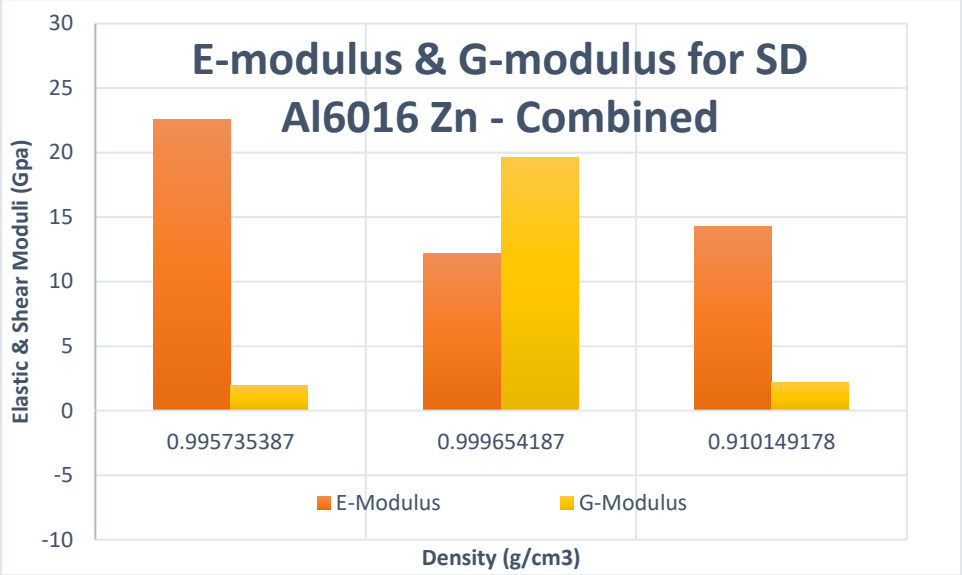

Figure 4.42: Mean Young and Shear Moduli for SD Al6016 Zn - Combined

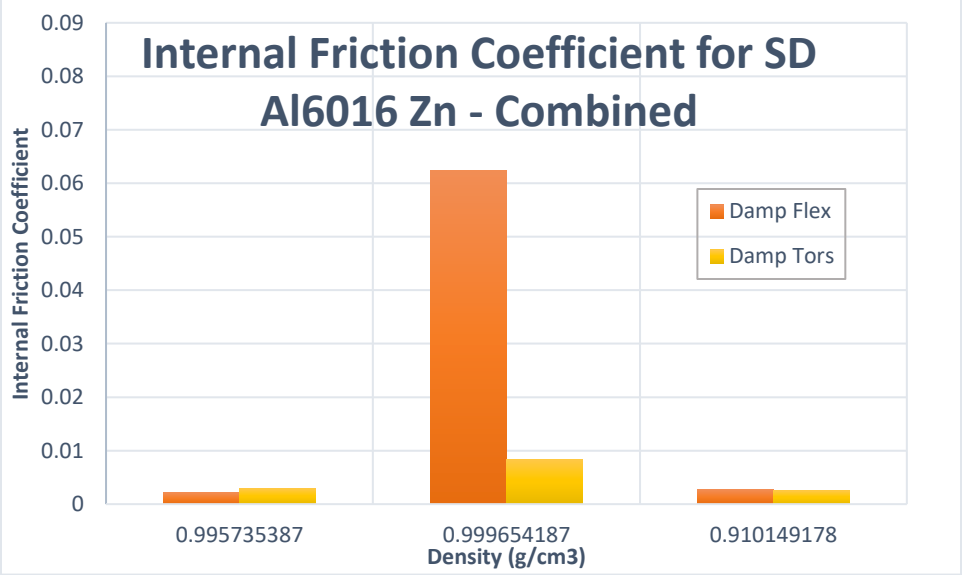

Figure 4.43: Mean Internal Friction Coefficient in flexion and torsion for SD Al6016 Zn - Combined

4.5. RESULTS FOR AL-2%-ZN SANDWICH (SD AL6016 AL 2 ZN)

The results for Al-2%-Zn Sandwich (SD Al6016 Al 2 Zn) are being obtained for Youngs Modulus, internal friction coefficient in flexion, shear modulus and internal friction coefficient in torsion. These plots are segregated for each of the three samples S1, S2 and S3. The combined plots are then prepared for elastic and shear moduli of the Aluminum 6016 plate and internal friction coefficient in flexion and torsion by averaging the values obtained for each run of the data.

4.5.1. RESULTS FOR SD AL6016 ZN2AL S1

The figures below represent the elastic and shear modulus and internal coefficient of friction in flexion and torsion for SD Al6016 Zn2Al S1.

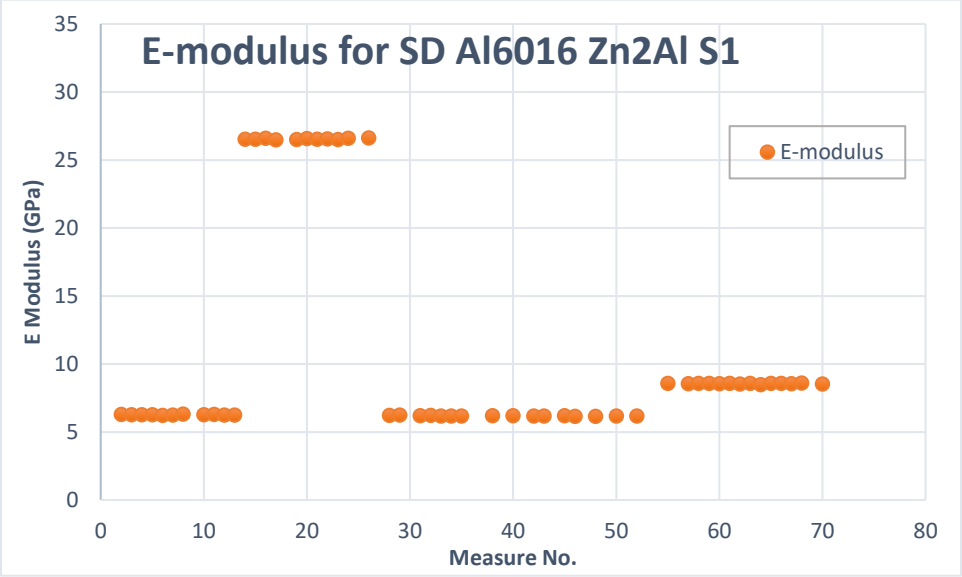

Figure 4.44: Youngs Modulus for SD Al6016 Zn2Al S1

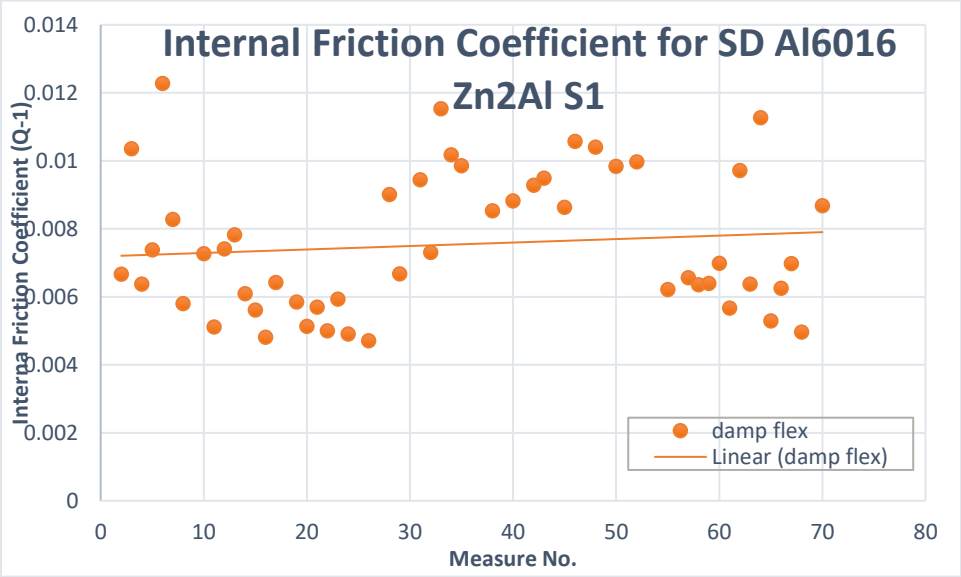

Figure 4.45: Internal Friction Coefficient in flexion for SD Al6016 Zn2Al S1

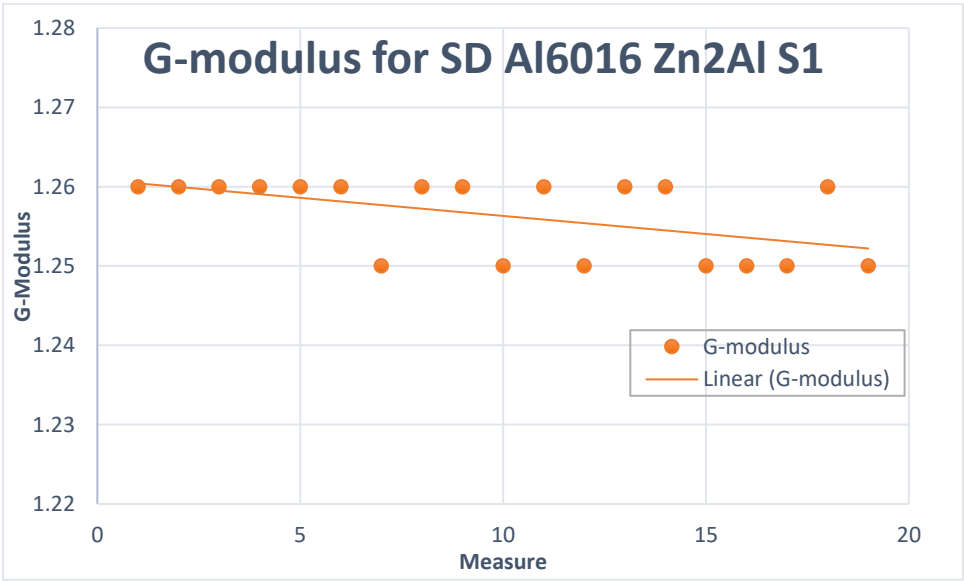

Figure 4.46: Shear Modulus for SD Al6016 Zn2Al S1

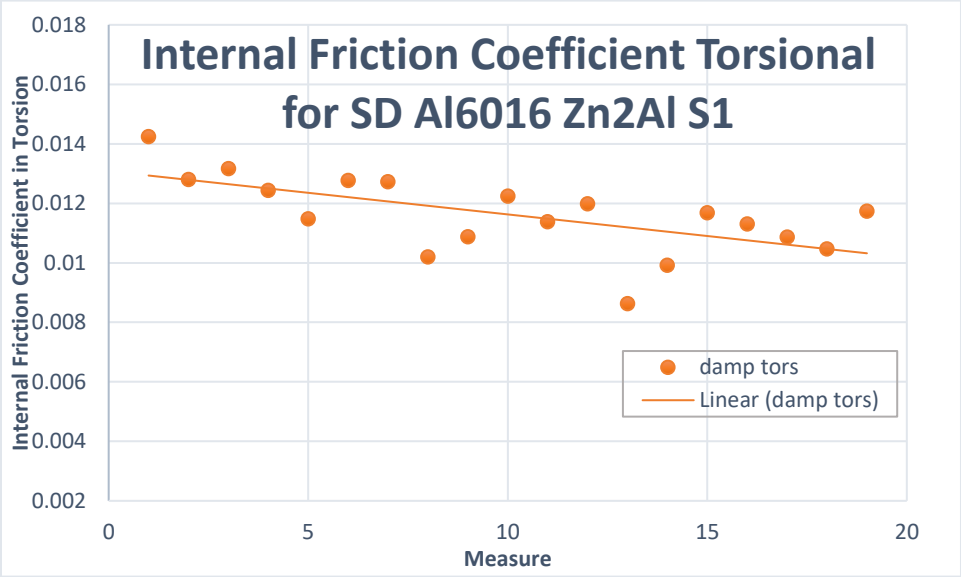

Figure 4.47: Internal Friction Coefficient in torsion for SD Al6016 Zn2Al S1

4.5.2. RESULTS FOR SD AL6016 ZN2AL S2

The figures below represent the elastic and shear modulus and internal coefficient of friction in flexion and torsion for SD Al6016 Zn2Al S2.

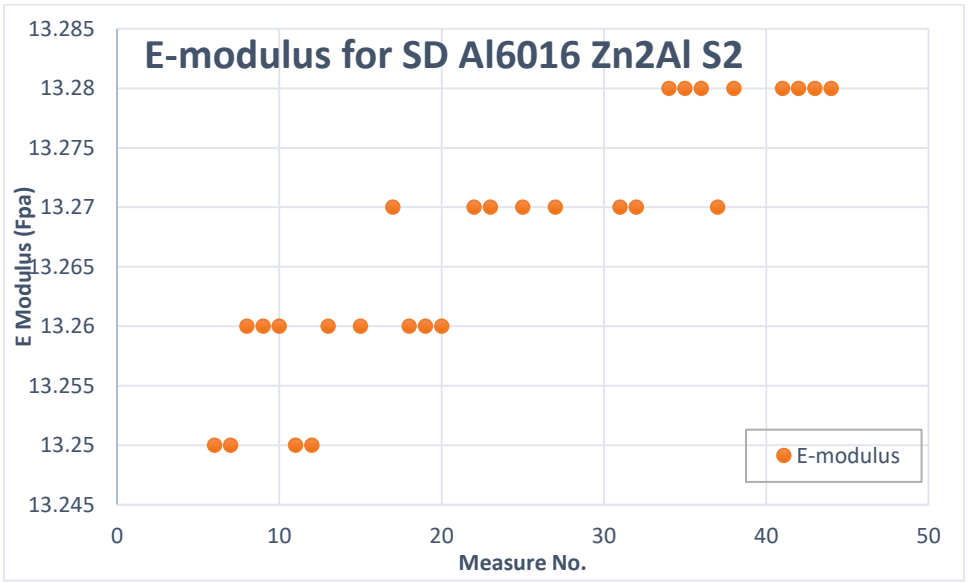

Figure 4.48: Youngs Modulus for SD Al6016 Zn2Al S2

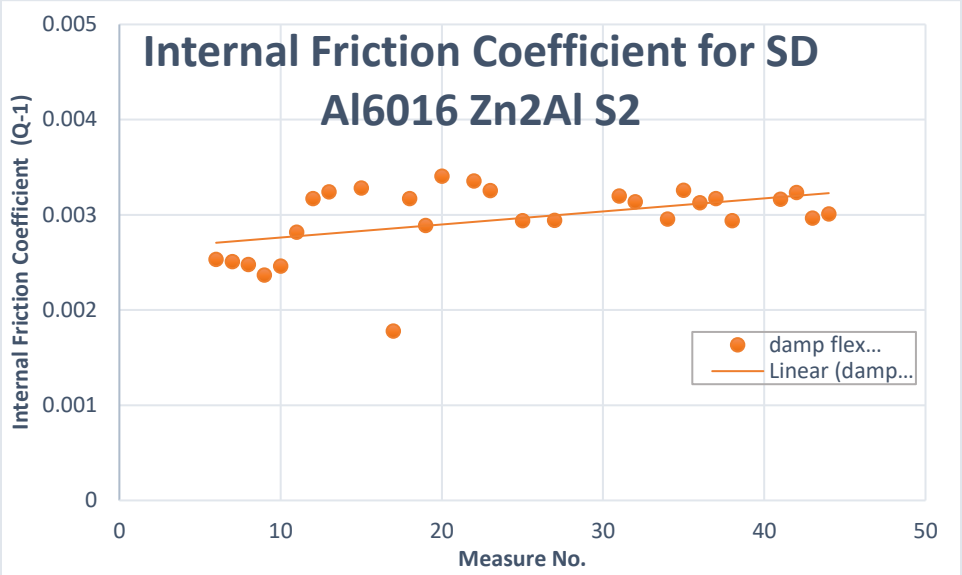

Figure 4.49: Internal Friction Coefficient in flexion for SD Al6016 Zn2Al S2

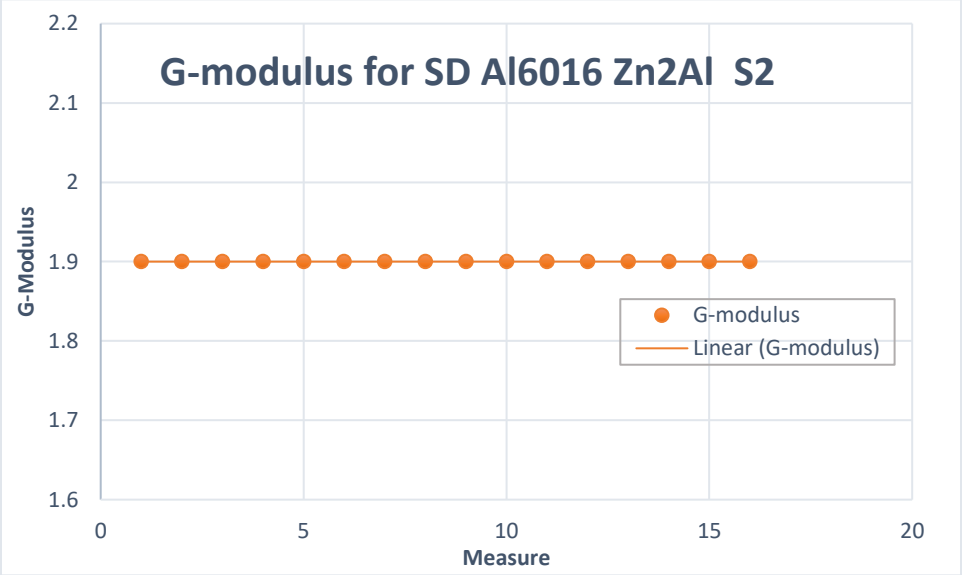

Figure 4.50: Shear Modulus for SD Al6016 Zn2Al S2

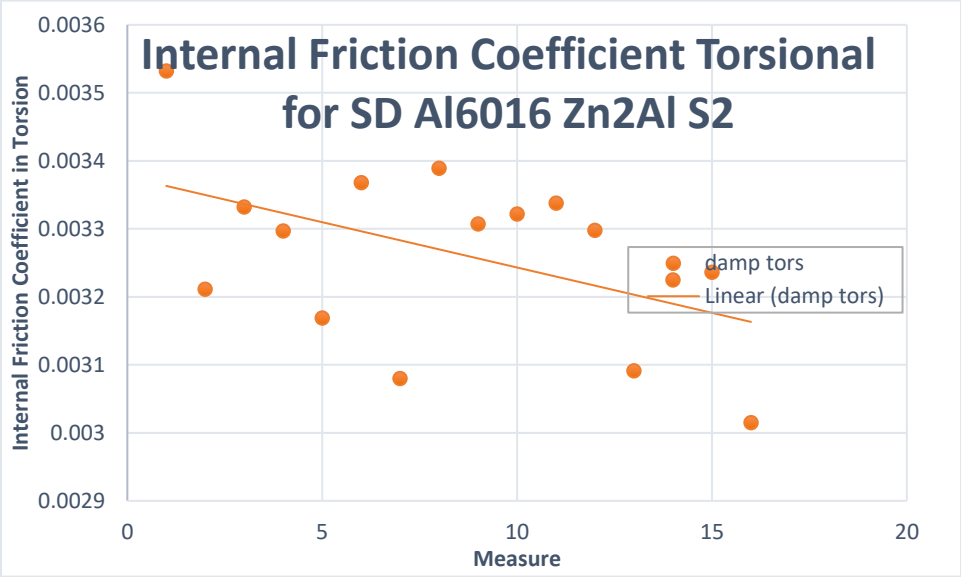

Figure 4.51: Internal Friction Coefficient in torsion for SD Al6016 Zn2Al S2

4.5.3. RESULTS FOR SD AL6016 ZN2AL S3

The figures below represent the elastic and shear modulus and internal coefficient of friction in flexion and torsion for SD Al6016 Zn2Al S3.

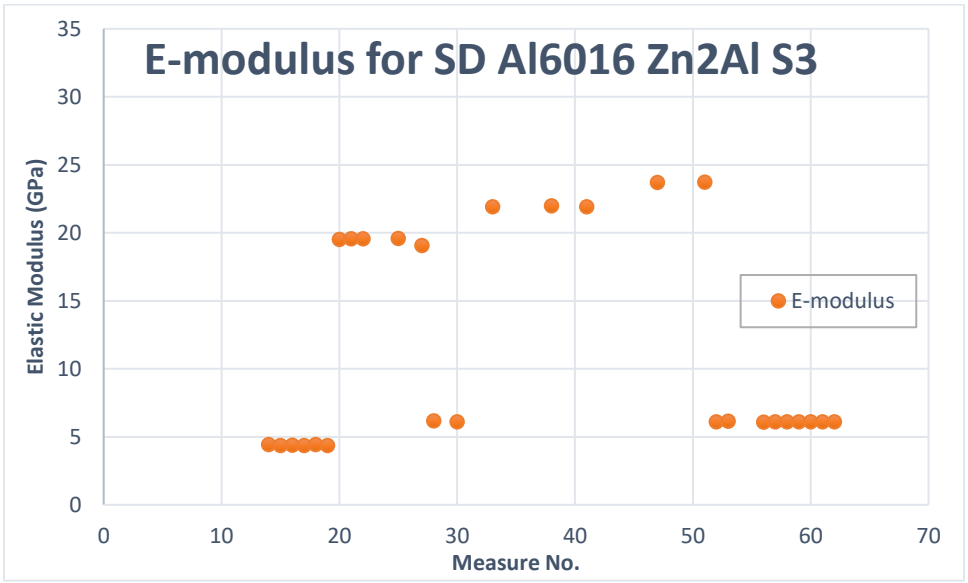

Figure 4.52: Youngs Modulus for SD Al6016 Zn2Al S3

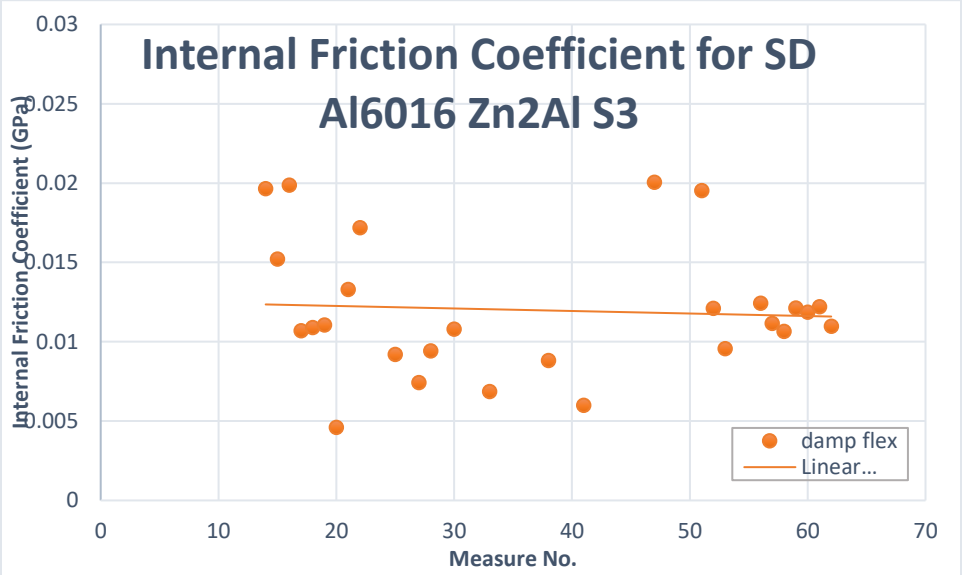

Figure 4.53: Internal Friction Coefficient in flexion for SD Al6016 Zn2Al S3

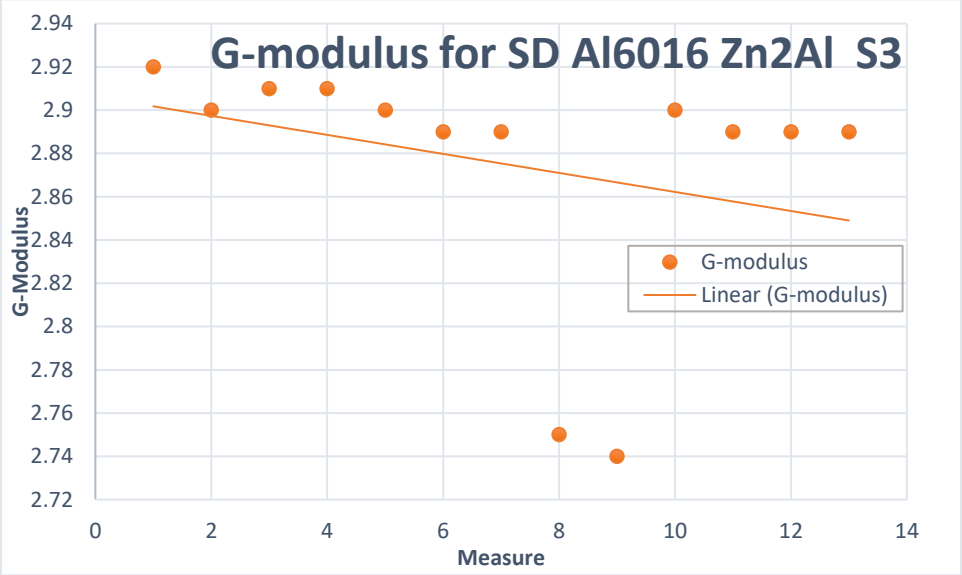

Figure 4.54: Shear Modulus for SD Al6016 Zn2Al S3

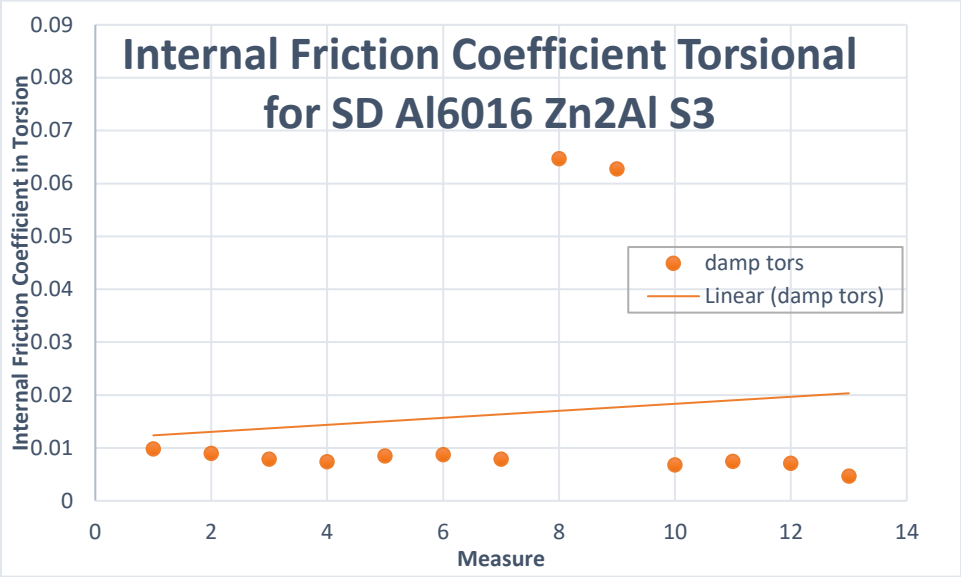

Figure 4.55: Internal Friction Coefficient in torsion for SD Al6016 Zn2Al S3

4.5.4. RESULTS FOR SD AL6016 ZN2AL COMBINED

The figures below represent the mean elastic and shear moduli and internal friction coefficient in flexion and torsion combined for SD Al6016 Zn2Al.

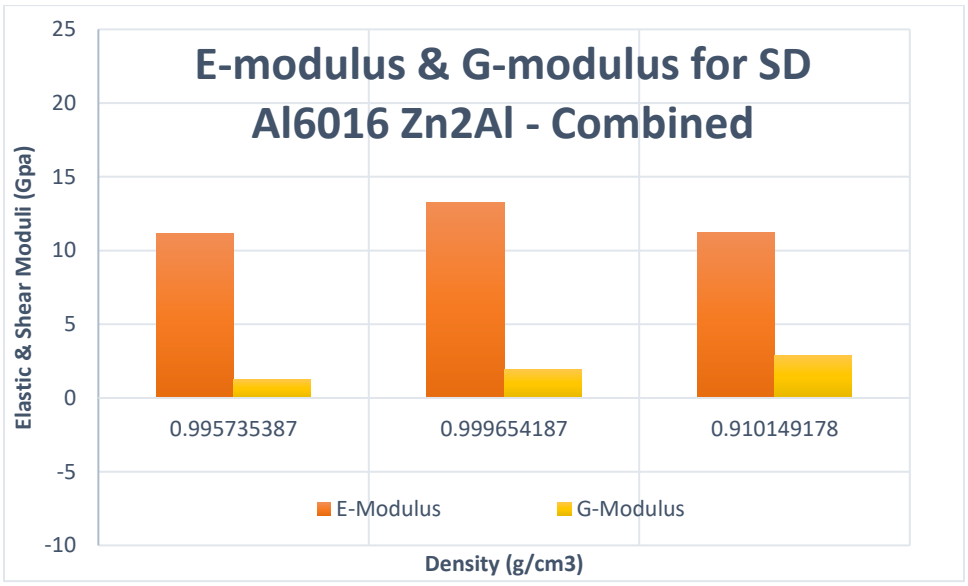

Figure 4.56: Mean Young and Shear Moduli for SD Al6016 Zn2Al - Combined

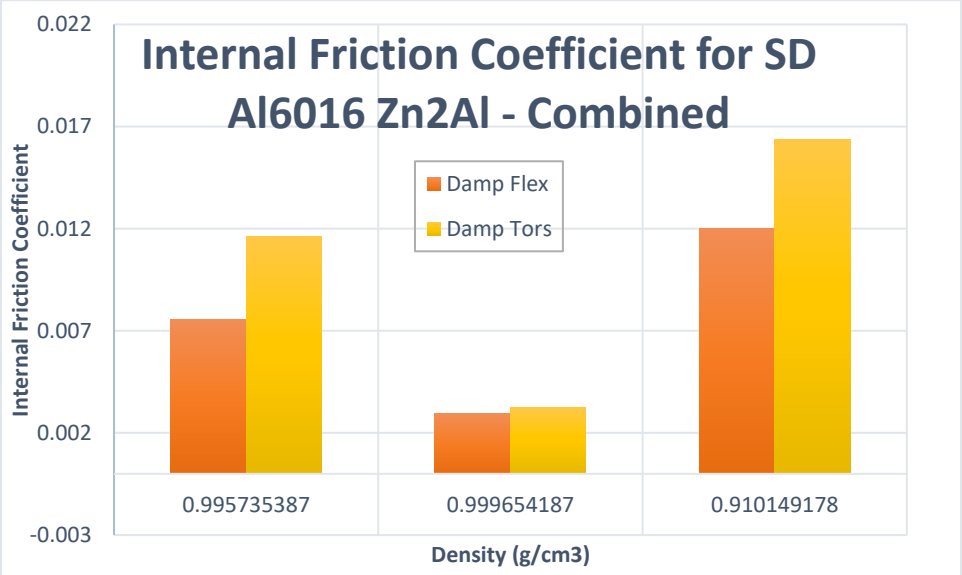

Figure 4.57: Mean Internal Friction Coefficient in flexion and torsion for SD Al6016 Zn2Al - Combined

4.6. COMPARISON PLOTS

The figures below represent the elastic and shear moduli and internal friction coefficient in flexion and torsion for all 4 materials. The values of material are averaged for all individual samples of each material of plate, foam and both variants of aluminum sandwich.

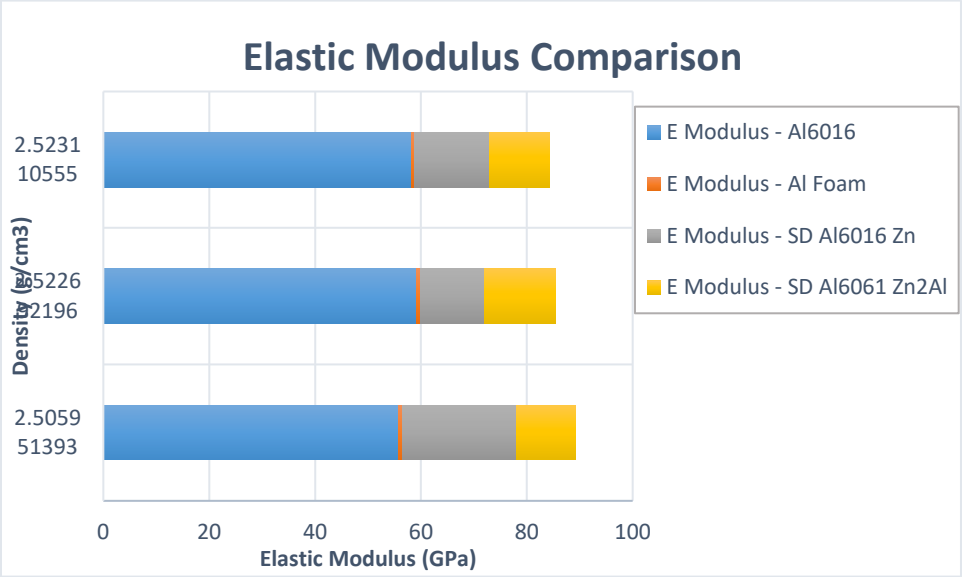

Figure 4.58: Comparison plot for Youngs Modulus of Al 60616 plate, Al foam, SD Al6016 Zn and SD Al6016 Zn2Al

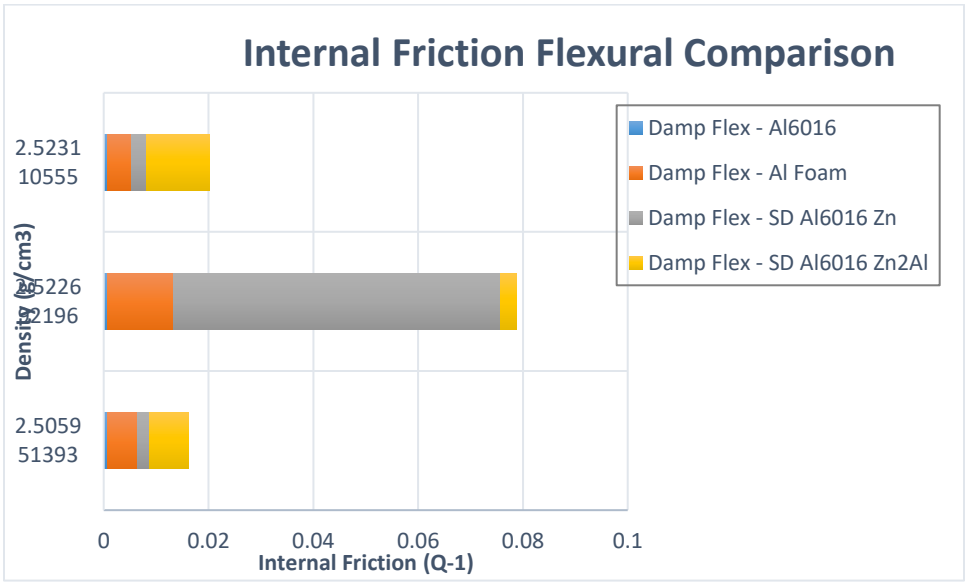

Figure 4.59: Comparison plot for Internal Friction coefficient in Flexion Al 60616 plate, Al foam, SD Al6016 Zn and SD Al6016 Zn2Al

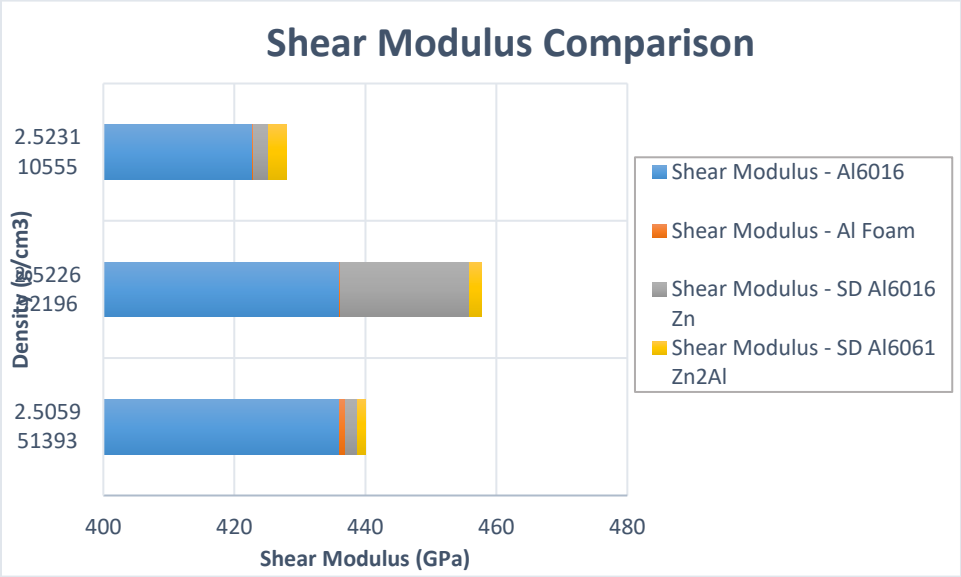

Figure 4.60: Comparison plot for Shear Modulus of Al 60616 plate, Al foam, SD Al6016 Zn and SD Al6016 Zn2Al

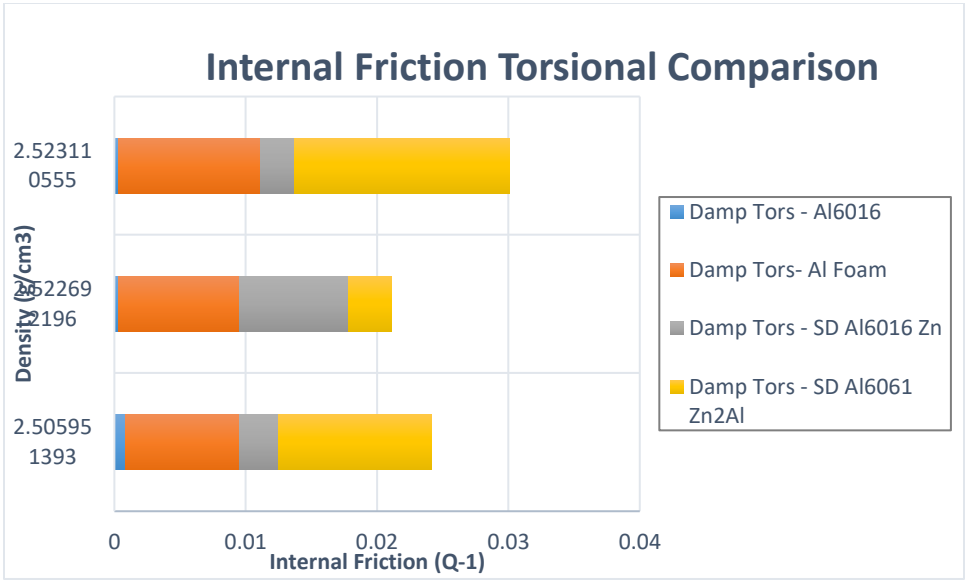

Figure 4.61: Comparison plot for Internal Friction coefficient in Torsion Al 60616 plate, Al foam, SD Al6016 Zn and SD Al6016 Zn2Al

4.7. RESULTS FOR TENSILE TEST EXPERIMENT

The tensile test was performed on aluminum foam and the two variants of aluminum sandwich foam. The load versus extension graphs provide a comprehensive

insight into the mechanical behavior exhibited by each tested sample under tensile loading conditions. These graphs portray the relationship between the applied load and the corresponding extension, offering a visual representation of the material's response to external forces. The analysis encompasses Aluminum 6016 Plate, Aluminum Foam, and the sandwich structures SD Al6016 Al-Zn and SD Al6016 Al-2-Zn. Each graph delineates the unique mechanical response of the materials under tension, highlighting their distinct yielding points, ultimate strengths, and deformation characteristics. These representations serve as vital indicators elucidating the material's performance and its ability to withstand tensile stresses before failure. The details of test from 1 to 8 are as follows:

Table 4.3: Details of Test 1 to 8

Sr. No.	**Sample Material**
TEST 1	ALZN S1
TEST 2	ALZN S2
TEST 3	ALZN S3
TEST 4	Al2Zn s1
TEST 5	AL2ZN s3
TEST 6	Foam s1
TEST 7	Foam s2
TEST 8	Foam s3

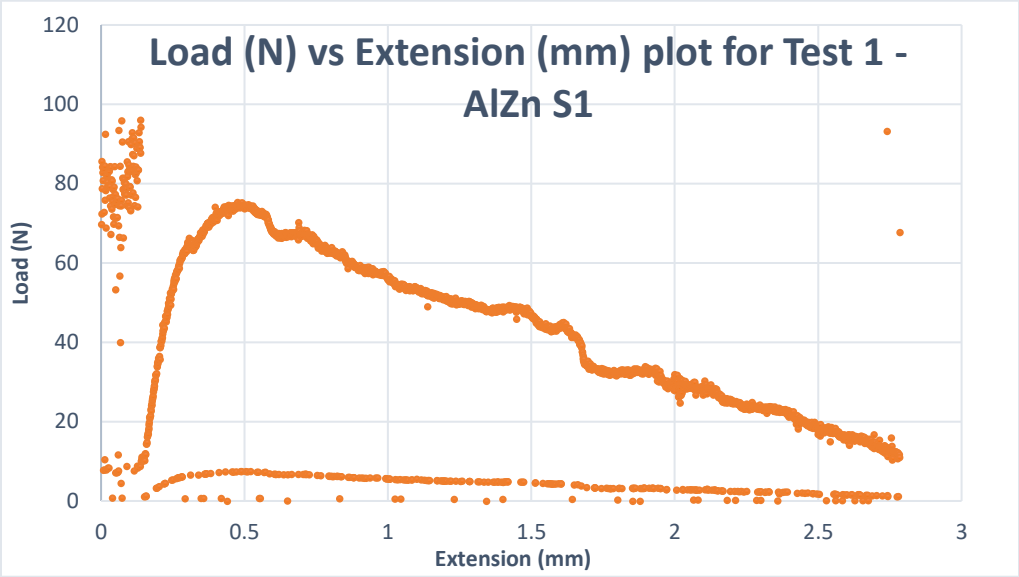

Figure 4.62: Load vs extension plot for test 1 – AlZn S1

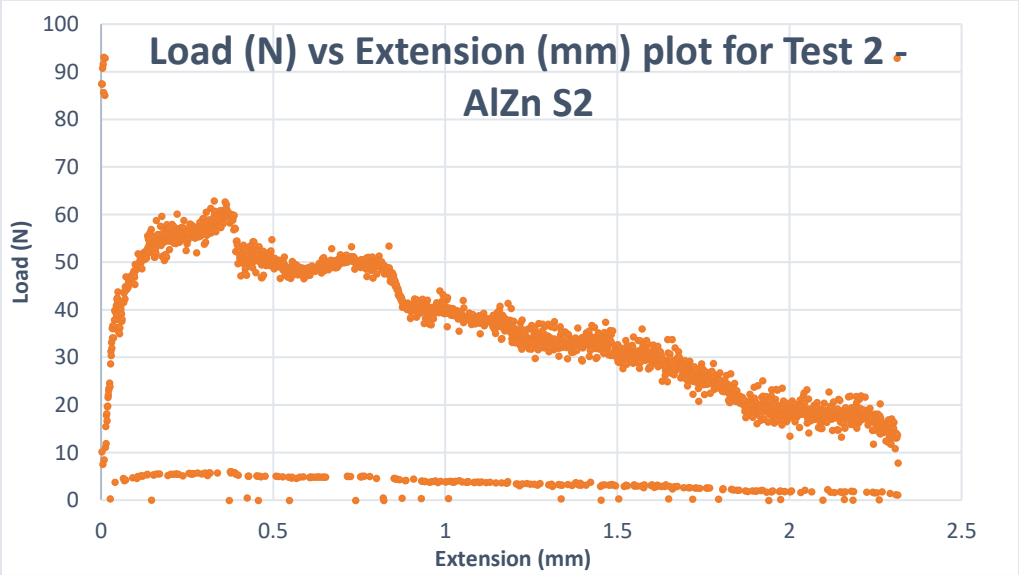

Figure 4.63: Load vs extension plot for test 2 – AlZn S2

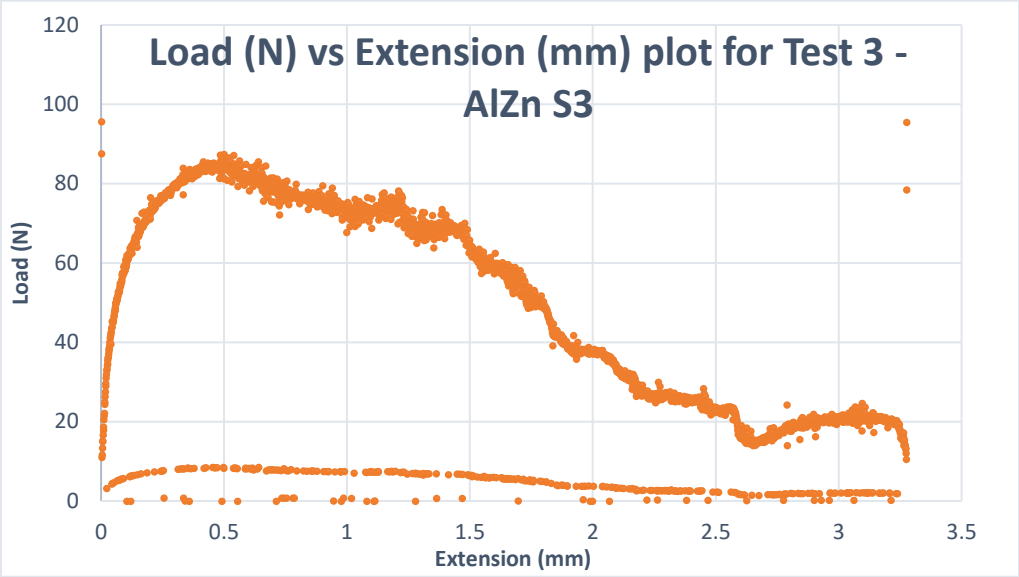

Figure 4.64: Load vs extension plot for test 3 – AlZn S3

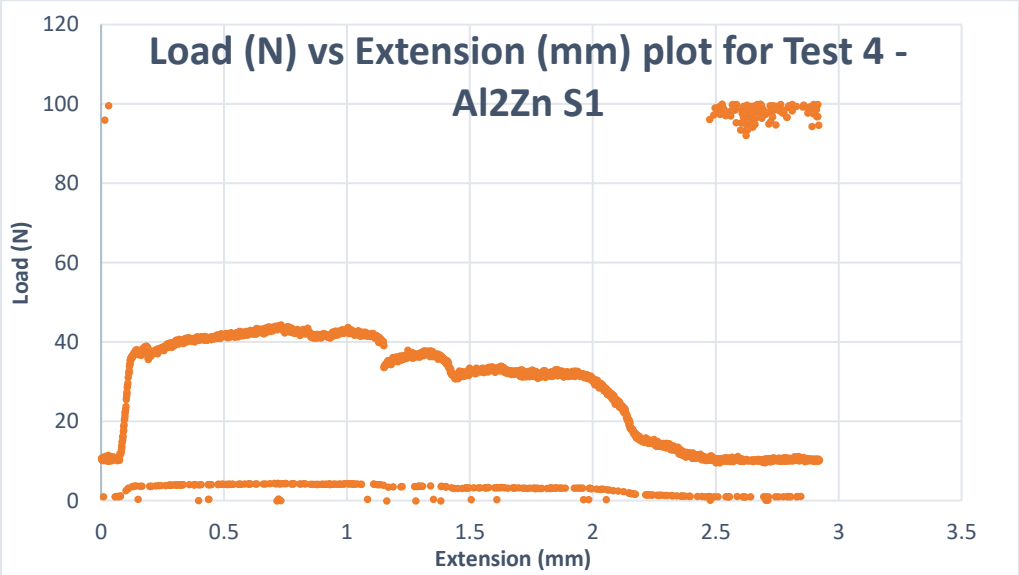

Figure 4.65: Load vs extension plot for test 4 – Al2Zn S1

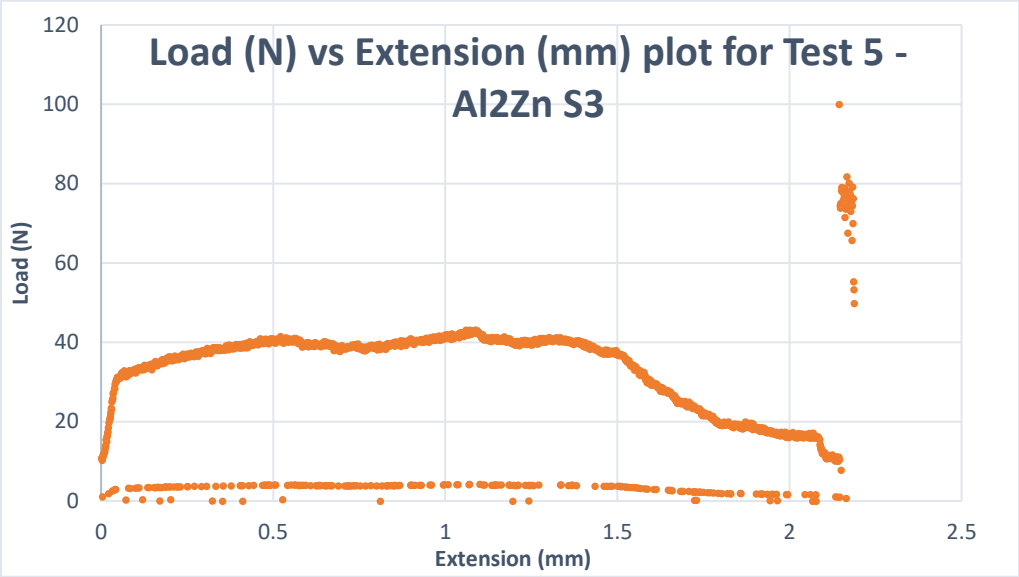

Figure 4.66: Load vs extension plot for test 5 – Al2Zn S3

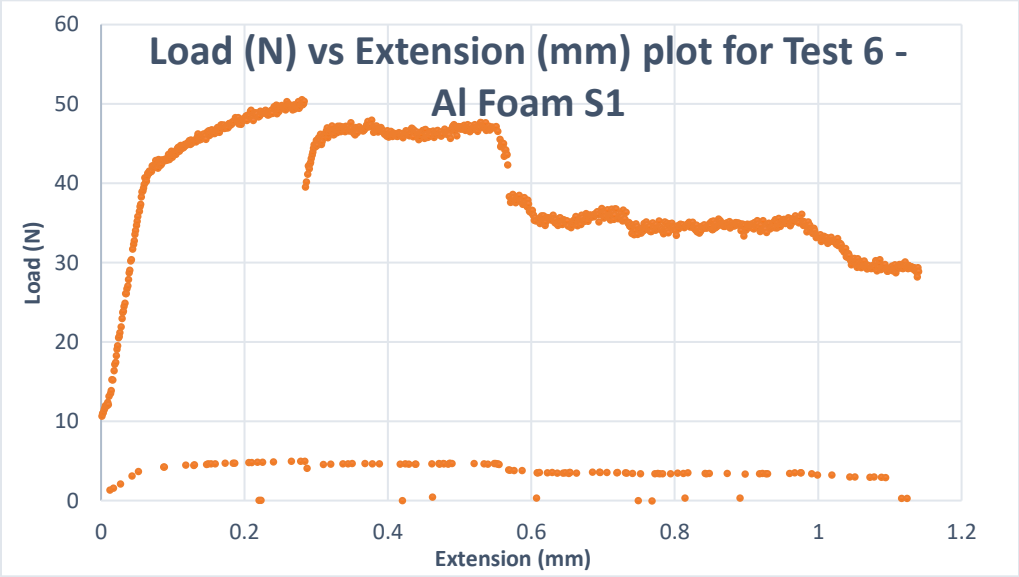

Figure 4.67: Load vs extension plot for test 6 – Al Foam S1

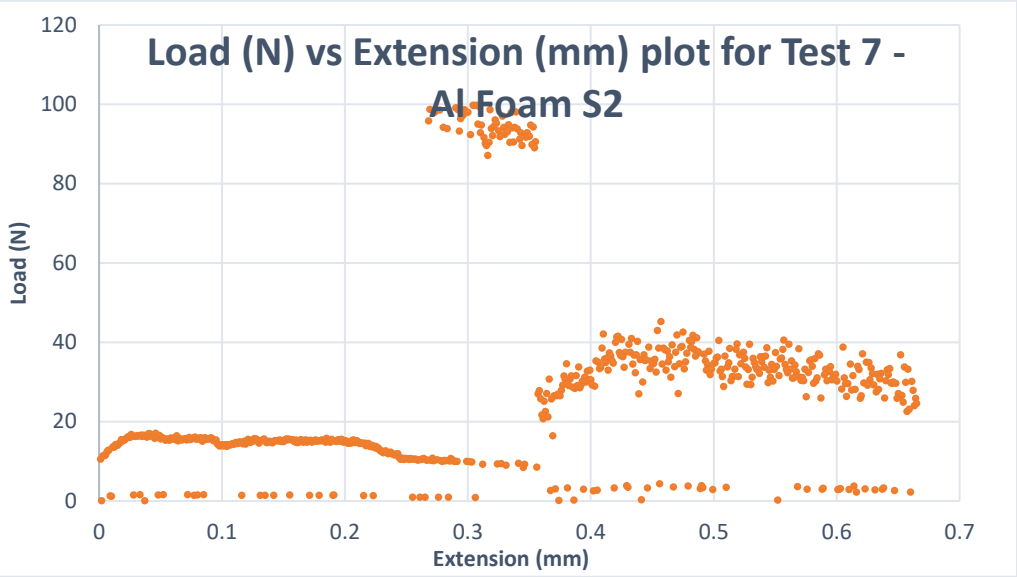

Figure 4.68: Load vs extension plot for test 7 – Al Foam S2

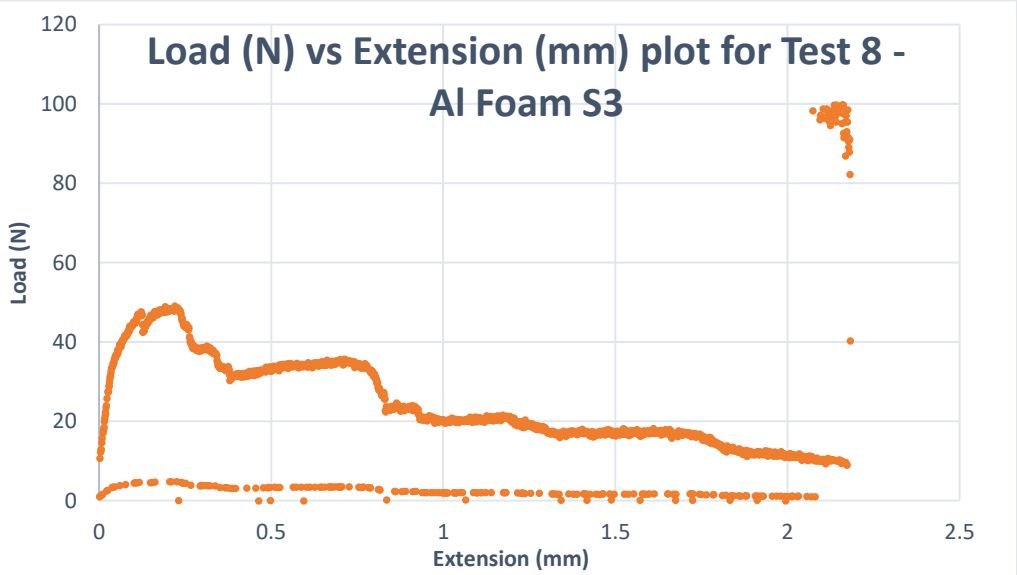

Figure 4.69: Load vs extension plot for test 8 – Al Foam S3

Each sample of the material was subjected to tensile test which resulted in the load vs displacement graph as shown in the figure below:

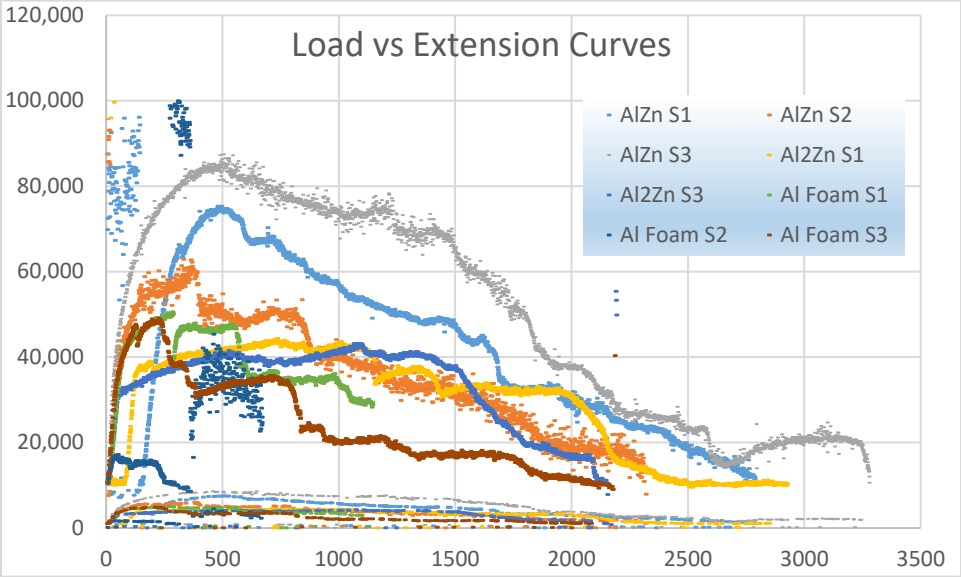

Figure 4.70: Load vs displacement plot for tensile test experiment

The results were compiled in the table below. The results from the tensile tests indicate various properties of the tested materials. Peak Load in N represents the maximum load or force applied to the sample before failure. The values range from 17.2 N to 87.4 N. Peak Stress in MPa is the maximum stress experienced by the material sample, calculated by dividing the peak load by the initial cross-sectional area of the specimen. The values range from 0.1 MPa to 0.8 MPa. Elastic Modulus in MPa measures the stiffness of the material. It's calculated as the ratio of stress to strain within the elastic deformation range. The values range from 16 MPa to 521 MPa. Strain at Failure in % represents the percentage elongation or deformation of the material at the point of failure. The values vary from 0.2% to 2.4%. Reason for Test Termination column provides information about how each test ended. It shows whether the test was interrupted or if failure was observed. And Percentage Strain at Peak indicate the deformation at the point of peak load.

Table 4.4: Tensile test results for Al foam and AFS

Sample Material	Peak Load in N	Peak Stress in MPa	Elastic Moduli measured in MPa	Strain at Failure in %	Reason for Test Termination	Percentage Strain at Peak %
ALZN S1	75.3	0.7	227	0.7	Detected Rupture	0.7
ALZN S2	62.9	0.6	521	0.7	Detected Rupture	0.7
ALZN S3	87.4	0.8	502	1.1	Detected Rupture	1.1
Al2Zn S1	44.4	0.4	293	1.5	Test Interrupted	1.5
AL2ZN S3	43.1	0.4	285	2.4	Test Interrupted	2.4
Foam S1	50.6	0.3	185	0.3	Test Interrupted	0.6
Foam S2	17.2	0.1	16	0.2	Test Interrupted	0.2
Foam S3	49.1	0.3	221	0.5	Test Interrupted	0.5

The figures below further represent a visual comparison of the percentage strain observed at peak stress, yield strength and peak load borne by each sample.

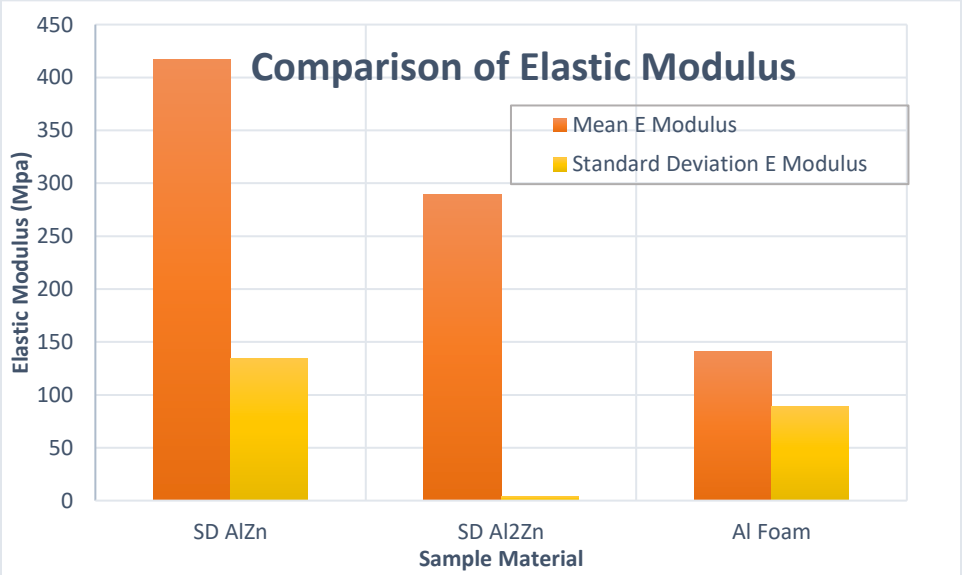

Figure 4.71: Comparison of mean and standard deviation of elastic modulus between tested materials

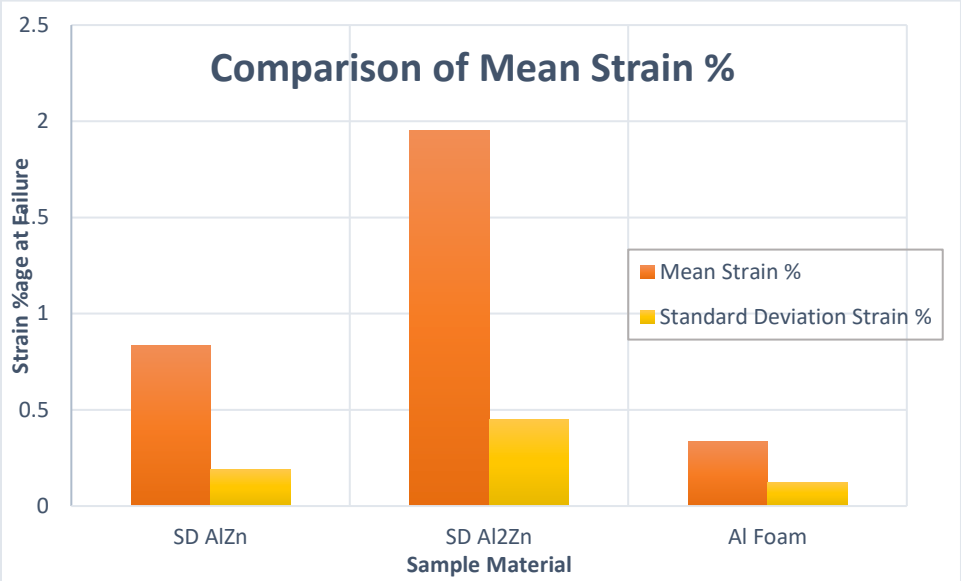

Figure 4.72: Comparison of mean and standard deviation of strain % between tested materials

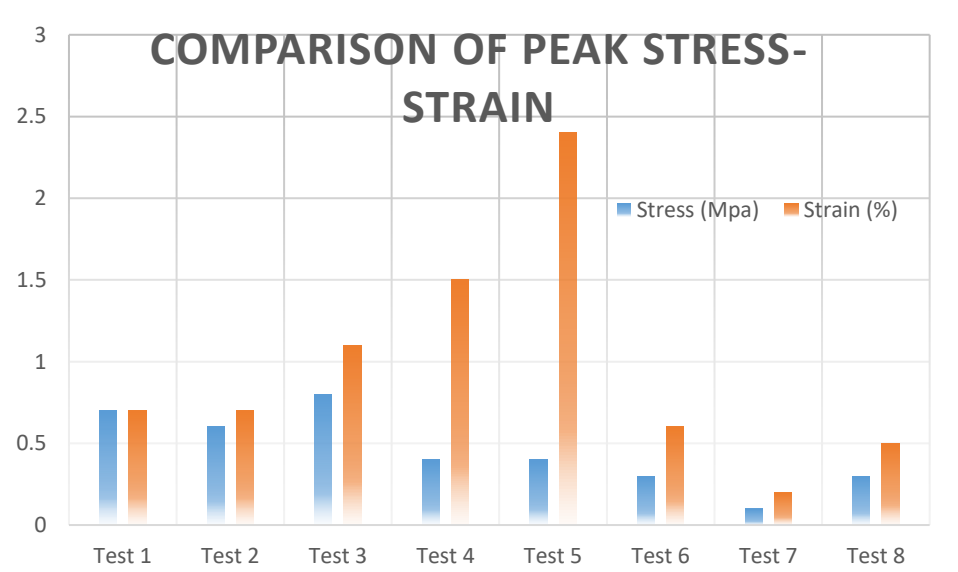

Figure 4.73: Comparison of percentage strain observed by each sample of material at peak stress

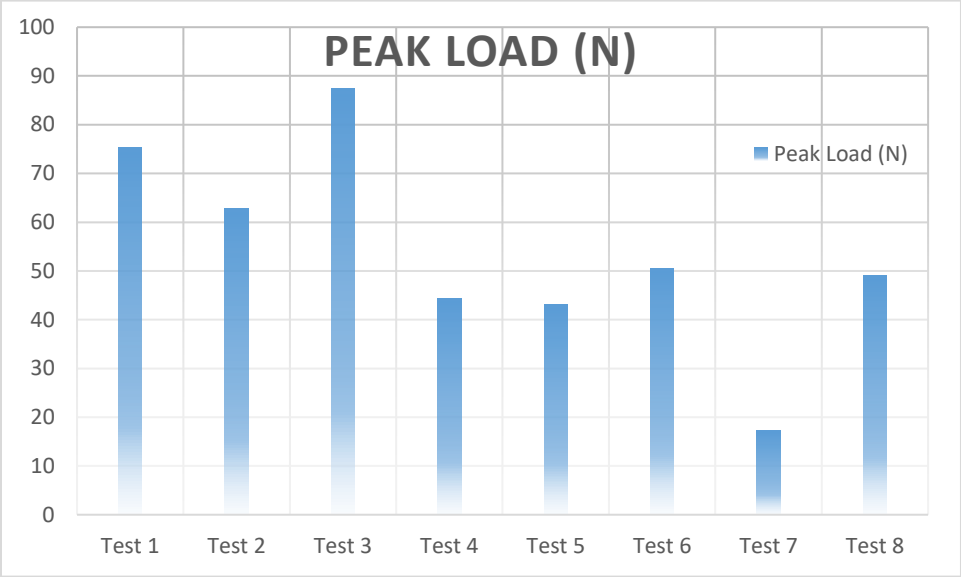

Figure 4.74: Comparison of peak load observed by each sample of various material

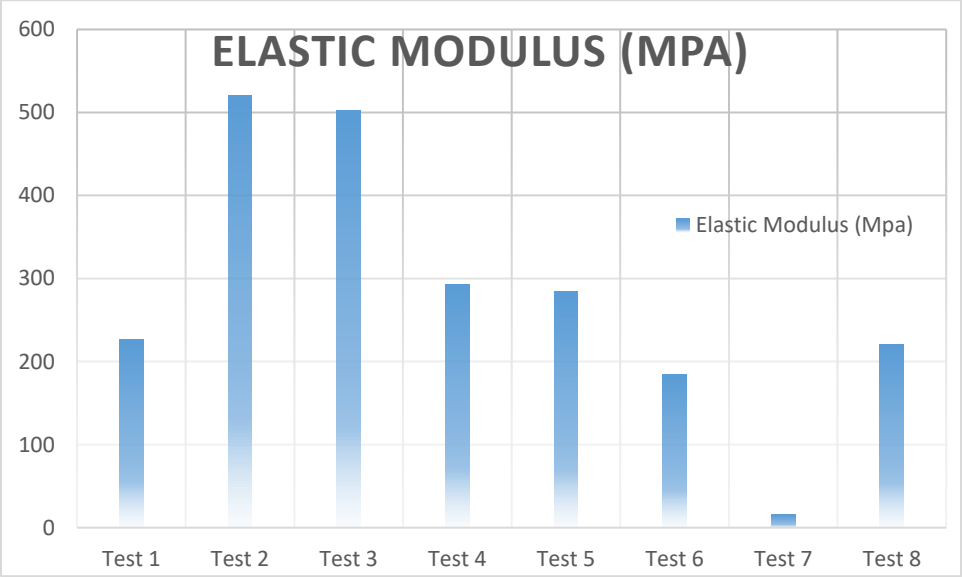

Figure 4.75: Comparison of elastic modulus depicted by each sample of various material

4.8. RESULTS FOR ELECTRON MICROSCOPY

In the electron microscopy analysis, detailed images were obtained for various samples, shedding light on the microstructural characteristics at different magnification

levels. Sample 3 of aluminum foam, was investigated at 50 micron with 400x magnification and at 10 micron with 1000x magnification. The images are shown in figure 4.74 below. These images provided a close examination of the foam's structure at different scales, capturing intricate details of the cell walls and overall morphology.

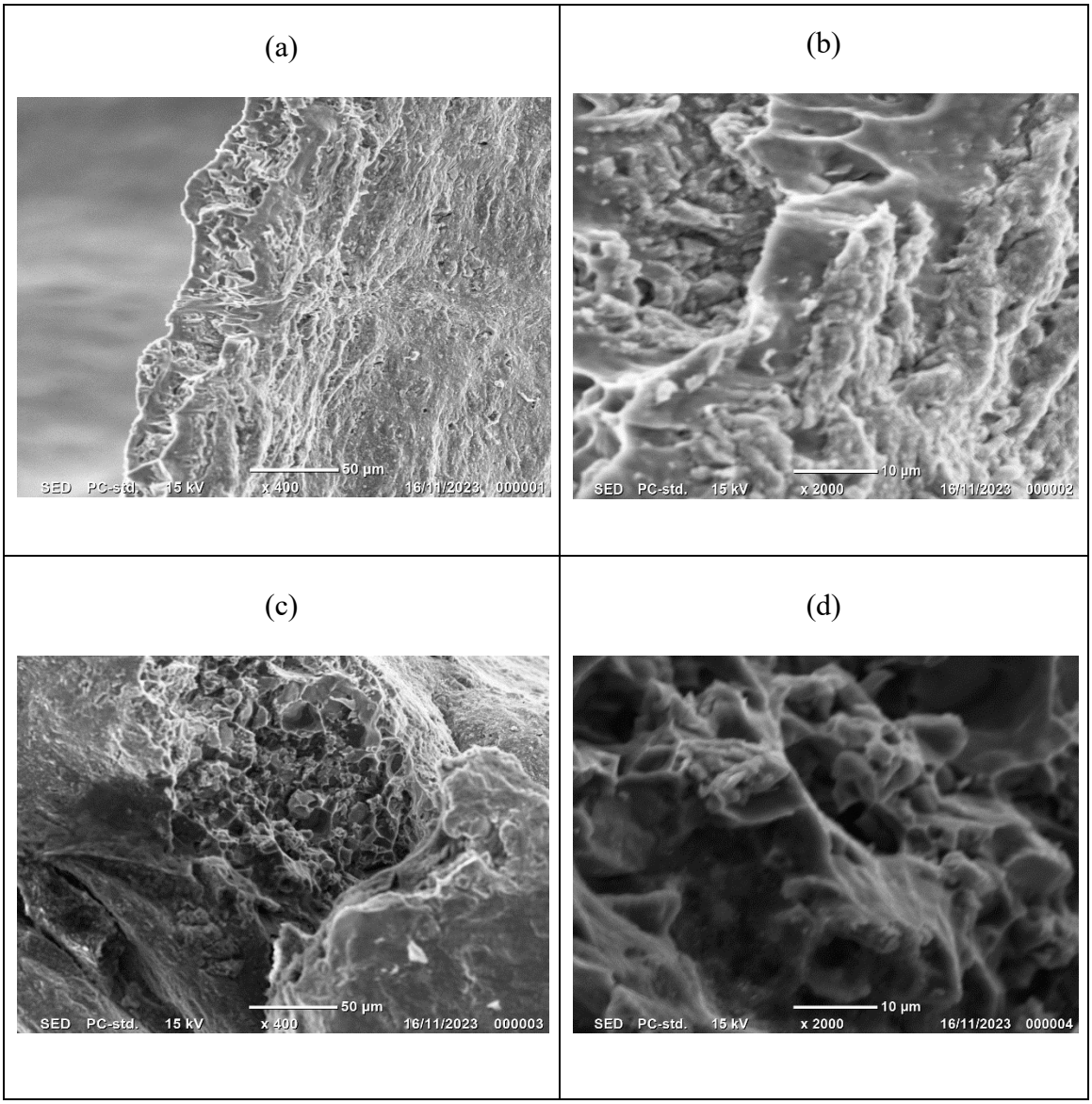

Figure 4.76: Varying magnification images of Aluminum foam

Similarly, the SD Al6016 Zn sandwich structure of Sample 3 underwent scrutiny at 10, 20, 50, 200 and 500 microns with magnification ranging from 40× to 2000×. The

images are displayed in figure 4.75. Images are representative of fractured surfaces and show mainly ductile fracture of the Al foam. Few fragile zones can be observed probably related to the presence of ceramic inclusions. In every case the fracture happened in the foam demonstrating the strength of the joint.

(a)

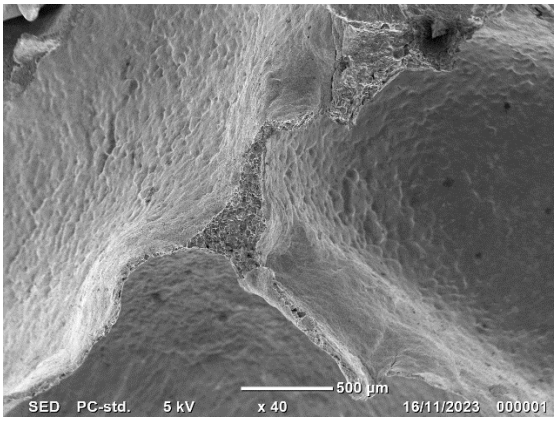

(b)

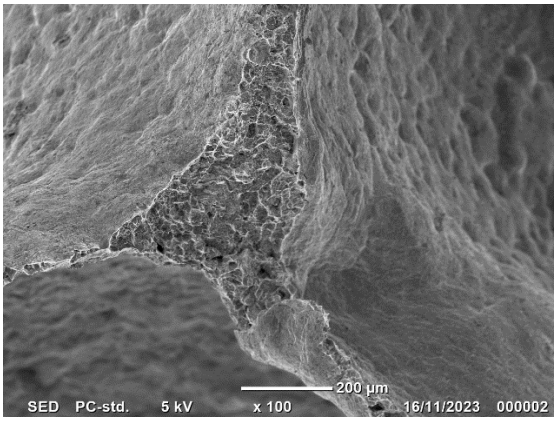

(c)

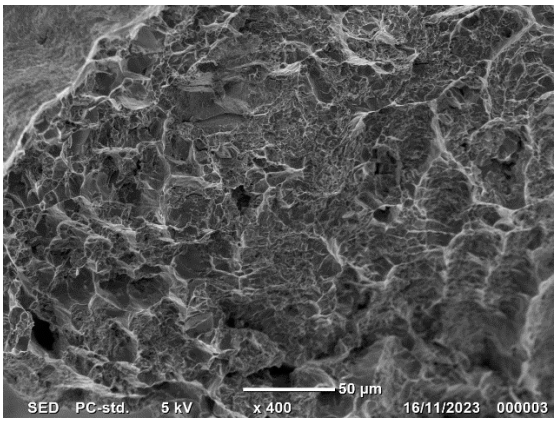

(d)

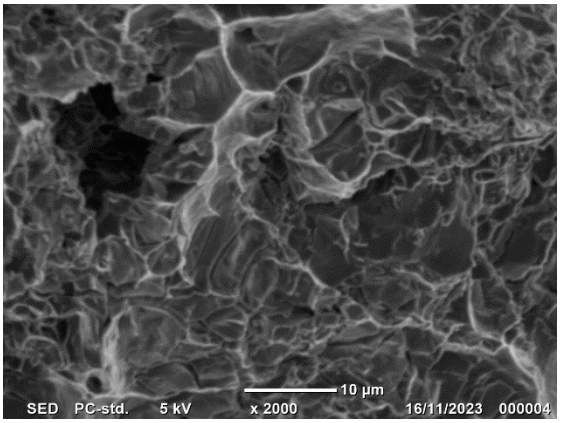

(e)

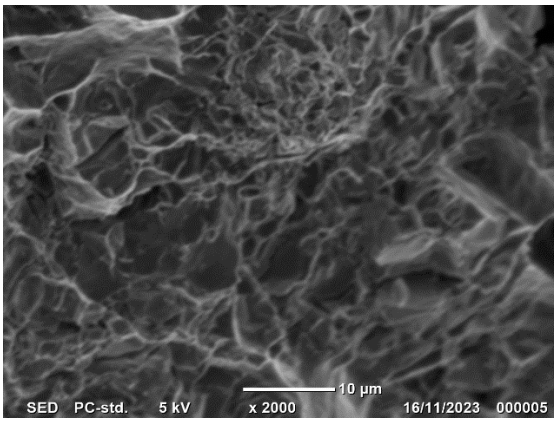
10 µm
SED PC-std. 5 kV x 2000 16/11/2023 000005

(f)

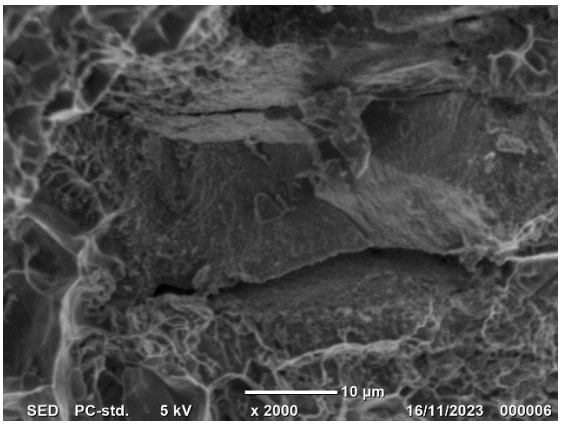
10 µm
SED PC-std. 5 kV x 2000 16/11/2023 000006

(g)

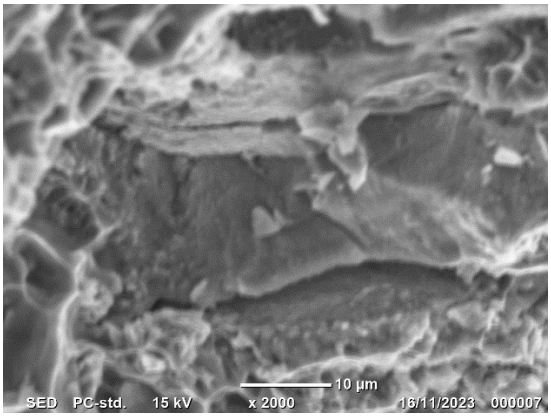
10 µm
SED PC-std. 15 kV x 2000 16/11/2023 000007

(h)

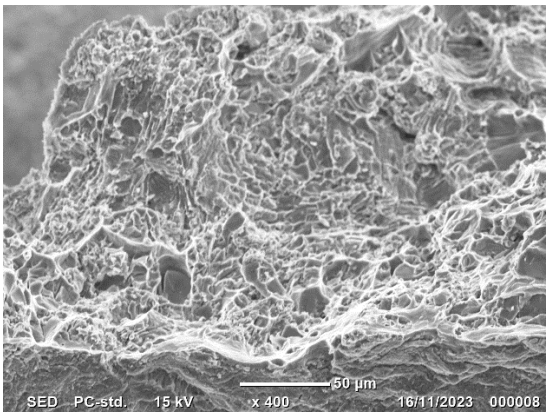
50 µm
SED PC-std. 15 kV x 400 16/11/2023 000008

(i)


10 µm
SED PC-std. 15 kV x 2000 16/11/2023 000009

(j)

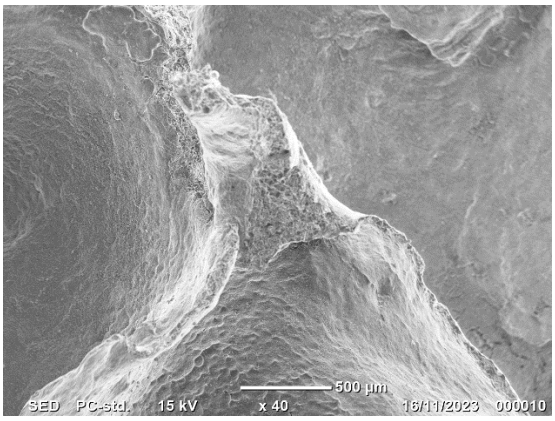
500 µm
SED PC-std. 15 kV x 40 16/11/2023 000010

(k)

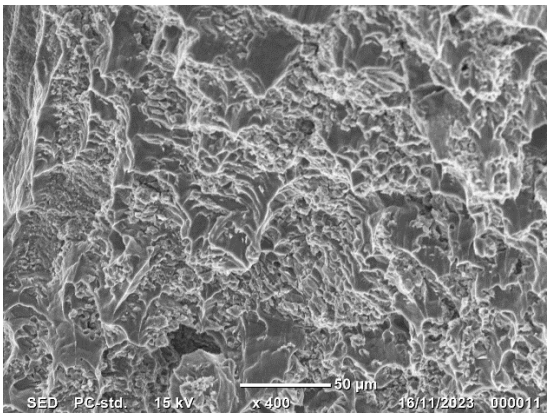
50 µm
SED PC-std. 15 kV x 400 16/11/2023 000011

(l)

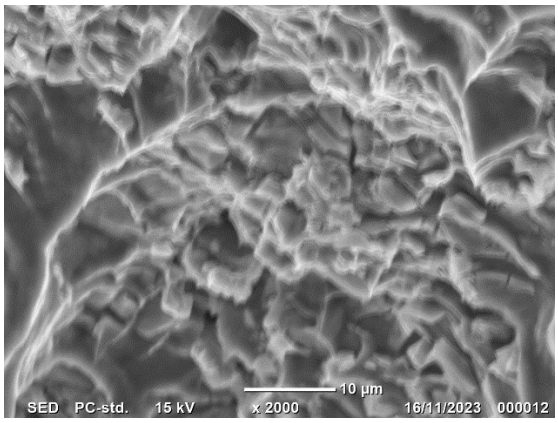
10 µm
SED PC-std. 15 kV x 2000 16/11/2023 000012

(m)

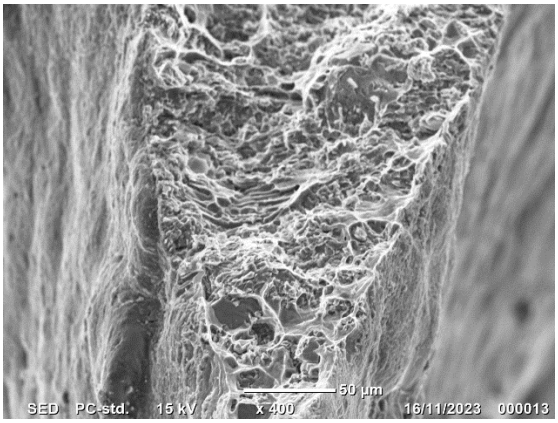
50 µm
SED PC-std. 15 kV x 400 16/11/2023 000013

(n)

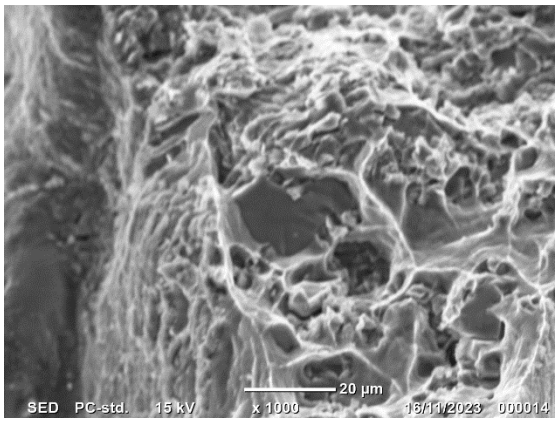
20 µm
SED PC-std. 15 kV x 1000 16/11/2023 000014

(o)

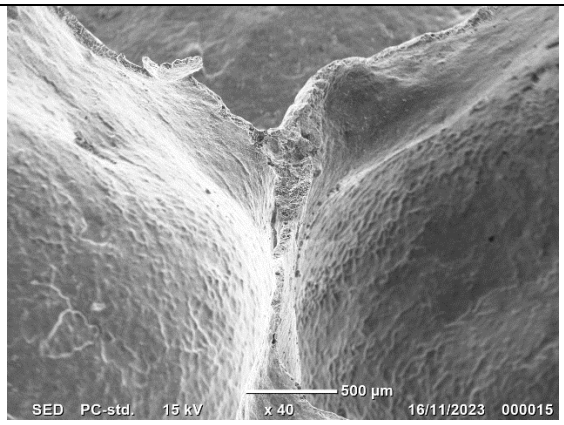

Figure 4.77: Varying magnification images of AFS component brazed with pure Zn foil as soldering material (SD Al6016 Zn)

The electron microscopy analysis extended to the SD Al6016 Zn2Al sandwich structure of Sample 3, with imaging at 50 micron and 400x magnification, as well as at 20 micron with 1000x magnification, repeated for further clarity. These images probed into the nuances of the observation of surface fracture developed in tested materials. The images are presented in figure 4.78 below.

(a)

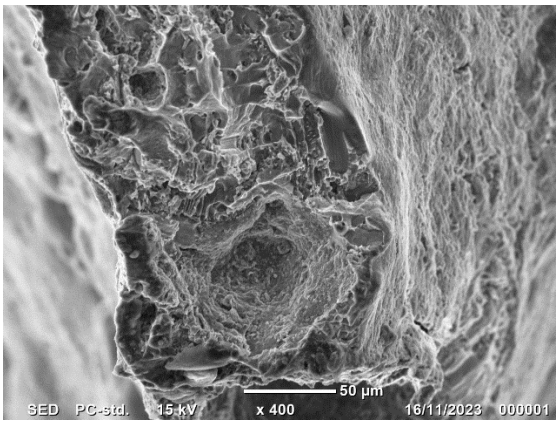

(b)

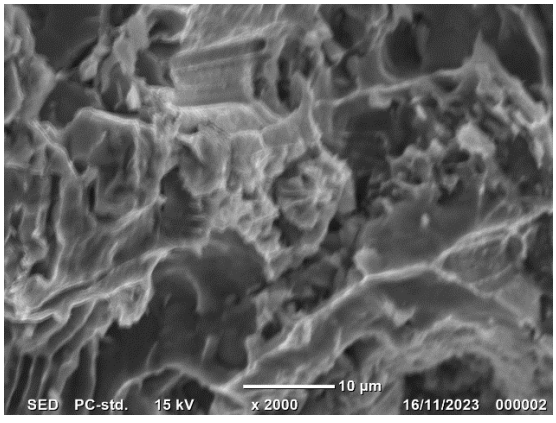

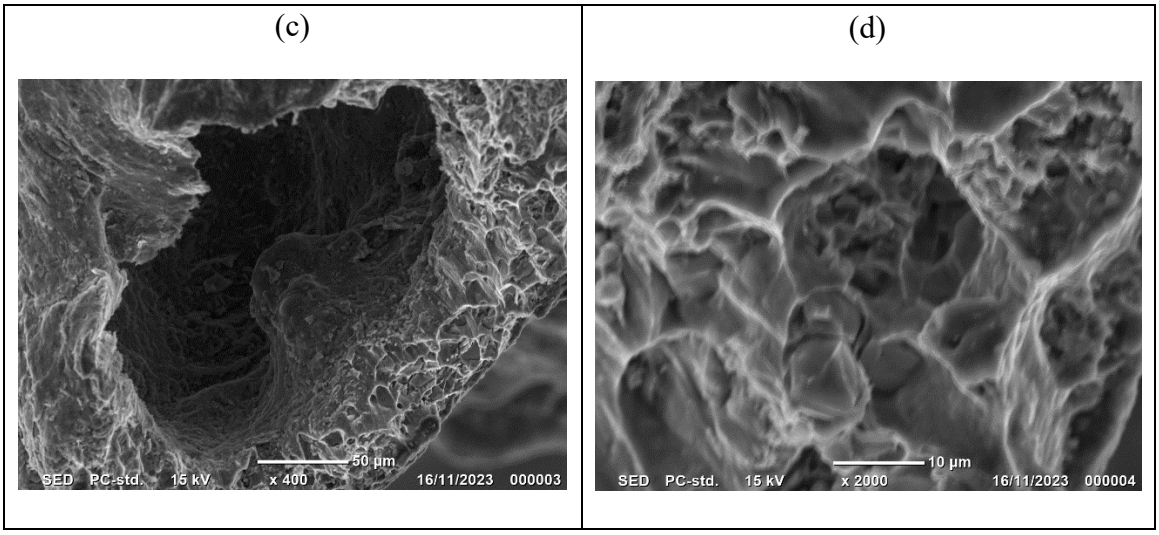

Figure 4.78: Varying magnification images of AFS component brazed with pure Zn2Al foil as soldering material (SD Al6016 Zn2Al)

The results of EDS performed on foam sandwich SD Al6016 with zinc brazing is shown in figure 4.79 through (a) to (e) and further in table 4.5.

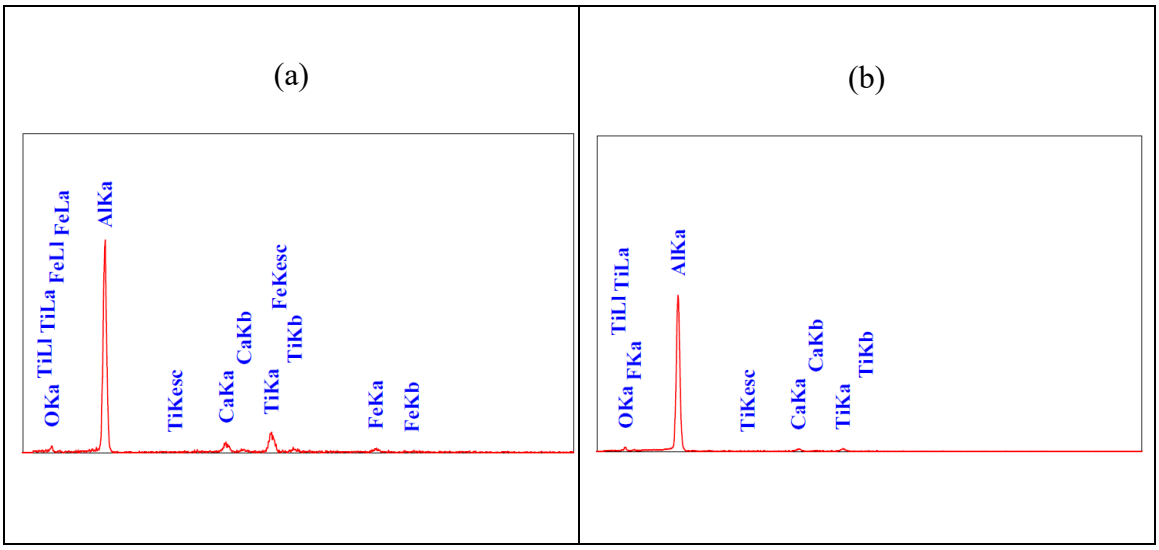

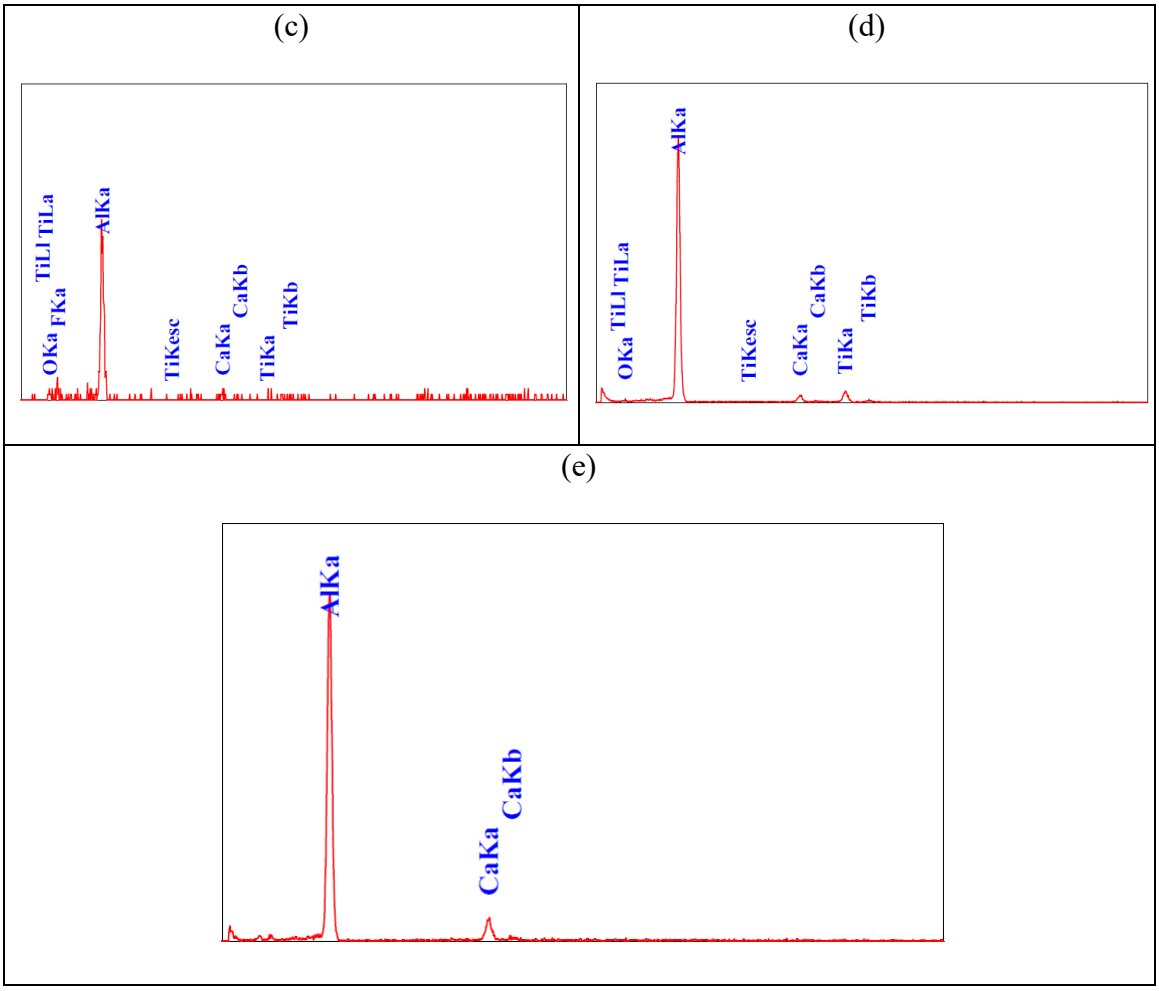

Figure 4.79: EDS Spectra results of SD Al6016 foam sandwich

Table 4.5: EDS results with composition (wt%)

Reference Figure	EDS	Composition (wt%)
Figure 4.79 (a)	EDS1	57%Al-9%O-6%Ca-21%Ti-7%Fe
Figure 4.79 (b)	EDS2	82%Al-8%O-4%Ca-3%Ti-3%F
Figure 4.79 (c)	EDS3	64%Al-13%O-8%Ca-4%Ti-11%F
Figure 4.79 (d)	EDS4	77%Al-3%O-5%Ca-15%Ti
Figure 4.79 (e)	EDS5	84%Al-16%Ca

The discussion section will explore into the significance of these microstructural features, correlating them with the mechanical and damping properties observed in the broader experimental study.

5. CHAPTER 5 – DISCUSSION

In this section, detailed discussion will be made on the results obtained for each sample of the material. The experimentally obtained values of Youngs modulus, shear modulus and internal friction coefficient in flexural and torsional measurement mode shall be compared with theoretical values from literature.

5.1. ANALYSIS OF RESULTS

5.1.1. ALUMINUM 6016 PLATE

For the aluminum 6016 plate, the figures 4.14 and 4.15 has been generated from the data shown in the table below. The data shows that Youngs modulus for aluminum 6016 plate varies from 55 MPa to 59 MPa while the shear modulus is 430 MPa. The value of shear modulus for S1 is an outlier.

Table 5.1: Experimental results of Youngs and Shear Moduli & internal friction coefficient for varying densities of Al 6016 Plate

Sample	Density	E-Modulus	Damp. flexural	G-Modulus	Damp. torsional
	kg/m3	GPa		GPa	
S1	2.505951	55.74667	0.000757	1.75	0.000819
S2	2.522692	59.07842	0.000756	436.122	0.000301
S3	2.523111	58.21467	0.000779	422.7317	0.000291

Experimental results in the above table shows that increasing the density of the material resulted in an increase in value of Youngs Modulus and shear modulus.

5.1.2. ALUMINUM FOAM

The research delved into the examination of the mechanical and damping characteristics of solid aluminum foams created through powder metallurgy,

encompassing various densities, through the utilization of impulse excitation technique testing on RFDA. The empirical findings demonstrate that, in both vibrational modes, Young's modulus and shear modulus exhibit an upward trend as density increases as evident in figure 4.28. In the context of flexural and torsional vibration of rectangular bar specimens, as illustrated in Figure 4.29, the results reveal that a reduction in relative density is associated with an escalation in the internal friction coefficient (Q−1). The results are presented in the table below:

Table 5.2: Experimental results of Youngs and Shear Moduli & internal friction coefficient for varying densities of Al Foam

Sample	**Density**	**E-Modulus**	**Damp. flexural**	**G-Modulus**	**Damp. torsional**
	kg/m3	**GPa**		**GPa**	
S1	0.288188	0.761628	0.005544	0.900588	0.008709
S2	0.28675	0.679333	0.014355	0.07	0.009208
S3	0.20342	0.409063	0.007395	0.205455	0.010835

5.1.3. AL-ZN SANDWICH (SD AL6016 AL ZN)

This experimental study for samples of Al-Zn Sandwich (SD Al6016 Al Zn) ventured into an exploration of the mechanical and damping characteristics which were manufactured via the powder metallurgy process, highlighting a spectrum of densities. Through the employment of IET testing, the outcomes unveiled intriguing trends which are shown in the table below:

Table 5.3: Experimental results of Youngs and Shear Moduli & internal friction coefficient for varying densities of SD Al6016 Al Zn

Sample	**Density**	**E-Modulus**	**Damp. flexural**	**G-Modulus**	**Damp. torsional**
	kg/m3	**GPa**		**GPa**	
S1	0.995735	22.5905	0.002249	1.92	0.002985

S2	0.999654	12.16333	0.062451	19.65556	0.008333
S3	0.910149	14.2516	0.002794	2.21	0.002588

It was observed that, and as evident in figure 4.42, for both modes of vibration, Young's modulus displayed a propensity to ascend with increasing density, while the shear modulus demonstrated a similar upward trajectory. As illustrated in Figure 4.43, the vibrational behavior of rectangular bar specimens, subject to flexural and torsional modes, exposed a contrasting pattern. In this context, the internal friction coefficient (Q^{-1}) experienced an intriguing ascent as relative density decreased.

5.1.4. AL-2%-ZN SANDWICH (SD AL6016 AL 2 ZN)

The elastic and damping properties of Al-2%-Zn Sandwich (SD Al6016 Al 2 Zn) is shown in table 5.4. A similar behavior is observed where higher density sample depicts higher Youngs and Shear moduli while a reverse trend is evident in the internal friction coefficient values. The figures 4.56 and 4.57 are the graphical evidence of this trend.

Table 5.4: Experimental results of Youngs and Shear Moduli & internal friction coefficient for varying densities of SD Al6016 Al 2 Zn

Sample	**Density**	**E-Modulus**	**Damp. flexural**	**G-Modulus**	**Damp. torsional**
	kg/m3	**GPa**		**GPa**	
S1	0.995735	11.13865	0.007541	1.256316	0.011628
S2	0.999654	13.26714	0.002955	1.9	0.003263
S3	0.910149	11.25556	0.011987	2.875385	0.016358

5.1.5. COMPARATIVE ANALYSIS BETWEEN THEORETICAL AND EXPERIEMNTAL VALUES

A comparative analysis between the theoretical predictions and the experimental findings for the selected materials, aiming to discern the alignment or disparities between

anticipated and observed behaviors. The materials under scrutiny encompass Aluminum 6016 Plate, Aluminum Foam, Al-Zn Sandwich (SD Al6016 Al Zn) and Al-2%-Zn Sandwich (SD Al6016 Al 2 Zn) each undergoing a battery of tests to evaluate key mechanical properties. By contrasting the theoretical expectations with the actual experimental results, it is aimed to unravel insights into the accuracy of predictions and potential variations in material performance, shedding light on the reliability of theoretical models in predicting the mechanical characteristics of these materials. A comparison of elastic modulus obtained through RFDA flexural mode test and tensile test is being made in table 5.5 below:

Table 5.5: Disparity between theoretical and experimental values of Youngs Modulus

Material	**Theoretical Value**	**RFDA Flexural *(averaged)***	**%age Difference**	**Tensile Test *(averaged)***	**%age Difference**
	GPa	**GPa**	**-**	**GPa**	**-**
Al 6016 plate	68.9	57.68	16.3%	-	-
Al Foam	0.1	0.62	500%	0.14	40%
SD Al6016 Al-Zn	0.4 – 1.0	16.3	15.3 *times from higher side*	0.42	4.7% *from lower side*
SD Al6016 Al-2-Zn	0.4 – 1.0	11.89	10.89 *times higher side*	0.29	27.5% *from lower side*

A comparative analysis reveals that theoretical value of elastic modulus is reported as 68.9 GPa revealing a percentage difference of 16.3%. In case of Aluminum foam, both RFDA flexural and tensile tests are in line as range of values exist for aluminum foam, with RFDA showing a 500% increase and tensile test a 40% increase. For Alporas SD Al6016 Al-Zn the RFDA flexural test indicated 15.3 times from higher

value, while the tensile test showed a 4.7% lower value compared to the theoretical range. The RFDA flexural test for SD Al6016 Al-2-Zn indicated a 10.89 times higher value, while the tensile test showed an 27.5% lower value compared to the theoretical range. These results highlight the discrepancies between theoretical expectations and experimental outcomes for each material and testing method.

The presented table 5.6 compares the theoretical values of elastic modulus (GPa) with the averaged values obtained from RFDA (Resonance Frequency and Damping Analysis) in the torsional mode

Table 5.6: Disparity between theoretical and experimental values of Shear Modulus

Material	**Theoretical Value**	**RFDA Torsional *(averaged)***	**%age Difference**
	GPa	**GPa**	**-**
Al 6016 plate	26	286	1000%
Al Foam	0.2	0.39	95%
SD Al6016 Al-Zn	0.3 – 0.35	7.92	21.62 *times from higher side*
SD Al6016 Al-2-Zn	0.3 – 0.35	2.01	4.74 *times from higher side*

The RFDA torsional results for aluminum 6016 plate significantly deviate from the theoretical value, showing an exceptionally higher modulus. Such a substantial difference suggests a potential anomaly or error in the experimental measurements or a limitation in the applicability of the torsional mode for this material. While there is still a notable difference, the percentage deviation for aluminum foam is comparatively lower than that of aluminum 6016 plate. This suggests that the experimental values are closer to the theoretical expectations, though some discrepancies may still exist.

The RFDA torsional results for Al-Zn sandwich indicate a higher modulus compared to the theoretical range, but the percentage difference is relatively moderate. This suggests that, despite being on the higher side, the experimental values align more closely with the theoretical expectations compared to aluminum 6016 plate. Similar to the Al-Zn sandwich, the Al-2%-Zn sandwich shows a higher modulus in the RFDA torsional results, with a percentage difference on the higher side. The experimental values, however, exhibit a closer alignment with the theoretical range compared to some other materials.

5.2. BEHAVIORAL & STRUCTURAL RESPONSE OF SAMPLES

The behavior of increase in Young's and shear moduli with increasing density in aluminum foam and aluminum foam sandwich can be attributed to both the structural characteristics of the closed-cell aluminum foam having more cell walls and the resulting material properties that emerge from this denser structure.

Aluminum foams have a cellular structure, where the material is divided into small cells. These cells are like tiny interconnected pockets within the foam. When the density of the foam increases, it results in circumstances that provide more cells per unit volume. The walls of these cells are made of the same material (aluminum), and they provide the structural integrity of the foam. As the density is increased, it effectively increases the number of these cell walls within the material. More cell walls indicate that there is more material to resist deformation, which results in increased stiffness or rigidity.

Young's modulus (E) and shear modulus (G) are material properties that quantify a material's stiffness to deformation under stress. Young's modulus measures the material's stiffness to stretching or compression in the direction of the applied force, while shear modulus quantifies the resistance to shearing or sliding deformation. Both moduli depend on the material's composition and microstructure. In closed-cell aluminum foams, the material is the same, but by increasing density, we effectively changed the microstructure by packing more material into the same volume. The increased number of cell walls results in a stiffer structure, leading to higher values of Young's and shear moduli.

Mathematically, Young's modulus (E) is related to stress (σ) and strain (ε) as $E = \sigma/\varepsilon$. In a material with more cell walls (higher density), it can withstand higher stress for a given amount of strain, indicating a higher Young's modulus. Shear modulus (G) is related to the shear stress (τ) and shear strain (γ) as G = τ / γ. Similarly, increasing density leads to a higher shear modulus because more cell walls provide greater resistance to shear deformation.

The findings in the combined plots in figure 4.58 & onwards highlight the trade-offs between stiffness and damping in material samples and structures selected for analysis, which can be important considerations in engineering applications where both properties matter. The selection of the material should align with the specific requirements of the application.

Aluminum 6016 Plate (Al 6016) material has the highest E-modulus among the tested materials. The high E-modulus of solid aluminum plate is expected because it's a dense, solid material with minimal voids. It offers high stiffness and is used in

applications where structural rigidity is critical. Sandwich Structure with Aluminum 6016 Faces and 2% Zinc based joining material (SD Al 6016 Zn2Al) has the second highest E-modulus. The sandwich structure typically combines the stiffness of the face sheets (Al 6016) with the lightweight core of aluminum foam ensuing in good stiffness-to-weight ratio, resulting in a relatively high E-modulus. Sandwich Structure with Aluminum 6016 Faces and Al foam (SD Al 6016 Zn) material has an intermediate E-modulus. Contrarily, Aluminum foam has the lowest E-modulus. It's designed to be lightweight and offers less structural stiffness than solid materials due to its porous structure.

The high E-modulus of the solid aluminum plate (Al 6016) is due to its dense structure. In the AFS, the aluminum foam core reduces the overall stiffness compared to a solid plate, resulting in an intermediate E-modulus. The joining materials play a role in connecting the face sheets and the foam core.

Aluminum foam continues to depict the highest damp flex values, as it is designed for excellent damping, as mentioned earlier while the relation between density and internal friction coefficient is being explained. The AFS structure exhibit intermediate damp flex values. The sandwich structure is providing inherent damping benefits due to the presence of the aluminum foam core, which helps with noise and vibration control. However, the aluminum face plates reduce the performance of AFS in damping while granting the strength and higher Youngs modulus. Similarly, aluminum 6016 plate exhibits the poorest damping properties because of its solid state closely bound molecular structure.

5.3. ANALYSIS OF TENSILE TEST RESULTS

Load vs displacement graph for the specimens reveal that SD Al6016 Al Zn curves represent highest load taken indicating that this is the best material for undertaking higher loads and representing highest resistance to failure. Similarly, the load-displacement curve indicates that SD Al6016 Al 2 Zn shows that lowest curve leading to earlier failure and termination of experiment.

From figure 4.63 to 4.65, variation in peak stress can be observed in the samples of aluminum foam and aluminum sandwich variants. The peak stress values range from 0.1 MPa to 0.8 MPa across the different test specimens. SD Al6016 Al Zn S3 exhibits the highest peak stress at 0.8 MPa, indicating its ability to withstand a substantial load before failure. Aluminum Foam S2, on the other hand, shows the lowest peak stress at 0.1 MPa. The strain at rupture varies widely, ranging from 0.2% to 2.4%. SD Al6016 Al 2 Zn S3 experiences the highest strain at rupture, reaching 2.4%, suggesting a significant deformation before failure. SD Al6016 Al 2 Zn S1 shows the second-highest strain at rupture (1.5%), indicating notable ductility before fracture. This result indicates that SD Al6016 Al 2 Zn shows the highest strain rate when compared with aluminum foam and SD Al6016 Al Zn. Whereas, SD Al6016 Al Zn samples represent the trend of withstanding highest stress. As a result, peak loads are borne by SD Al6016 Al Zn which ranges from 62 N to 87 N.

Generally, there is a positive correlation between peak stress and strain, with higher stresses corresponding to higher strains. The relationship between these factors provides insights into the material's deformation behavior under applied load. Tests with higher peak stress and strain values suggest better material performance in terms of

strength and ductility. Understanding these characteristics is crucial for assessing the material's suitability for specific applications.

It can be further observed by comparing the previous sections that in case of aluminum foam sandwich variants, the findings of tensile test experiment are in accordance of the RFDA flexural mode analysis. The RFDA analysis indicated that SD Al6016 Al Zn has the higher elastic modulus in flexion as compared to SD Al6016 Al 2 Zn which is also evident from the results and plotted curves of tensile test experiment. The aluminum foam results however, show discrepancy where aluminum foam shows enhanced performance in tensile test experiment as compared ton in RFDA where they reported lowest elastic modulus.

5.4. ANALYSIS OF FAILURE MODE IN TENSILE TEST

The analysis of failure mode in tensile test of each material reveal interesting facts that shed more light on the bonding strength of the adhesive material for sandwich panels. The failure mode analysis of aluminum foam however, reveal the only possible scenario of core yield or core failure since there are no face plates in these specimens. This failure occurs due to the failure of the core material occurring when the combined principal stresses within the core surpass the yield criterion. The aluminum foam core failure mode is shown in figure 5.1.

Figure 5.1: Aluminum foam core failure mode

The failure of aluminum foam is also observed due to the failure of adhesive bonding of aluminum foam surface with the holder, due to few contact points between the foam and the holder of the test piece thus resulting in the constant interruption of tests being the only reason for termination of experiments as indicated in figure 5.2. the possible reason for this failure is the even surface of foam which hinders uniform bond between holder and foam core.

Figure 5.2: Failure mode showing failure of adhesive bond between Al foam and holder

In case of Aluminum foam sandwich, SD Al6016 Al 2 Zn, test interruption was observed due to the failure of adhesive bond between the face plate and the foam core. This type of failure was congruent in all the specimen of SD Al6016 Al 2 Zn. The figure 5.3 below shows the failure of adhesive bond between aluminum face plate and foam core of the sandwich panel.

Figure 5.3: Failure of adhesive bond between aluminum face plate and foam core of the sandwich panel SD Al6016 Al 2 Zn

However, in case of SD Al6016 Al Zn it is observed that test was terminated rather than interrupted. And the observation of the failed specimen shows that failure mode occurs due to two reasons. One possible reason being the failure of bond between face plate and foam core while the other being the foam core yield. The failures are evident from the figures 5.4 and 5.5.

Figure 5.4: Failure of adhesive bond between aluminum face plate and foam core of the sandwich panel SD Al6016 Al Zn

Figure 5.5: Failure of foam core of the sandwich panel SD Al6016 Al Zn

6. CONCLUSION

This comprehensive study explored the mechanical and damping characteristics of various aluminum-based materials through extensive experimental testing and theoretical comparisons. The materials under scrutiny included Aluminum 6016 Plate, Aluminum Foam, Al-Zn Sandwich (SD Al6016 Al Zn), and Al-2%-Zn Sandwich (SD Al6016 Al 2 Zn). Young's modulus for aluminum 6016 plate varied from 55 MPa to 59 MPa, with a shear modulus of 430 MPa. Increasing material density resulted in higher values of Young's modulus and shear modulus. The high E-modulus of solid aluminum plate is expected due to its dense, solid structure. For Aluminum Foam Young's and shear moduli exhibited an upward trend with increasing density. Internal friction coefficient increased as relative density decreased. Aluminum foam demonstrated the lowest E-modulus, as expected from its lightweight, porous structure.

In case of Al-Zn Sandwich (SD Al6016 Al Zn) Young's and shear moduli ascended with increasing density while internal friction coefficient exhibited an intriguing ascent as relative density decreased. The sandwich structure with aluminum foam core and face sheets of Al 6016 showed intermediate properties. For composite bonding material of ASF Al-2%-Zn Sandwich (SD Al6016 Al 2 Zn) similar trends were observed with higher density samples depicting higher Young's and shear moduli. Internal friction coefficient displayed an interesting ascent as relative density decreased. The elastic and damping properties aligned with the behavior observed in other materials.

The increase in Young's and shear moduli with density in aluminum foam and sandwich structures can be attributed to the structural characteristics of closed-cell

aluminum foam, resulting in a denser structure. Trade-offs between stiffness and damping were evident, crucial for engineering applications where both properties matter.

From tensile test results, it can be concluded that SD Al6016 Al Zn exhibited the highest peak stress, indicating superior resistance to failure. Aluminum foam showed the lowest peak stress, with varying strain at rupture across specimens. Positive correlation between peak stress and strain suggested better material performance in terms of strength and ductility. Furthermore, comparative analysis between theoretical and experimental values for Young's and shear moduli revealed significant disparities between theoretical and experimental values, especially in aluminum foam, SD Al6016 Al Zn, and SD Al6016 Al 2 Zn.

The failure analysis shows that in tensile testing aluminum foam sandwich with zinc rich bonding material shows higher strength of the bond as evident in from the results of the experiment showing higher elastic modulus and peak stresses. The result is also supported by the fact that delamination of Aluminum skin sheet was frequently observed in samples of Zn + 2%Al bonding material with lower elastic moduli in the tensile tests. The result is in liaison with the findings of the RFDA test where sandwich with zinc rich bonding material depicts higher elastic modulus as compared to composite bonding material of Zn and Al.

BIBLIOGRAPHY

1. Baumeister, J.J.G.P.D., *Porous metal body production-involves compaction at low temperature followed by heating to near melting point of metal.* 1990. **4018360**.
2. Akiyama, S., H. Ueno, and K.J.A.E.P.I. Imagawa, *Foamed metal and method of producing same.* 1987. **3**(6): p. 241.
3. Orovčík, Ľ., et al., *Effects of chemical composition on the pore structure and heat treatment on the deformation of PM aluminium foams 6061 and 7075.* 2016. **54**(06): p. 463-70.
4. Banhart, J. and H.W.J.A.e.m. Seeliger, *Recent trends in aluminum foam sandwich technology.* 2012. **14**(12): p. 1082-1087.
5. Hohlfeld, J., T. Hipke, and F. Schuller. *Sandwich manufacturing with foam core and aluminum face sheets–a new process without rolling*. in *Materials Science Forum*. 2018. Trans Tech Publ.
6. Ubertalli, G., et al., *Joining of AL-6016 to Al-foam using Zn-based joining materials.* 2017. **96**: p. 122-128.
7. Hannemann, C., et al., *Manufacturing of foamable semin-finished products for aluminium foam sandwiches produced by extrusion.* 2018. **26**: p. 2018.
8. Hommel, P., D. Roth, and H. Binz. *Deficits in the application of aluminum foam sandwich: An industrial perspective*. in *Proceedings of the design society: DESIGN conference*. 2020. Cambridge University Press.
9. Baumeister, J., J.J.S.M. Weise, and P.i. Transportation, *Metal foams.* 2013: p. 415-444.
10. Lefebvre, L.P., J. Banhart, and D.C.J.A.e.m. Dunand, *Porous metals and metallic foams: current status and recent developments.* 2008. **10**(9): p. 775-787.
11. Schwingel, D.D., et al. *Aluminium foam sandwich structures for space applications*. in *57th International Astronautical Congress*. 2007.
12. Xu, Z., H.J.J.o.A. Hao, and compounds, *Electromagnetic interference shielding effectiveness of aluminum foams with different porosity.* 2014. **617**: p. 207-213.
13. Zhao, A. and Y.J.T.S. Hu, *Numerical simulations of effective thermal conductivity in aluminum foam sandwich panel.* 2018. **22**(6 Part B): p. 2827-2834.
14. Ventech. *Heat Insulation Materials Phenolic Aluminum Foam Sandwich Panel for HVAC Air Duct Panel*. 2023 [cited 2023 11-11-2023]; Available from: https://fsventech.en.made-in-china.com/product/SQrpbsoGbmcZ/China-Heat-Insulation-Materials-Phenolic-Aluminum-Foam-Sandwich-Panel-for-HVAC-Air-Duct-Panel.html.
15. ASTM, E.J.A.B.o.A.S., *Standard Test Method for Dynamic Young's Modulus, Shear Modulus, and Poisson's Ratio by Impulse Excitation of Vibration*, in *ASTM E1876-22*. 2022, ASTM.
16. Materials, A. *Aluminium / Aluminum 6061 Alloy (UNS A96061)*. 2023 [cited 2023 11-11]; Available from: https://www.azom.com/article.aspx?ArticleID=6636.

17. Goodfellow. *Aluminium Foam – Structure, Properties and Benefits*. 2014 [cited 2023 11-11]; Available from: https://www.azom.com/article.aspx?ArticleID=10529.
18. M.F. Ashby, A.G.E., N.A. Fleck, L.J. Gibson, J.W. Hutchinson and H.N.G. Wadley, *Metal Foams: A Design Guide*. 2000: Butterworth-Heinemann. 247.

APPENDICES

Finally, leave a blank page at the end of your thesis. This page is not numbered.